An MR Compatible Olfactometer For Clinical Research Use

By

JOHNNY NG

A dissertation submitted to the Graduate Faculty in Biomedical Engineering in partial fulfillment of the requirements for the degree of Doctor of Philosophy, The City University of New York

2012

This manuscript has been read and accepted for the
Graduate Faculty in Engineering in satisfaction of the
dissertation requirement for the degree of Doctor of Philosophy.

Professor Marom Biskon

Date — Chair of Examining Committee

Dr. Cheuk Yang Tang

Date — Co-Chair of Examining Committee

Professor Mumtaz K. Kassir

Date — Executive Office

Professor Lucas Parra

Professor Maribel Vazquez

Professor Simon Kelly

Supervisory Committee

THE CITY UNIVERSITY OF NEW YORK

Abstract

An MR Compatible Olfactometer for Clinical Research Use

by

Johnny Ng

Advisors: Professor Cheuk Y. Tang

Professor Marom Bikson

The sense of smell is part of our chemical sensing system. It not only has a role in helping to interpret smells, but also taste flavors. The olfactory system is the first sensory system to develop in a fetus. However, it is one of the most neglected sensory systems in human research compared to visual and auditory sensory systems. It is difficult to objectively quantify exploration of the olfactory system. Different adequate methods to produce a selective and controlled stimulation of the olfactory system are lacking.

Recently, more studies have used functional imaging techniques to investigate the olfactory system in humans. Functional magnetic resonance imaging (fMRI) is the main technique used in recent studies. fMRI is a non-invasive method which allows researchers to study the functions of the human olfactory system without any contrast agent. However, there are a few commercial olfactometers in the field that are compatible to MR imaging. The cost of commercial olfactometers is not always affordable for most research institutes. Therefore, most of the olfactory system studies require a specifically-built olfactometer for their particular needs.

The purpose of this study is to build a cost effective olfactometer, which can be used not only in a research, but also in a clinical environment. Its main feature is MR compatible, so that

studies with functional imaging will be easily adapted to this olfactometer. Different tests have been applied to determine the characteristics of the olfactometer and its delay time, sometimes called the “rise time” or “fall time”. A mask and cannula were also tested to determine which would be best for olfactory stimulation. The results showed that the custom-built olfactometer has less than 1 second delay time. For human subjects testing with fMRI showed positive results. Brain activations were recorded from olfactory stimulation by using this olfactometer to deliver the odorant stimuli. It is now being used with a new research project that involves obsessive-compulsive disorder patients with the use of pleasant and unpleasant odorant stimuli. Some test subjects showed activations in the orbitofrontal cortex.

Acknowledgments

I would like to express my sincere thanks to everyone who made my doctoral studies the best experience anyone could imagine.

First, I would like to extend my sincere gratitude to my advisor, Professor Cheuk Tang. He has been a constant source of encouragement, immeasurable support and guidance every step of the way towards the completion of my doctoral studies. It was an honor to learn from him, and I am grateful beyond words for his mentorship. Also, I would like to thank my other advisor, Professor Marom Bikson for his generous help, guidance, and encouragement throughout my doctoral studies.

My sincere thanks to Professor Lucas Parra, Professor Maribel Vazquez and Professor Simon Kelly for being members of my dissertation committee and the sincere efforts they have put into the review of my thesis manuscript. I thank all the members of the Translational and Molecular Imaging Institute at Mount Sinai Hospital, including Emily Eaves, David Carpenter, Yu Zhou, Lena Marra, Elana Pessin, Daniel Samber, Edmond Wong, and Tuyen Nguyen, for their endless support during my research. I also want to thank Professor Susannah Fritton and Professor Mitchell Schaffler for their valuable guidance and generous help.

I would like to thank my parents and my family for their love and unlimited moral support. I especially thank my sponsor, Otto Schmitt. Without his guidance, advice, love, help and teaching me to think outside the box, I would not be able to be who I am today. I also appreciate all the trips we took, which showed me much of the United States and its history, and taught me about the cultural diversity of this country. I deeply appreciate his being part of my life in New York. Thanks to all the people whom I met and who have become my friends

through these years. They were interested in my studies and were part of my New York and American experience.

I would like to dedicate this thesis to my dearest friends, who are no longer with us, Anita and Martin Saunders. I appreciate not only their friendship, but also their generosity, caring and always treating me as a son of their own. Thank you and you will always be in my heart.

Table of Contents

List of Figures

List of Tables

Chapter 1

Introduction

The olfactory system is vitally important to humans and animals for sensing environmental changes and helping to trigger proper behavioral and physiological responses. In all animals, it is the primary mode of communication, helping with reorganization of kin, aiding in navigation, marking of territory and detecting of both predators and prey. It also influences many bodily functions, including reproduction and taste. Likewise in humans, the sense of smell significantly contributes to a person's quality of life.

Olfaction is considered one of the oldest senses and is perhaps the most important sense for most organisms. Human interest in scents or odors can be traced far back in ancient history. However, human olfaction still is not well understood and is an often neglected and misunderstood topic of study compared to our other senses, such as visual and auditory.

The air we breathe contains many diverse odorant molecules, yet human perception selects only those that attract or distract. Odor is perceived by the human brain in response to the chemical mixture present in the air when breathing, and is the effect of those chemicals. The human olfactory system can detect odor even when the chemicals producing them are present in a very low concentration.

At least 3,000,000 Americans suffer from chemosensory disorders, and this figure is more likely to increase as the aging group of the population grows[1-3]. A study in 2002 by Murphy et al. found that about 24% of individuals aged 53-97 years had impaired olfactory function. This dysfunction ranges from a generally diminished sense of smell to complete inability to detect odors at all, which is called anosmia. Common causes for olfactory dysfunction are: head trauma, nasal and/or sinus disease, upper respiratory disease, stroke, cigarette smoking and aging[4-8]. Recently, an increased numbers of neurological and psychiatric diseases have been reported to be associated with olfactory dysfunction. These neurological and

psychiatric diseases are: Alzheimer's disease (AD), schizophrenia, multiple sclerosis (MS), epilepsy, Parkinson's disease (PD) and obsessive-compulsive disorder (OCD)[2, 9-19]. Some studies are also trying to determine the possibility of using olfactory dysfunction as a biomarker for these neurodegenerative diseases – such as Alzheimer's disease, Parkinson's disease and obsessive-compulsive disorder[17, 19-21].

The olfactory process begins when odorant molecules from the surface of an object are released into the air and reach the nose. These chemicals move across the olfactory epithelium and dissolve in its mucous sheath. Then they bind to the olfactory receptors in the cilia, which are located in the olfactory epithelium on the dendrite side of the olfactory neurons. Olfactory receptor cells are then activated and send electric signals to glomeruli in the olfactory bulbs through their axons. The signals are relayed from the glomeruli to both the mitral and tufted cells which then transmit them onto higher regions of the brain, such as the primary olfactory cortex (anterior olfactory nucleus, piriform cortex, olfactory tubercle, amygdala and the entorhinal cortex), hippocampus, insular cortex and orbitofrontal cortex[14, 22-26].

Functional neuroimaging of the olfactory system has gained increased interest during recent years. High resolution coronal Magnetic Resonance Imaging (MRI) images, with and without contrast material and with fat suppression techniques, offer the best opportunity to study the olfactory bulbs and tracts anatomically[27]. Moreover, MRI is a valuable tool for the investigation of brain structure and functional activation in special regions of interest[28]. Functional Magnetic Resonance Imaging (fMRI), which requires no injection of radioactive material into the circulatory system is a non-invasive method, and has been used to quantify brain activation with different subjects using olfactory stimulation. These studies of the olfactory system place special demands on how to present the odorant stimulus to the participants. There

are commercial olfactometers on the market, but most are not magnetic resonance compatible and are typically used for environmental odor detection. Therefore, the majority involved in olfaction research with fMRI are usually custom-built for particular research.

Several research studies using fMRI to investigate certain olfactory functions need to build their own olfactometer to accomplish their research. One research project[29], a study of the function of human olfaction which declines with advancing age, demonstrated that aged adults showed less brain activity in olfactory structures, especially those elderly with Alzheimer's disease. These investigators built their own odorant delivery system for their fMRI research. Another research project[30] studied the olfactory system activation from sniffing. They found significant activity in the piriform and orbitofrontal cortexes (OFC) during odorant sniffing, which suggested that sniffing might play an important role in facilitating the higher-order analysis of odors. They also built an eight-channel computer controlled olfactometer, following the MR compatible air-dilution olfactometer developed by Lorig et al. (1999)[31]. Rolls et al.[32] constructed a purpose-built 10-channel olfactometer for their research in 2003. The aim of their research was to investigate the different representations in the human brain with 'pleasant' and 'unpleasant' odorant stimuli. They found activations in piriform cortex, anterior cingulate cortex (ACC) and the OFC. Other fMRI studies[33-35] also used custom-built or purpose-designed olfactometers to deliver the odorant stimuli to the subjects.

There is no uniform standard for building an olfactometer, which remains largely laboratory specific. Most of these olfactometers are built under the principle of air dilution olfactometry. Since an olfactometer works by bubbling air at a fixed flow rate through solutions (odorant stimuli), most of the researchers expect that the odorant concentration does not vary during normal use for a given odorant solution. Therefore, no validation of the odorant

concentration is tested. But, if the odorant concentration varies, the end result will undoubtedly be affected. Also, the time when a subject receives the odorant stimulus is equally important and will affect the outcome when analyzing the data. There is a company making commercial olfactometers for olfactory research compatible with MR usage – Burghart Medizintechnik, Hamburg-Blankenese, Germany. Many olfactory research projects use these olfactometers to accomplish their research[8, 36-38]. The price of a Burghart's olfactometer ranges from US$ 45,000 to 240,000. This price range is much too high for most of the laboratories doing olfactory research.

The majority of the custom-built olfactometers used for laboratory research are not always considered for clinical use. An olfactometer is rarely available or used in a clinical setting. The aim of this project is to build an MR compatible and cost-effective olfactometer, which can be used not only in laboratories but also in a clinical environment.

Chapter 2

Background

2.1 A Brief History of the Sense of Smell

The topic, 'the sense of smell', has been of great interest and can be traced back to ancient history. The Greek philosopher, Democritus of Abdera (460-360 B.C.), and his countryman, Aristotle (384-322 B.C.), had their own hypothesis concerning this matter. Democritus thought that we smelled the "atom" of different sizes and shapes, which came from objects. On the other hand, Aristotle suggested that odors were detected when the "cold" sense of smell met with "hot" smoke or steam from the object. Not until the late eighteenth century did most scientists and philosophers agree that Democritus was right – the object that we smell was due to volatile molecules that it emitted.

In the 5th century B.C., Alcmaeon, an ancient Greek, associated the brain with sensation. He proposed that smell was produced by the aspiration of odorous particles through the nose to the brain.

Perfumes consisted only of thick resins, gums and gooey unguents. Avicenna, the 11th century Arabian alchemist and physician, discovered the process of extracting and preserving the flower's scent by using alcohol distillation. Avicenna also used the change in the smell of patients' urine to diagnosis illness. However, he wasn't the first doctor to diagnose diseases by the patients' smell. Many centuries earlier, the ancient Greek physician, Hippocrates, sniffed patients' body odor as an effective means to identify their ailments. In the 17th and 18th centuries, doctors suggested the use of perfumes to fight infection.

Carolus Linnaeus (1707-1778), the Swedish botanist, physician and zoologist, is known as the father of modern taxonomy and is famous for his system of classification of plants and animals. Moreover, it is almost unknown that he suggested a seven-category system for odors –

camphoraceous, musky, floral, pepperminty, ethereal, pungent and putrid, since John E. Amoore is often credited with the classification of primary odors in 1952, almost 200 years later.

The French anatomist, Hippolyte Cloquet (1787-1840), stated in 1821 that smell was important to animal survival and reproduction. However, his other theories of the role of smell in human sex and mental disorders were controversial.

In 1883, an Austrian physiologist and physician, Ernst Fleischl von Marxow (1846-1891), observed that electrical brain potentials were produced when ammonia was presented to a rabbit's nose[39, 40]. However, the first electrophysiological recording from the human nasal mucosa was not obtained until the 1960s[40].

In the first half of the twentieth century, more studies of the sense of smell were making real progress. Spanish neuroanatomist, Santiago Ramon y Cajal (1852-1934), traced the olfactory system where the nerves lead from the nose to and through the brain. Some other scientists investigated how the nose detects odor molecules, the sensitivities of the human nose, and the difference of the olfactory system between animal and human. Currently, the recent application of molecular science is applied to investigate the odor-sensitive cells of the nasal cavity.

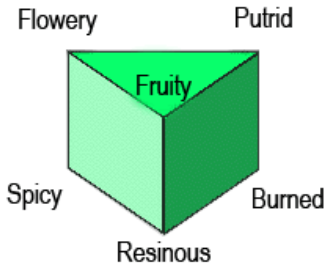

Figure 2.1-1: Henning's smell-prism. *Jim LaMar*

In 1916, Hans Henning (1885-1946) suggested that a 'smell prism', which used six primary odors, would represent the range of human olfaction (figure 2.1-1). He thought that any olfactory stimulus would be in a position in one of the three-dimensional spaces – flowery, foul, fruity, spicy, burnt and resinous. In 1927, Crocker and Henderson invented a system, which involved four basic odors – fragrant, acid, burnt, and caprylic (smelling like a goat). This system

became a commercial product, which came as a kit with comparison vials and each was labeled with the basic odor and its rating on a nine-point scale (odors were rated from zero to eight).

Smell was even used in the theater as early as 1916 in the Family Theater in Forest City, Pennsylvania. The machine, which delivered the scent in the theater while the film was being projected, was invented by Hans Lube. It was first named "Scentovision", and later, after modification in 1930's, it was named "Smell-O-Vision" (figure 2.1-2). Hans Lube introduced his system in the 1939 New York World's Fair and later signed a movie contract with film producer Mike Todd Jr. They produced the movie "Scent of Mystery" in the 1960, the only appearance of the Smell-O-Vision. Thirty different smells were injected into the theater's seats with triggering by the film's soundtrack. With negative reviews of the film and technical problems, Smell-O-Vision technology wasn't used after this movie until the 1980's. A few movies tried to adopt this technology, but were not successful. Recently, this technology seems like it is making a comeback and growing in popularity. In 2006, the Japanese telecom giant, NTT Communications, developed a new way (through the internet) to synchronize the odors generated with the movie scenes. In 2008, a Portuguese designer, Nuno Teixeira, developed a device called "Smellit" (figure 2.1-2). This system introduced the Smell-O-Vision technology into the home and works with DVD players to release odors to the corresponding scene[41, 42].

Figure 2.1-2: Smell-O-Vision and Smellit home systems. Mike Todd Jr., Hans Lube and the Smell-O-Vision system (top). Smellit home system by Nuno Teixeira is shown in the middle and bottom pictures. *wired.com and behance.net*

The first prototype electronic nose was developed by the Institute of Olfactory Research at Warwick University in the United Kingdom in July 1987[43]. This electronic nose mimics the functions of the human nose, but with more precision and it never has adaptation problems. The concept of an electronic nose is widely used in industry as an analytical tool[44]. Most of the applications involve the grading of the odors of foodstuffs – especially the quality of freshness. Perfume makers are also using the electronic nose to protect their patented scents against imitators. Scientists at Warwick University are researching the use of the electronic nose to diagnose illnesses by smelling patients' breaths – this method has been used for centuries by Chinese doctors[43, 45]. Moreover, Warwick University was recently awarded an European Union grant to investigate the possibility of installing a tiny electronic nose in telephone receivers, into which patients can breathe and wait for a diagnosis from doctors[43, 46].

Recently a dating website – Basisnote from Bern, Switzerland – announced that it will be able to compare partners' personal body odors to determine whether they will be a potential match, in addition to looks and interests in the profile[47]. A digital code from a saliva test result combined with a chromatographic process is entered on an online profile. If a potential partner has also entered his/her smell profile, the database of the website can find out whether these potential partners will like each other.

Also, a company called ScentSational Technologies from Jenkintown, Pennsylvania has released a new consumer product, Aroma Water, which uses smells to duplicate flavors[48]. A thin layer of plastic with FDA-approved flavors sealed inside is placed inside the bottle cap. Not only is the fragrance with the fruity scent infused into the water, it is also released into the air when the seal is broken and the top is popped open. This fragrance then travels along the back of

the throat and up into the nasal passage. Retronasal stimulation will enhance the fruity taste of the water.

Smell is one of the senses (compared to vision and sound) which was considered as a lower order, primitive and with no control, since each intake of breath sends air molecules over the receptors in the nose and produces uncensored information to the brain. However, the topic of 'sense of smell' is always being researched with great interest; and always involves our daily lives.

2.2 Human olfactory system

2.2.1 Anatomy of the olfactory system

The olfactory system consists of the primary olfactory nerves in the nasal cavity (olfactory epithelium), olfactory bulbs and tracts, and numerous intracranial connections and pathways, such as the olfactory cortex.

The olfactory epithelium (also called the olfactory mucous membrane or olfactory mucosa) is located in the roof of the nasal cavity and occupies areas of the cribriform plate, dorsal portions of the superior turbinate, and the superior part of the nasal septum. These two patches of yellowish mucous membrane are about 7 cm up from each nostril, and their areas are about 2 to 2.5 cm^2 and about 60 microns thick. The olfactory epithelium is made up of four primary cell types: the olfactory receptor cells, the supporting cells or the sustentacular cells, the basal cells, and the duct cells of Bowman's gland (figure 2.2-1). The supporting cells cover the receptor

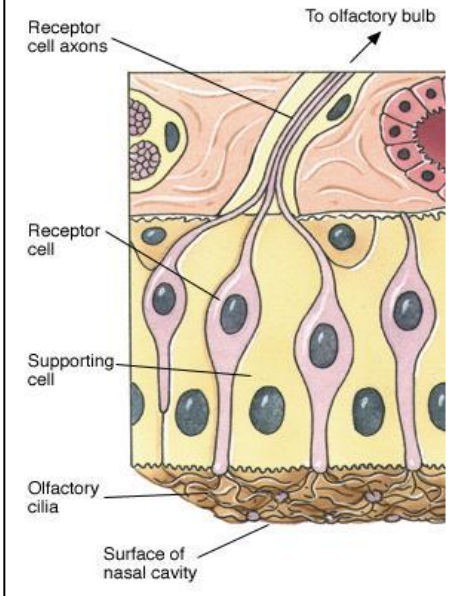

Figure 2.2-1: The olfactory epithelium. *University of Illinois at Urbana-Champaign*

neurons to maintain the normal extracellular potassium levels needed for neuronal activities[49]. The Bowman's gland, which penetrates the epithelium and subepithelium connective tissue, secretes mucus to cover this tissue. These mucous lipids keep the tissue surface moist, and dissolve odoriferous substances before they can effectively stimulate the sensory cells. The basal cells, small polygonal cells, are located in the lower part of the epithelium and in contact with the underlying basement membrane[50, 51]. There are approximately 20 million olfactory receptor cells in the epithelium[22, 52]. Each olfactory receptor is a neuron, and all of the neurons are regenerated every 40 to 60 days as shown in previous studies[22, 50, 53-55], but more evidence shows that this is not true. There is long-live neuron in a mouse model; therefore it is not necessarily true that the neurons will be regenerated every 40 to 60 days[51]. These neurons are the only group of neurons capable of regeneration, and undergo self-renewal throughout adult life[50, 54, 56, 57]. They can be regenerated from basal cells after damage, and project directly into the brain before their first synapse. They are the only cells that directly contact both the central nervous system and the external environment.

Olfactory receptor neurons are bipolar in which the dendrite and axon connect directly to the cell body[6, 23, 50]. These axons are extremely small, approximately 0.2 μm in diameter, and are among the thinnest axons in the nervous system. Moreover, they are the slowest conducting axons in the nervous system, approximately 1 meter per second[51]. Each neuron lies between supporting cells in the middle of the epithelium. The apical end of the neuron has an unmyelinated axon, which joins others in olfactory nerve filaments. These penetrate the base of the skull through openings in the

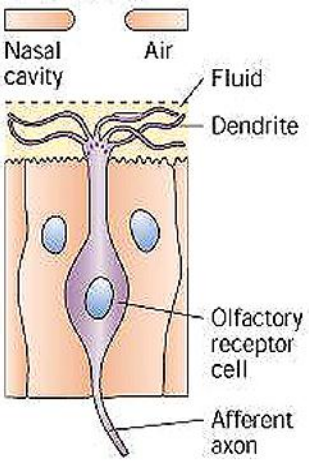

Figure 2.2-2: The olfactory receptor cell. *University of Illinois at Urbana-Champaign*

cribriform plate of the ethmoid bone. The olfactory nerves connect synaptically to the olfactory bulb. On the other end of the neuron, the dendrite has hair-like fibers on the surface, called olfactory cilia, which are up to 200 μm long. The cilia have a nine plus two pattern of microtubules, characteristic of motile cilia. However, there is only one center pair towards the tip. There are approximately 20-30 cilia where the initial events of olfactory transduction occur[23, 50] (figure 2.2-2). Olfactory cilia, which are non-motile, contain olfactory receptors and project from the receptor neurons into the mucus layer lining the nasal cavity. They detect odorants dissolved in the overlying mucus layer, where interactions with the odorants take place. Each olfactory receptor neuron appears to express only one type of receptor protein, and detects only one particular class of odorant molecules. There are about 1,000 of these receptors[22, 25, 54, 58]. All olfactory receptor neurons, expressing a particular type of receptor, converge their axons into a single spherical mass, called the glomerulus[54].

The olfactory bulb is an oval structure that lies on the ventral surface of each frontal lobe and supported by the cribriform plate of the ethmoid bone. The olfactory receptors leave the olfactory epithelium and come together to form a large number of bundles. These bundles together form the olfactory nerve. Each olfactory nerve projects to the same side of the olfactory bulb. There are three main cell types in the olfactory bulb: the mitral cells, tufted cells, and interneurons – granule cells and periglomerular cells[22, 25, 53]. The tufted cells are smaller than the mitral cells, and have thinner axons. Both cells send their axons into the olfactory bulb, and have similar functions. Periglomerular cells are the inhibitory neurons connecting the glomeruli. Granule cells have no axons and make reciprocal synapses with the lateral dendrites of the mitral and tufted cells[24].

The anterior and posterior axons of olfactory receptor neurons project to the anterior and posterior part of the olfactory bulb in a topographic manner. These axons then terminate in the glomeruli, which lie beneath the surface of the olfactory bulb. The glomeruli are formed by the terminals of the olfactory nerve fibers and surrounded by tufted cells and periglomerular cells. These cells receive synapses from the olfactory nerve terminals. The apical dendrites of mitral and tufted cells divide into several branches in the glomeruli. These dendrites are targeted by the olfactory synaptic nerve endings. Therefore, each glomerulus is not only formed by thousands of olfactory cells' axon terminals, but is also connected to the dendrites of the mitral, tufted and periglomerular cells. The granule cells, the other major neurons, can be found deeper in the olfactory bulb. These neurons form dendrodendritic synapses with the lateral and secondary dendrites of mitral and tufted cells. Axons of mitral and tufted cells constitute the primary output pathway of the olfactory bulb[22, 24, 25, 54, 55, 59, 60] (figure 2.2-3).

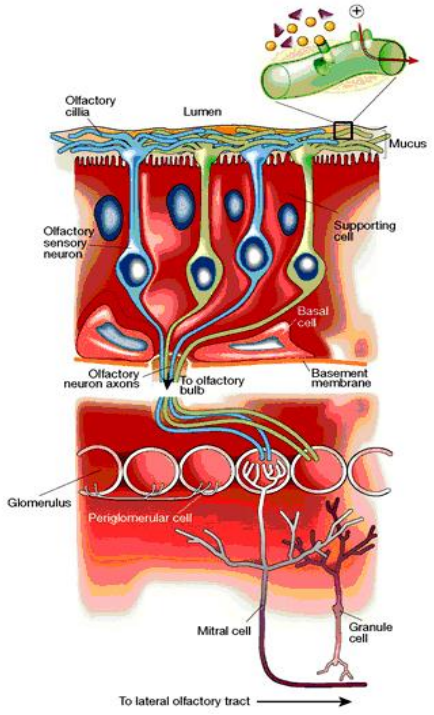

Figure 2.2-3: The olfactory epithelium and the olfactory bulb. *University of Colorado at Boulder*

2.2.2 Olfactory pathways

In the glomerulus of the olfactory bulb, the axons of the olfactory receptor neurons transmit the signals to mitral and tufted cells. The axons of mitral cells form a bundle, the lateral olfactory tract, which projects to the olfactory cortex. The olfactory cortex is divided into five main areas: 1) the anterior olfactory nuclei, which connect the two olfactory bulbs through a

portion of the anterior commissure; 2) the olfactory tubercle; 3) the piriform cortex; 4) parts of the entorhinal cortex; and 5) portions of the amygdala. The major target of the olfactory tract is the piriform cortex, which is located in the ventromedial section of the temporal lobe near the optic chiasm. Information is relayed from the last four areas to the orbitofrontal cortex via the thalamus. However, the olfactory cortex has direct contact with the frontal cortex. Moreover, the amygdala transmits olfactory information to the hypothalamus; and the entorhinal cortex transmits information to the hippocampus[23-25, 59]. The olfactory pathway is the only sensory system, which does not have synaptic relay in the thalamus (figure 2.2-4).

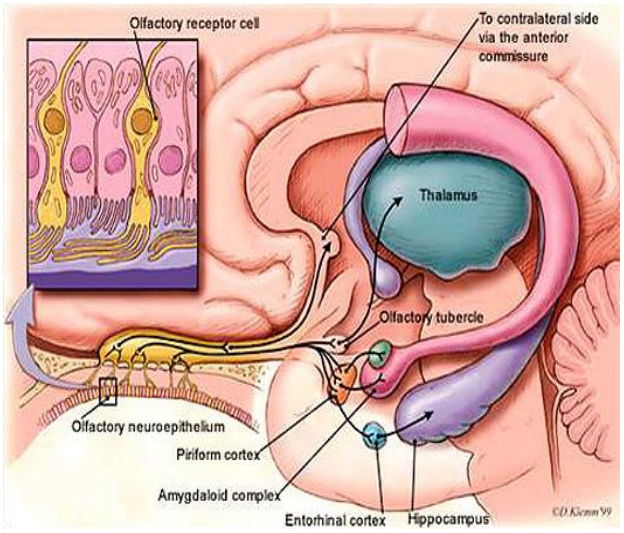

Figure 2.2-4: The olfactory pathways. *David Klemm 2000*

2.2.3 Transduction Mechanism

When odorant molecules reach the mucus layer, they bind to the special protein molecules of the receptors in the cilia. An odorant molecule combines with a receptor molecule just like a key fits in a lock, the right key for the right lock. This activates an odorant-specific G-protein (guanine nucleotide-binding protein) – G_{olf}, which combines with a molecule of GTP and displaces GDP. G protein α subunit dissociates from the receptor protein

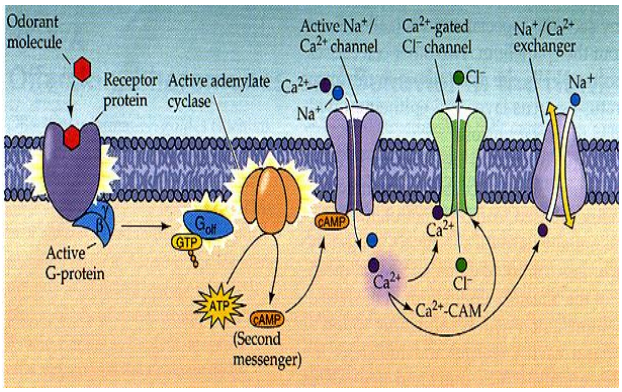

Figure 2.2-5: Olfactory transduction. *Menini 1999*

and activates the enzyme adenylate cyclase (ATCase). The activated ATCase then converts adenosine triphosphate (ATP) to cyclic adenosine monophosphate (cAMP), the second messenger. cAMP then binds to the cation sensitive channel, which opens up and permits calcium (Ca^{++}) and sodium (Na^{+}) ions to flow into the cilia[22, 25, 55, 61]. This creates an inward-directed Ca^{++} current, which causes a depolarization in the membrane. Moreover, the influx of Ca^{++} opens up calcium gated chlorine (Cl^{-}) channels. Cl^{-} flows out of the cells resulting in further depolarization. This triggers a train of action potentials across the membrane. This spatial pattern of action potentials is carried into the brain by an array of axons – glomeruli, periglomerular cells, mitral and tufted cells, granule cells – constituting the olfactory nerve. When cAMP is broken down by specific phosphodiesterases (PDE) to reduce its concentration, the magnitude of the receptor potential is reduced. At the same moment, Ca^{++} combines with calmodulin (Ca^{++} - CAM) and binds to the channel, reducing its affinity for cAMP. Then Ca^{++} is extruded through the Ca^{++}/Na^{+} exchange pathway[22-25, 61] (figure 2.2-5).

There is another transduction path in which the G protein dissociates from the receptor protein and activates phospholipase C, which generates IP_3 – the second messenger. IP_3 activates and opens the Ca^{++} channels, causing a depolarization. The influx of Ca^{++} opens up the calcium gated chlorine channels, which makes the membrane further depolarize[22-25].

There are at least 350 types of receptor molecules in the cilia, and they are unevenly distributed in the mucosa. Therefore, different odors elicit different spatial patterns of neural activity in the mucosa[23, 55, 62].

2.3 A Brief History of the Olfactometer

Many of the olfactometry systems were developed from the 19th to the mid-20th century in Europe. Gabriel Valentin (1810-1883) described a static olfactometry in 1848, which was

based on the evaporation of odorants in vessels presented in a single dilution step. This was the first reported apparatus to study olfaction in 1850. The procedure of his apparatus was a measured amount of a particular substance sealed in a small, thin-walled glass tube; then it was put inside a larger, thick-walled tube and corked. When the smaller tube broke, the larger container would fill with a known volume and a known quantity of odorous material. Several similar modifications of this procedure were followed by Berthelot, Passy, Hans Henning, Fischer and Penzoldt.

Not until 1887, was the first olfactometer constructed by Dutch physiologist Hendrik Zwaardemaker (10 May 1857, Haarlem – September 19, 1930, Utrecht) while he was working at the College of Veterinary Medicine in Utrecht to measure olfactory thresholds. He believed that smell should be related to vision, which should follow the laws of mixture and adaption. He constructed the first draw-tube olfactometer to study olfactory perception of the sense of smell[7, 63-67] (figure 2.3-1). He placed the stimulus material in an enclosed long, hollow tube, with one end sealed. Holes were made on the inner surface. This tube slid over a glass tube, which was opened on both ends. This glass tube led through a screen to the subject's nose. When the inner tube was less and less covered by the outer tube, more and more of the holes of the inner surface were exposed. This allowed a greater amount of the odor to escape into the glass tube and be delivered to the subject's nose when the subject sniffed. His olfactometer first appeared in the British Medical Journal in 1888.

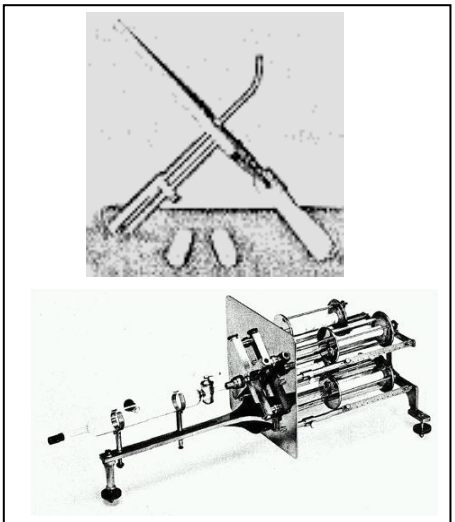

Figure 2.3-1: An illustration of Zwaardemaker's olfactometer (top). Bottom picture shows the modified Zwaardemaker olfactometer, *The Netherlands, 1886.*

Hofmann and Kohlrausch stored saturated fumes over mercury in a tube and mixed them with air in a graduated cylinder. This diluted air was then blown under low pressure through nosepieces into the nostrils. Savelieff's method was connecting two flasks with glass tubing, placing odorous liquid in one flask and allowing it to diffuse into the other, to which a nosepiece was attached. Specific quantities of water were added to accomplish the dilution of the contents in the first flask. Ónodi soaked a ball of cotton in one of the odor concentrations that he had prepared. Then the ball of cotton was attached to the stopper of a bottle, which had another opening. The odor on the cotton diffused through the bottle when a subject sniffed at the second opening. Grazzi's method was a bit different. He used a strip of filter paper, which was soaked in a substance dissolved in alcohol as the odorant source. When the filter paper was dry, the alcohol odor would disappear. Only the substance odor would remain on the paper. Then this paper was hung in a small-enclosed pasteboard box, with a hole in the top. A paper funnel was fit into the hole. The subject sniffed at the open funnel to detect the odor[68].

Not until Sternberg and von Rothe, was a pump used to deliver the odorous air into the subject's nostrils. Sternberg placed his desired concentration substance in a flask, which had a pump attached at the neck. This mixture was then blown into the subject's nose. Von Rothe's method was slightly different. He soaked a piece of filter paper in a desired concentration of an odorous liquid, and hung the filter paper in a wide glass tube. Air was blown by a pump through the paper and into the subject's nostrils[69].

Henry, a French scientist, interested in the perfume industry, created an olfactometer, which was modified from Zwaardemaker's method, in 1890. His modification consisted of using an odorous cylinder, which was a porous hollow paper cylinder with the bottom closed. The cylinder was saturated with the fumes of an odorous liquid from a surrounding glass reservoir.

The subject would inhale from the glass inhaling-tube, which entered from the top, and would be raised with a uniform movement during inspiration. The intensity of the stimulus was determined by the exposed surface of the paper cylinder and the time it took for the odorous vapor to be diffused into the paper cylinder, from the lifting of the inhaling tube[70].

In 1893, Dr. N. Savelieff built an olfactometer in the laboratory of Morokschowetz, which was different in principle from Zwarrdemaker's olfactometer. He used two flasks of glass, each of which had two corks. The two flasks were connected by a glass tube bent into a U-shape, and each end of the U-shaped tube went through a cork in each flask. One flask's cork was inserted into a glass tube, which reached the bottom, into which a liquid mixture (usually ethereal oil) and water would be poured and would not reach the connecting tube. The cork of the second flask, which would fill only with air, was inserted with a glass inhaling-tube, which divided into two nose-pieces for the nostrils. The subject would inhale on this side while water would be added to the liquid mixture to vary the intensity of the stimulus, which would be measured[70].

Little work had been done until the late 1970s and 1980s, when air-dilution olfactometry was being investigated more closely. All this progress in the development of olfactometers is the foundation of present-day olfactometers. In recent decades, different equipment (olfactometers) has been created to evaluate the odor of air pollution in buildings, from industrial processes, ill-smelling bodies of water, and other sources. Most of these olfactometers are based on two main principles – gas or liquid

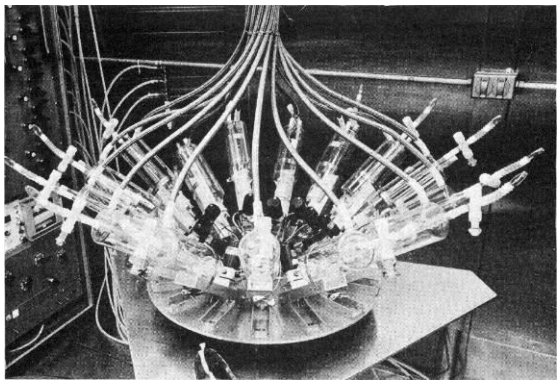

Figure 2.3-2: A ten-stage dynamic air-dilution olfactometer. *Doty et al. 1988a*

phases. Gases were mixed with a known proportion of non-odorous gases or mixtures, such as nitrogen or clean air. There are two exposure systems to which subjects may be exposed – target odors (gas or liquid), static or dynamic. In static exposure, the target odor is stationary. The subject's inhalation creates movements and exposes the target odor; this involves using a closed vessel or container. Dynamic exposure requires a continuous flow of gas to expose the target odor to the subject, similar to Sternberg's and von Rothe's olfactometers.

The air-dilution olfactometer provides a continuous flow of control odorant concentration, and a change of the relative volume flow of clean and odor-saturated air. In the 1980s, the University of Pennsylvania, under the direction of Richard L. Doty, developed a ten-stage dynamic air-dilution olfactometer, which had a rotating stimulus-sampling table (figure 2.3-2).

The air-dilution olfactometer offers the most precise measurement of psychophysical and electro-cortical responses today, but it is not used in a clinical routine. In recent years, computerized olfactometry has also been used. It provides versatility and precision of the stimulus presentation and data collection, but it is very expensive. Therefore, it is restricted to specialized centers only[71].

Chapter 3

Guide to Goals, Methods and Results

The purpose of this research project is to build an MR compatible olfactometer. It is not only for research laboratory use; but also suitable for a clinical environment. Several goals need to be reached to build such an olfactometer. The following table indicates the goals and the chapters associate with the testing the methods and their results. One can follow the table to locate the chapter for his/her interest.

Goals	**Methods and Results**
Build an MR compatible olfactometer	Chapter 4
Build a UV apparatus to test the olfactometer	Chapter 6.1
Develop software for performing and recording the experiments	Chapter 6.3
Determine the time response of each duration pulse and compare it with the actual durations	Chapter 6.4 and 7.1
Determine the rise time and fall time of the olfactometer	Chapter 6.4 and 7.1
Determine the shortest possible duration for the olfactometer	Chapter 7.2
Compare the air dilution method and the fix concentration method	Chapter 7.3
Use different flow rates to compare their delay time	chapter 6.4 and 7.4
Use different tube lengths to compare their delay time and investigate the delay time without any tubing	Chapter 6.4 and 7.5
Test the olfactometer's durability	Chapter 6.4 and 7.6
Develop protocol for human testing	Chapter 5.2
Determine stimuli for human obsessive-compulsive disorder research	Chapter 8.1 and 8.2

Determine the best acquisition method for the obsessive-compulsive disorder research	Chapter 9 and 11.2

Chapter 4

Constructing the Olfactometer

The custom-built magnetic resonance (MR) compatible olfactometer is based on the principles of air dilution olfactometry[33, 64, 72-75]. The olfactometer is composed of three main components – a controlled solenoid valves unit, a signal control unit and a Windows based laptop computer (figure 4-1and 4-2). It also consists of an air compressor and a vacuum pump (figure 4-3).

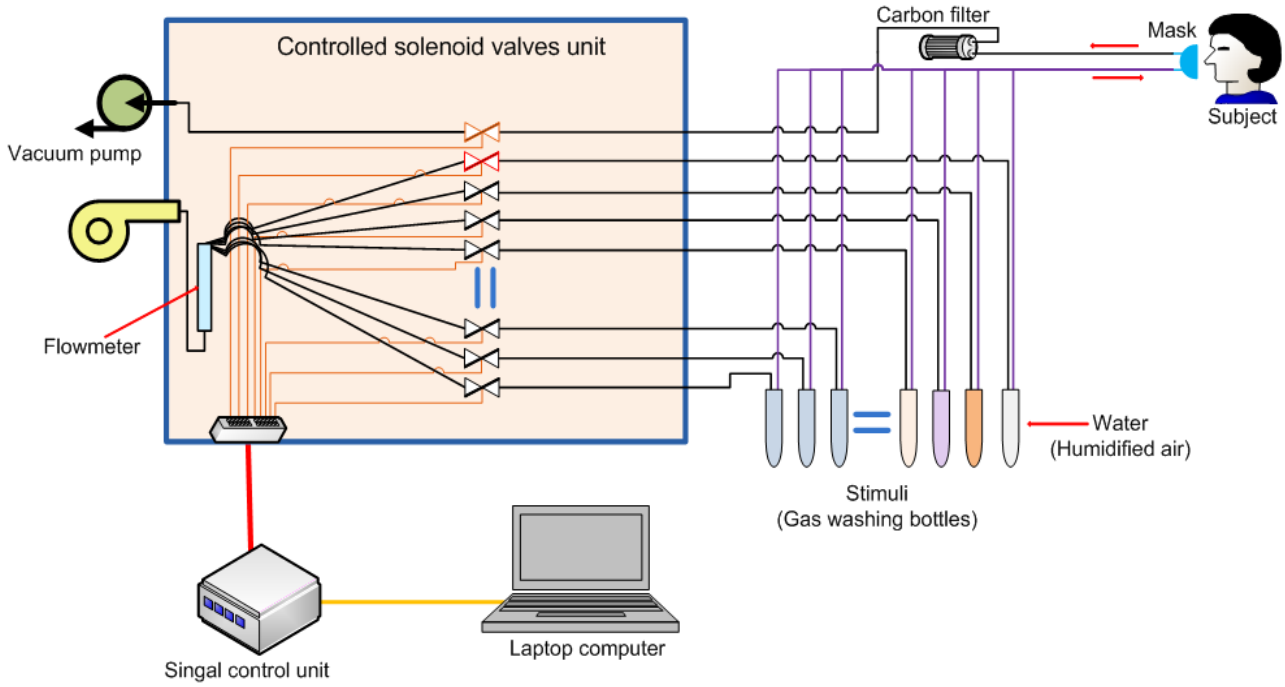

Figure 4-1: Simplified schematic of the olfactometer.

By using a laptop, one has the ability to transfer the system to different scanning rooms and storage is easy. The olfactometer is controlled by a laptop computer with a Windows based operating system, started with Windows XP Professional version and currently upgraded to Windows 7 Professional version. The special control interface program is written in the LabVIEW (started with version 7.1 and currently using version 2010) program, which is a graphical programming language from National Instruments (Austin, Texas). The interface of the

control program is easy for anyone to operate. Changes can be made to any input values for different protocols, such as different 'On' and 'Off' time boxcar paradigms, or pulse sequences. This interactive graphic program can switch between the odor and non-odor phase, which is pure air without any contamination by other odorants. Also, this switching between pure air and odorants does not cause any changes in the airflow. It can also indicate the status of the procedure on the computer screen. Moreover, it controls the time of the odor presentation with or without any delay. The control program passes the information through a USB connection to the signal control unit (NI USB-6221 Multifunction Data Acquisition unit, National Instruments, Austin, Texas), which is a multifunction I/O data acquisition device and has 16 analog inputs, 2 analog outputs, 24 digital I/O and 32-bit counters, from the laptop computer. Previously a NI DAQCard-6024E PCMCIA card (Personal Computer Memory Card International Association or PC card, National Instruments, Austin, Texas) was used. It has 16 single-ended analog inputs, two 12-bit analog outputs, 8 digital I/O (input/output) lines and 20 MHz counter/timers. It is connected to the SCB-68 terminal block, a shielded I/O connector block for interfacing I/O signals. The SHC68-68-EPM cable (National Instruments) connects the DAQ device with the

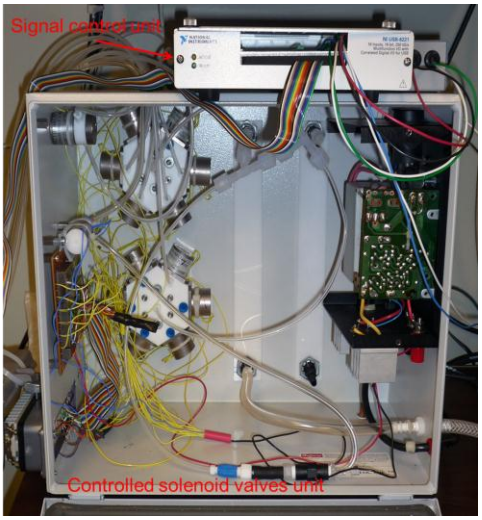

Figure 4-2: Inside view of the solenoid valves unit.

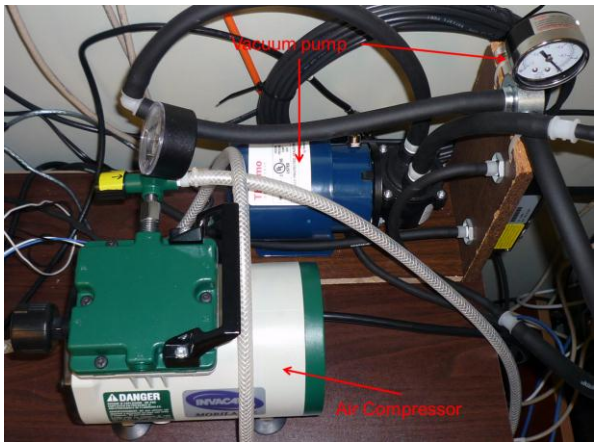

Figure 4-3: Air compressor and vacuum pump.

terminal block. The reasons to change to the USB connection are: 1) most of the new hardware uses USB connections, 2) National Instruments offers limited support of the PCMCIA connection, and 3) the maximum length of the SHC68-68-EPM cable is 2 meters; it may restrict the mobility of locating the control computer. Sometimes the waveguide, where all the tubing goes through to reach the scanning table, may not be next to the MR control panel. One does not want to increase the length of the tubing; it will increase the delay time when keeping the same flow rate. The USB connection can give the possibility of increasing distance of the connection between the control computer and the signal control unit without changing the length of the tubing.

The controlled solenoid valves unit, which is a 8 x 14 x 12 inches (depth, width and height) metal casing, contains 6-12 computer-controlled solenoid valves (Manifold Mixing Solenoid Valves, Cole-Parmer Instrument Co., Vernon Hills, IL) (figure 4-4) that provide multiple odor stimuli. Independent solenoid valves provide a constant airflow and a vacuum airway. These valves are open when not activated. The solenoid valves are operated with 12V DC (direct current), which lowers the cost of the olfactometer. A rectifier was built in the valves unit to convert the AC (alternating current) to the DC voltage to operate the solenoid valves. The stimuli solenoid valves are installed in two groups – 6 solenoid valves in each group. Each valve has its individual tubing for connecting to the air-washing bottle. A set of 6-solenoid valves was shown in figure 3-4 to illustrate the setting of the valves unit. For controlling our olfactometer, NI USB-6221 is used. This unit can provide 24

Figure 4-4: Manifold mixing solenoid valves.

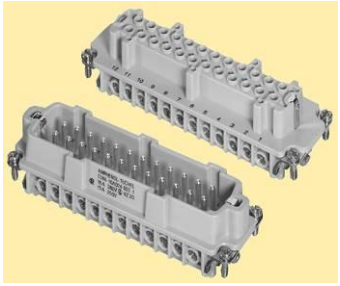

Figure 4-5: Heavy duty connectors C146.

digital I/O lines. If one wants to use more than all 12-output lines, more solenoid valves can be added in the controlled solenoid valves unit. All the valves are connected to a heavy-duty female connector (Amphenol-Tuchel Electronic GmbH, Germany) shown in figure 4-5. It secures the connections and provides extra ports for future expansion. The male connector is connected to the signal control unit (NI USB-6221), and all the solenoid valves are controlled by the computer through the USB connection with the signal control unit.

The continuous medical-graded air is provided by an air compressor device, Mobilaire 50psi Medication Compressor (Invacare Corporation, Elyria, Ohio). Omron NE-C25 CompAir XLT Compressor Nebulizer (Omron Healthcare Inc., Vernon Hills, IL) was used at the beginning of the project testing with the nasal cannula (figure 4-6). If nose cannula is use, this compressor will be fine to provide the necessary flow rate to deliver the odorant stimuli. However, if a mask is used, this compressor does not have enough power to supply the flow rate required – the Invacare, Mobilaire Medication Compressor is used. The filtered nebulizer system is mainly for patients who have asthma, *chronic obstructive pulmonary disease* (COPD) or other respiratory conditions. This compact nebulizer design weighs approximately 11 pounds and the dimensions are 8" L x 8" W x 10.5" H. Its weight (with a built in handle) and size offer portability. Its suction cup feet provide stable operation and it has an easy-to-read pressure gauge for adjusting the pressure to the satisfactory flow rate, especially suitable for our project.

Figure 4-6: Omron NE-C25 CompAir XLT Compressor Nebulizer. *Omron*

Figure 4-7: Gas-washing bottle holder (single version) and gas washing bottles.

The pumped air from the nebulizer is filtered with the built in filter, *MMAD (Mass Median Aerodynamic Diameter) approximately 5 microns*, before being delivered to the air outlet. This air is then connected to the controlled solenoid valves unit. The input air pressure is monitored by a flow meter (Gilmont Instruments, Barrington, IL) with a flow rate of 1.5 L/min. Air is then sent to all the solenoid valves via Teflon tubes (Cole-Parmer Instrument Co.), and they are connected to individual gas washing bottles (glass bottle, Fisher Scientific, PA) (figure 4-7). Teflon tubes with an inner diameter of 1/16 inch, an outer diameter of 1/8 inch and 25 feet in length are used since they are made of very low absorbent material (Teflon® Fluorinated Ethylene Propylene). However, when a birhinal nasal cannula (Cardinal Health, MaGaw Park, IL) is used, there will be approximately 4.5 feet of non-Teflon tube attached to the subject. If a SleepNet Phantom Nasal *Continuous Positive Airway Pressure* (CPAP) mask (SleepNet Corporation, Hampton, NH) is used, there is a 5-foot Teflon tube connected to the inlet of the mask. Each solenoid valve has Teflon tubing connected individually. These connections are also color-coded; so each valve can be identified with the stimulus to which it is connected. Each gas-washing bottle, which can hold 20 ml, contains a different odorant stimulus; up to 8 stimuli at this moment and can be upgraded to 12 stimuli if necessary. A separate gas-washing bottle contains distilled water for constant airflow. When the control interface program is on, air will flow through a tube on the vinyl stopper into the gas-washing bottle. The odorant stimulus then passes through the other tube of the vinyl stopper (Cole-Parmer Instrument Co.) and into a mask (or a nasal cannula if preferred), which will be placed near the subject's nostrils or over the nose (figure 4-8). A special holder is made to hold 4 gas-washing bottles, and it can be expanded as desired (figure 4-7). The final version of the holder for this olfactometer can hold 10 gas-washing bottles (figure 4-9). It is easy to change or replace a certain odorant stimulus in the

holder. The connectors for the tubing to the gas-washing bottles are color-coded. Stimuli can be pre-assigned to a color to minimize misconnecting the stimuli to their connecting valves (shown in figure 4-9).

Since the mask (or the nasal cannula) and the gas-washing bottle are non-metallic materials, they are safe to be used inside the scanner. The gas-washing bottles will be placed as close as possible to the subject and are outside the scanner to minimize any delay in delivering the stimuli. Velcro strips are used to secure the bottle holder on a non-magnetic intravenous (IV) stand. It can be wheeled as close as possible to the magnet without interference to the subject when lying on the sliding platform. All the tubing is extended through a porthole (waveguide) connected to the technician's booth, which is next to the MRI scanning room. The olfactometer is located outside the scanning room, since the magnetic environment of the scanning room hinders the use of electronic devices.

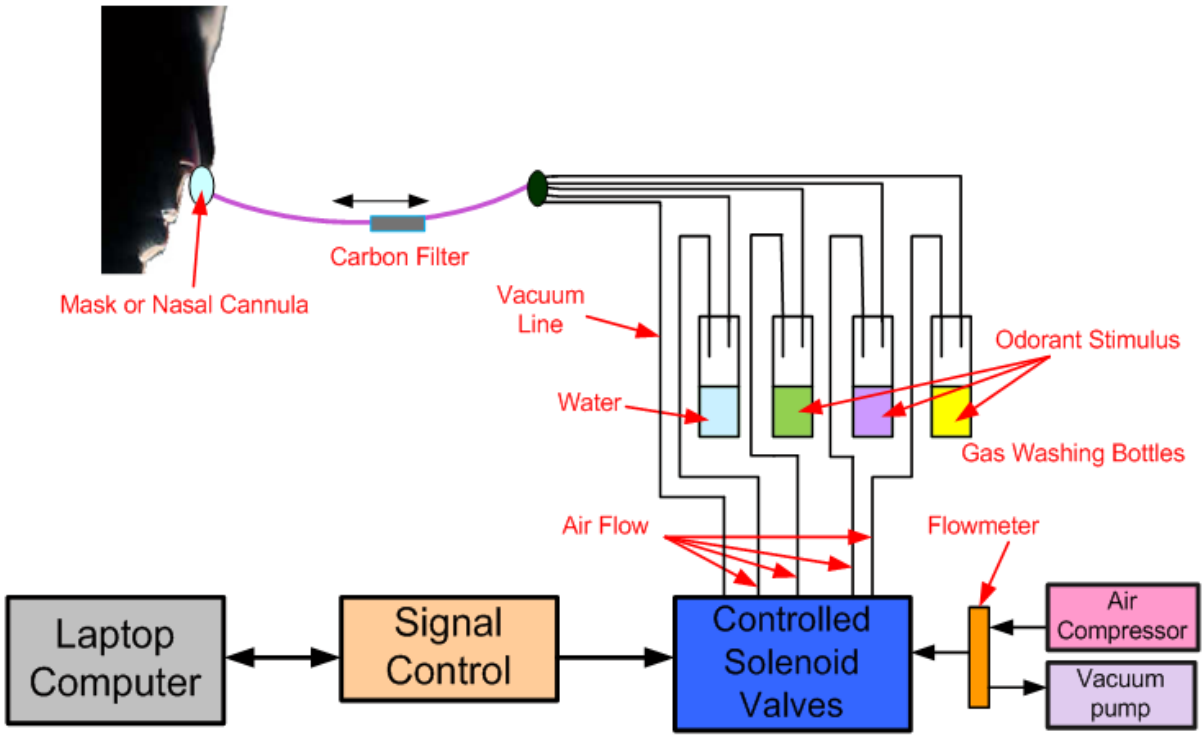

Figure 4-8: Schematic of how olfactometer works.

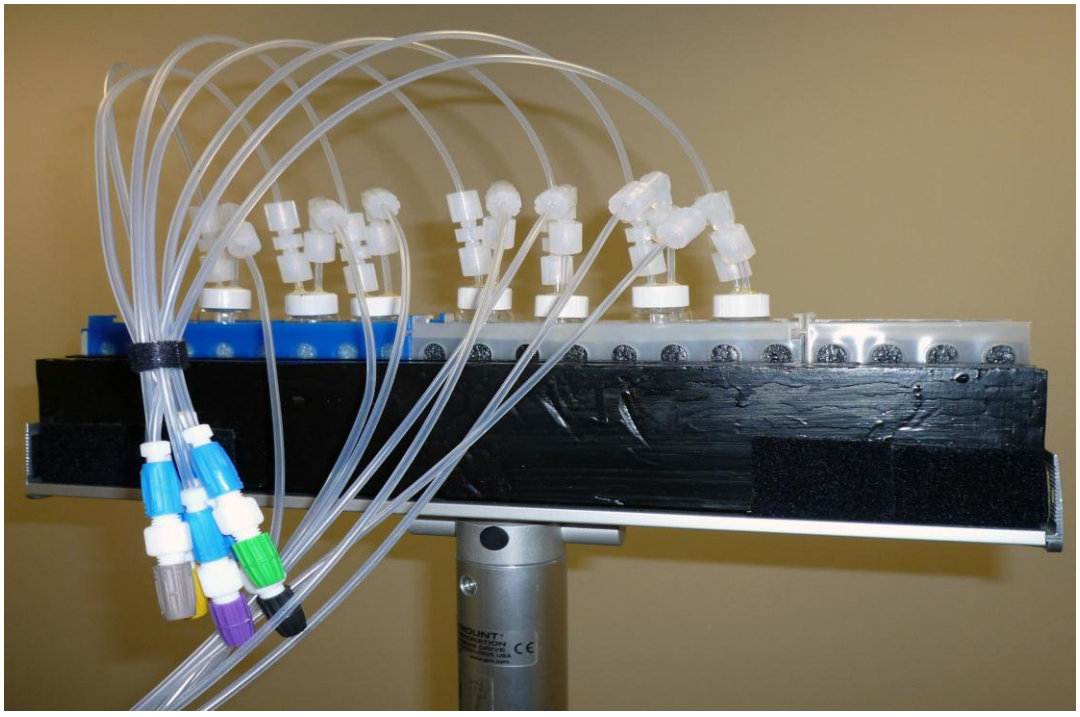

Figure 4-9: Final version of the gas-washing bottle holder. It can hold up to10 bottles.

Chapter 5

Software and Protocols for the Olfactometer

5.1 Control Software

LabVIEW (Laboratory Virtual Instrument Engineering Workbench) is a programming environment with which one can create programs with graphics – it does not require using text-based languages to create lines of code as traditional programs demand such as C, C++ or Java. It is easier for building a program development and execution system with people who do not have much experience in programming. In our case, it will be easier for researchers/technicians to modify the program (virtual instrument VI) to meet their needs. The control software was first developed with LabVIEW 7.1 version with the PCMCIA card (NI DAQCard 6024E). When the National Instruments signal control box was upgraded to NI USB6221, the LabVIEW software was also upgraded to 2010 version.

5.2 Designing Protocols

Most common protocol for olfactory stimulation is straight forward boxcar protocol, which usually sets the 'ON' time (stimulation period) varying from 6 to 30 seconds and the 'OFF' time (resting period) from 20 seconds to 1 minute[29, 38]. The 'ON' and 'OFF' blocks are fixed and repeated many times as designed during the entire experiment. However, a pulse sequence boxcar protocol has recently been used, which was suggested to further avoid olfactory habituation[76] (figure 5.2-1). There is a 6-pulse sequence in a block. Inside the block, the 'ON' time is short (usually 1 to 2 seconds) and there is a short 'OFF' time between each pulse of 6

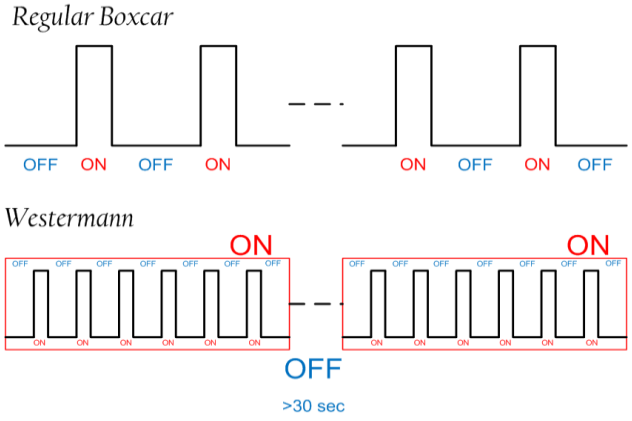

Figure 5.2-1: The regular boxcar protocol and pulse sequence protocol suggested by Westermann et al. 2008.

seconds. In this way, the olfactory epithelium will not be exposed to the stimulus continuously for a long period of time, which reduces the adaptation of the stimulus. After each block, there is a much longer time for the olfactory epithelium to rest (typically greater than 30 seconds), and then it will be ready for the next block of odorant stimulation. However, if the 'ON' time is no longer than or equal to 10 seconds, this protocol is not much different than a standard boxcar protocol when the 'OFF' time is much longer than the 'ON' time. Usually habituation starts when there is continuous stimulation of about 15 seconds (personal interview with Dr. Doty, March 2010).

The control interface program (virtual instrument – VI) for this project is written in LabVIEW 7.1 & 2010. Several different protocols were written for further testing. Besides the standard boxcar protocol VI, another was written based on Westermann's pulse sequence, which can easily be modified to a regular boxcar protocol. It will accommodate either paradigm that a researcher desires – especially if one desires a longer period of 'ON' time in his/her paradigm. A modified boxcar protocol is also written for the Obsessive-Compulsive Disorder project, which is similar to standard boxcar protocol with addition of jittered (figure 5.2-2). The 'ON' block of the protocol is fixed (with this project it is set at 10 seconds); and the only difference is the time of each 'OFF' block, which is varied between 30 to 45 seconds. Since there are six olfactory stimuli for this project, there will be six 'ON' blocks in the protocol – each stimulus only appears once. Four different protocols are created with randomized orders of the stimuli. Each 'OFF' block time is also randomized (except the first one which is fixed at 30

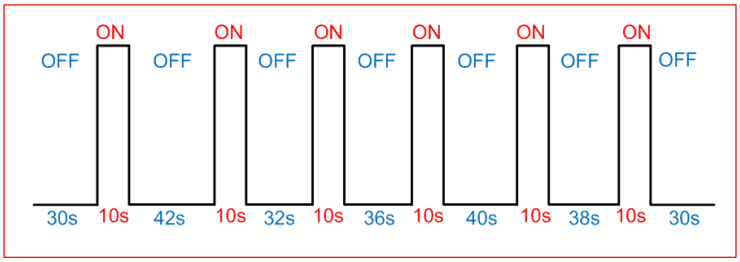

Figure 5.2-2: Example of the modified boxcar protocol.

seconds). In this case, the subject will not create a thought of anticipation for the next stimulus, which will activate areas in the brain that are not related to olfactory stimulation. The VI's interface is designed as simply as possible to minimize inputting parameter errors.

5.3 Self Triggering Vis

The software program to control the solenoid is written in LabVIEW; and the signal control box (NI USB6221) is from National Instruments, Texas. One wants the program synchronized with the scanner, so the start time of the program will be exactly at the time the scanner acquires the images.

When running the control program with the scanner for an experiment, one has to trigger both the scanner and the control software simultaneously to synchronize them to begin each MR scan. Generally speaking, it is not a big concern of creating too long of a delay. However, it is easier for the technician to just press/click on one button, which will avoid any distraction or causing an unnecessary delay.

The MR scanner, which is used for testing the olfactometer, is Gemini 3T (Philips, Netherlands). The default of the triggering pulse width from the scanner is 50 microseconds. It is too short a duration for the LabVIEW program to capture/acquire this signal. Therefore, this signal needs to be extended so that the LabVIEW can acquire this trigger pulse for self-triggering. A monostable circuit was built to extend the pulse width. However, the monostable circuit inverted the input signal – positive pulse becomes negative pulse. Therefore, the input signal must be inverted before being sent to the monostable circuit to maintain the correct output (figure 5.3-1).

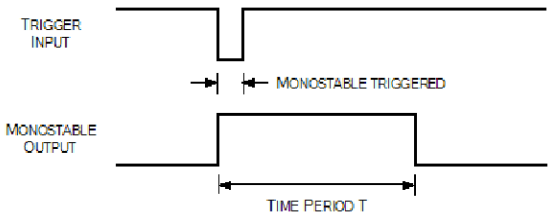

Figure 5.3-1: Trigger input and output of the monostable.

The modified monostable circuit consists of a 555 timer integrated circuit (IC) and a 7404 hex inverter integrated circuit (figure 5.3-2). A 555 timer IC is the most common component in electronic timers of school projects. It is very stable, relatively inexpensive and reliable. This IC was designed by Hans R. Camenzind in 1970. In 1971, Signetics Corporation (was once a major player in semiconductor manufacturing and later acquired by Philips) introduced the 555 Timer IC to the market. After 40 years, the regular type is still available, even though there have been many improvements and variations in its circuitry[77]. The schematic of the modified monostable circuit for self-triggering VI is shown in figure 5.3-3.

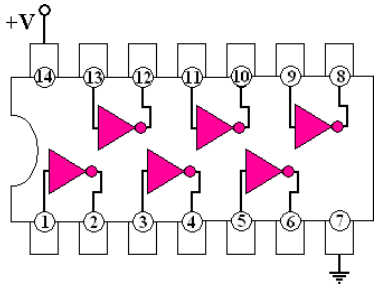

Figure 5.3-2: Layout of the 6 inverters in the 7404 IC.

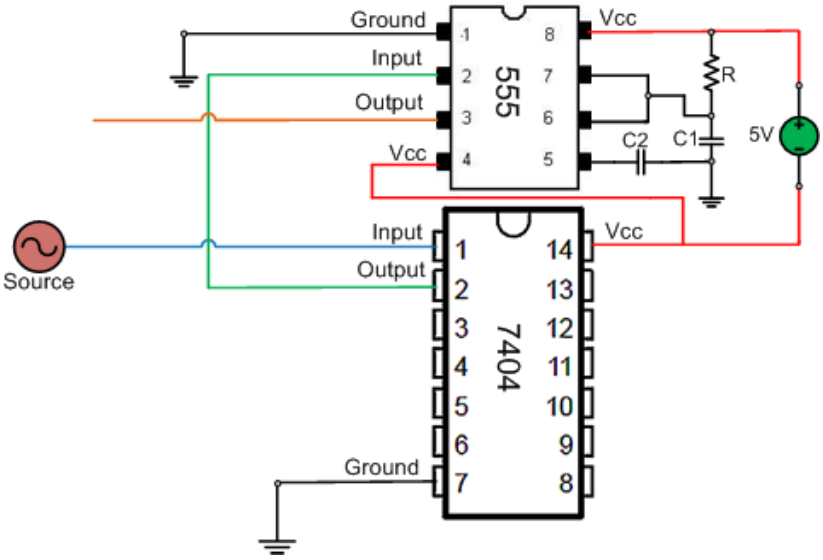

Figure 5.3-3: The schematic of the modified monostable circuit for the self-triggering VI.

A BNC cable is connected to one side of the monostable circuit box. The other side of the circuit box is connected to one of the digital lines of a digital port in the USB-6221 box, which

also provides a 5V source to power the monostable circuit. Then the USB-6221 box is connected to the laptop computer with a USB cable (figure 5.3-4).

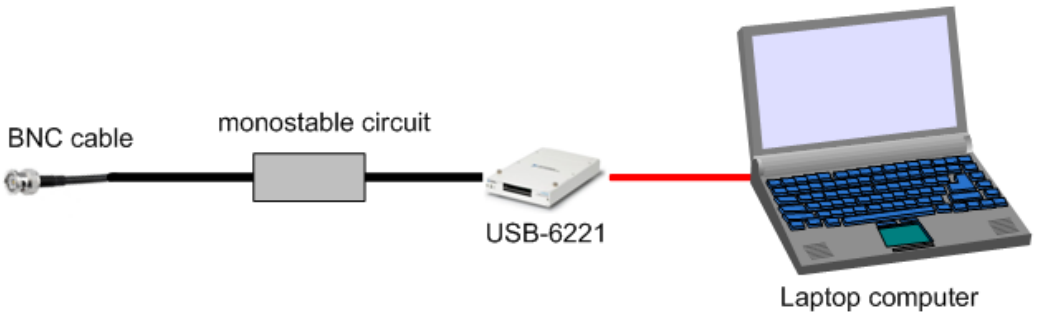

Figure 5.3-4: The connections of the trigger source to the laptop computer.

By consulting with the Philips engineers, the MR trigger pulse width actually can be adjusted between 50 microseconds to 5 milliseconds. However, the Philips engineer suggested that the trigger pulse should not adjust higher than 2 milliseconds. Otherwise, the scan time will increase and the images will be divided into two packages. It will affect other projects that perform their studies with the scanner. Therefore, we have to use the monostable circuit to increase the pulse width to reach our goal.

Chapter 6

Methods of Testing the Olfactometer

To test the characteristic of temporal dynamics of the olfactometer, a UV (ultraviolet light) apparatus was built similar to Johnson et al. 2003, which was based on the principles of ultraviolet light spectroscopy.

6.1 The UV test apparatus

An apparatus was built to determine the temporal resolution of the custom-built olfactometer in this study. It was built with the method similar to Johnson et al., 2003[78] (figure 6.1-1). Under the principles of ultraviolet (UV) light spectroscopy, techniques employ the interaction of electromagnetic radiation with matter. Instead of using an Hg(Ar) (Mercury and Argon) lamp as the light source, an ultraviolet light-emitting diode (UV LED) (Sensor Electronic Technology Inc., Columbia, South Carolina), with peak wavelength of 255 nm ± 5 nm, was chosen because of low heat generated and a longer life span. A quartz tube (Quartz Scientific Inc., Fairport Harbor Ohio) is placed between the UV LED (light source) and the UV-sensitive detector (silicon photodiode), with a spectral sensitivity range from 220 to 360 nm and maximum at 280 nm (Boston Electronics Corporation, Brookline, Massachusetts) (figure 6.1-2). A quartz tube must be used, because most regular glass tubes will absorb the shorter UV wavelength (320 nm and below) – in this study UV-C wavelength (190 nm to 280 nm) is used. The quartz tube, which is 8 mm in outer diameter (6 mm inner diameter) and 101.6 mm long, has

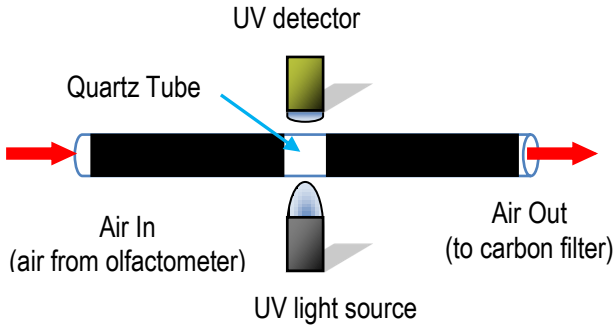

Figure 6.1-1: A schematic of the ultraviolet apparatus – similar to Johnson et al., 2003

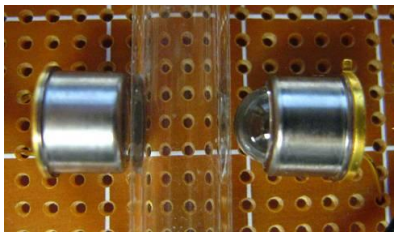

Figure 6.1-2: UV LED and detector with the quartz tube in between.

a high UV transmittance rate. About 75 % ± 2 % of the UV wavelength can be transmitted through it. Acetone (Sigma-Aldrich) is used as a UV absorber rather than ethyl acetate, which is one of the most commonly used solvents, because ethyl acetate absorbs in the wavelength range of 200 to 235 nm (figure 6.1-3). It is difficult to find a UV LED as a light source in this range and it will be extremely expensive if it is on the market. However, the acetone has a wider wavelength range of the electromagnetic energy spectrum and it is not that expensive and one can easily find a UV LED at this range as a light source.

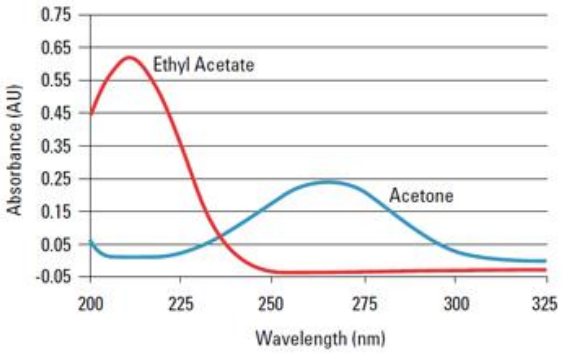

Figure 6.1-3: UV spectra of acetone and ethyl acetate. *Teledyne Tech. Co.*

This apparatus is then connected to the olfactometer with the same length and diameter tubing to the subject, including the nasal cannula/ mask's length. This tubing is then connected to one end of the quartz tube (air in). Another shorter length tube (approximate 3 feet) with the same diameter is attached to the other end of the quartz tube (air out). The other end of the shorter tube is connected to a carbon filter (Bickford Inc., New York) to absorb the exiting acetone.

6.2 Characterize the temporal dynamics of the olfactometer

The UV LED light source is powered by 6.5 volts and supplied by a DC power supply (BK Precision, Yorba Linda, CA). When the light source is turned on, it generates UV energy. This energy is transmitted through the quartz tube and activates the UV-sensitive detector. The voltage measured with a multimeter (Fluke 8060A multimeter, Fluke Corporation, Washington) from the UV-sensitive detector is approximately 2.3 V. When the olfactometer air flows through

the quartz tube, which is triggered by the LabVIEW software, the UV energy will be attenuated by any acetone in the air stream. Acetone absorbs the UV energy; this attenuation of the energy can be measured by the UV-sensitive detector as the voltage drops. Since this attenuation is very small (approximately a few millivolts [mV]), it is easier to display the output signal with a LabVIEW program rather than an oscilloscope. If an oscilloscope is used to display this signal, the output from the UV detector needs to be amplified before being displayed. However, the output measurements do not need to be amplified with the LabVIEW software, which is sensitive enough to detect the signal. No amplification is required before data is recorded and displayed. The displayed signals can be easily reproduced with a LabVIEW or other desired program from the recorded data for later analysis. Due to the low energy attenuation, the measured output can be noisy. When an oscilloscope is being used, not only the output signal needs to be amplified; it also needs to filter out the noise. The filter can be easily integrated into the LabVIEW program, and the output signal can directly be channeled into the SCB-68 terminal block and can be displayed on the computer screen without extra wiring.

6.3 Developing a virtual instrument (VI) for acquiring data

Since there is a limitation of the NI DAQCard-6024E, it cannot send out signals from the digital outputs and have an analog data acquisition at the same time. For the testing purpose, another VI (virtual instrument) was developed to acquire the analog signal from the UV apparatus circuit. A NI PCI-6221 pc card was installed in a desktop computer to execute this LabVIEW program. Also, another SCB-68 connector block and the SHC68-68-EPM cable are used.

The raw signal was very noisy (figure 6.3-1). A smoothing filter, called low-pass filter, was added in the VI to filter out the noise. Different moving averages (half-width) were tested. A moving average is commonly used to smooth out the fluctuations. The acetone air stream was then generated by the olfactometer, and the numbers of the moving averages were tested with the fluctuation signal, which was measured from the UV detector. When the moving averages were set to 15 or 31, some of the noise still could be seen at the edges of the signal. However, when the moving averages were set to 51 and 71, the noise was significantly reduced (figure 6.3-1). Even higher numbers were tried with no significant improvement and the setting at 71 achieved the maximum result. The moving average was then set to 71 for all the tests.

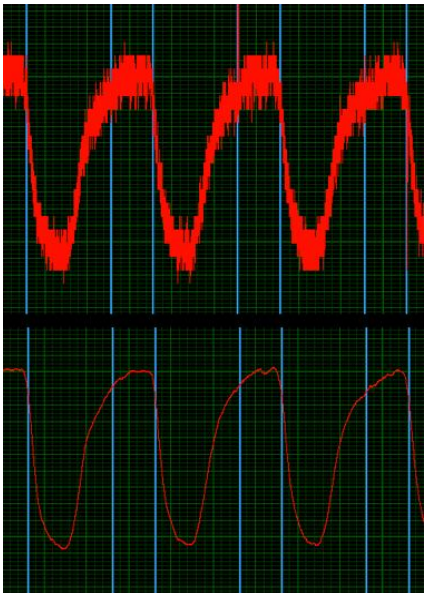

Figure 6.3-1: Only the original and the moving average of 71 signals are shown here.

The voltage changes in the UV detector with the acetone passing through was too small to see (in mV range) in the same graph with the boxcar protocol (trigger pulse), which was measured from the control valves VI and was shown only as a straight line. Therefore, signals were displayed in two different panels – one was the close-up of the UV voltage changes and the other was the triggering voltage and the UV voltage (figure 6.3-2). The sampling rate was set at 1 kHz, which National Instruments recommended to use. With this VI, the acquired sampling data is recorded in a regular “dat” extension data file and “lvm” extension LabVIEW file, which can be reproduced with a LabVIEW program as the screen display or other desired program for later data analysis. The display data could be inverted for the purpose of looking at the rise/fall time of the impulse.

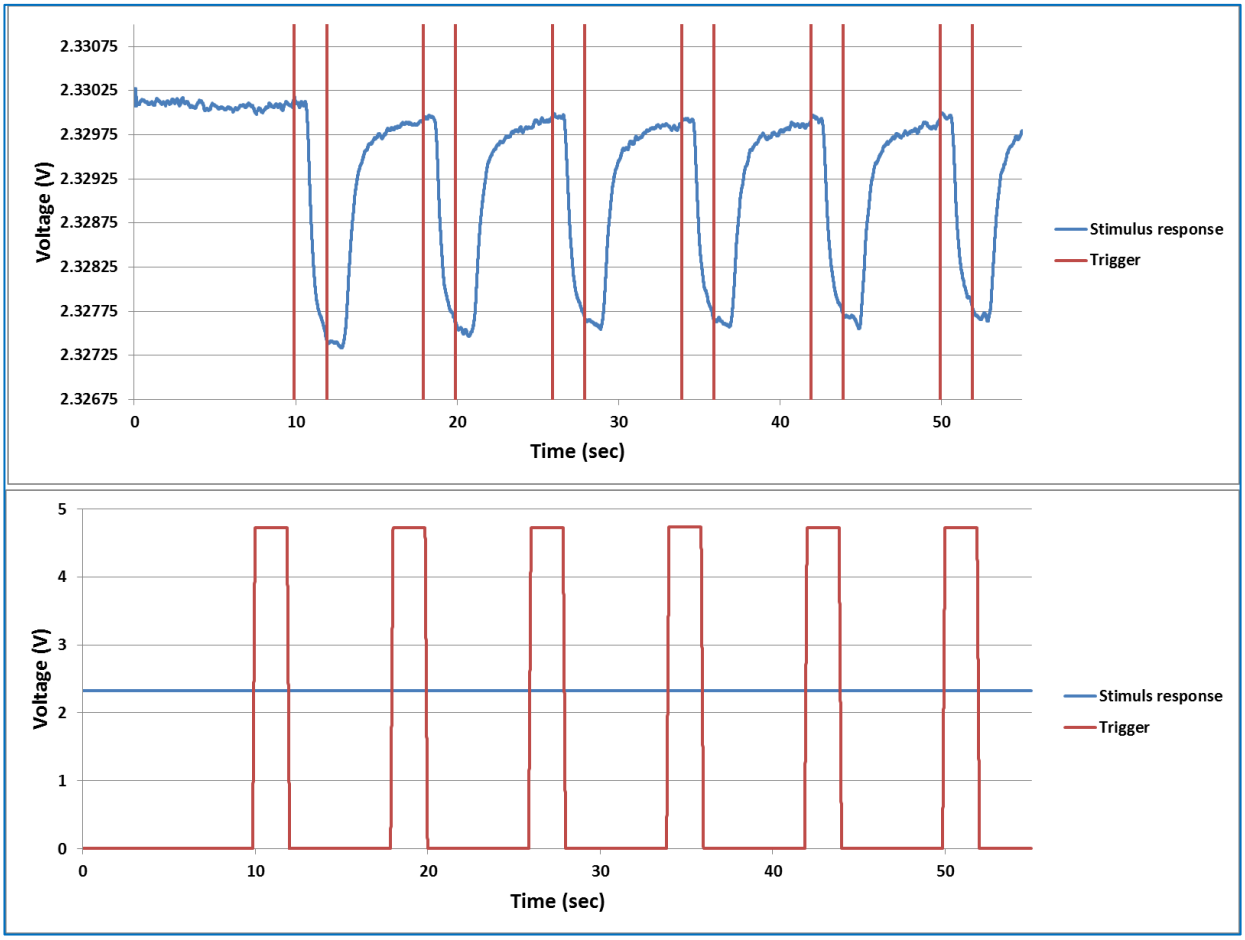

Figure 6.3-2: Dual displays showing the LabVIEW VI acquired data.

6.4 Testing methods

Pentyl acetate, linalyl acetate and acetone were used as the testing odorant. Each was prepared with a volume of 5 ml and was poured in a gas-washing bottle individually, which would be the standard volume for all the tests. Five bottles of linalyl acetate and acetone were mixed. Each bottle containing 5 ml in volume of the mixture was prepared with different concentrations of the acetone – 0%, 25%, 50%, 75% and 100%.

Impulse response and the characteristic of the olfactometer would be tested with different durations of the pulse, such as 0.1, 0.5, 1, 2, 4, 8, 10 and 20 seconds. Through these tests, the rise/fall time of the olfactometer (protocol triggered impulse) and the delay time of the

olfactometer (stimulus being delivered) were examined. Only acetone was used in these tests. The length of the Teflon tube would be the full tubing length of 25 feet.

Different 'ON' times of the pulse sequence were set from 0.25, 0.5, 1, 2, 3, 4 to 6 seconds to test the shortest possible presentation time ('ON' time) and rest time ('OFF' time) combination that could be used. The 'OFF' time was also set from 1, 2, 4, 6 to 8 seconds to test how long it would take to recover its original or closest to its original amplitude. The length of the Teflon tube connected to the olfactometer was 25 feet, and the flow rate was set at 1 LPM. Acetone was the testing odorant in these tests.

Three different flow rates, such as 0.25, 0.5, and 1 LPM (liter per minute), were tested for any delay of the delivery of the testing odorants. The 50% mixture of each linalyl acetate and acetone and 100% acetone were used as the testing odorants for these different flow rate tests. The full tubing length of 25 feet was used to connect the olfactometer. Also, four sets of 10 ml of each of the testing odorants (50% of the mixture and 100% of acetone) were prepared. Two 20-minute periods of olfactory stimulation were run with each of the four different flow rates (0.25, 0.5, 0.75 and 1 LPM) and the two testing odorants. The gas-washing bottle of each testing odorant was weighted, before and after each 20-minute period of the stimulation, to determine the concentration of the odorants delivered by these flow rates.

Three different lengths of the Teflon tubes were attached to the olfactometer (full length – 25 ft., 2/3 of the full length – 16 ft. 7 in., and 1/3 of the full length – 8 ft. 4 in.), and the length of the nasal cannula/ mask was kept the same. Also, two different settings of the testing odorants were used – 1) air-dilute combination of either pentyl acetate or linalyl acetate and acetone, 2) mixture of linalyl acetate and acetone in different concentrations. Through these tests, any

changes in the delay time of the delivery of the stimulus would be investigated. The flow rate was set at 1 LPM.

The olfactometer ran for a long period (approximate 30 minutes) to test its stability; the 'ON' time was set at 8 seconds and the 'Off' time was set to 30 seconds. Only acetone was used in the above tests. The length of the Teflon tube connected to the olfactometer was the full tubing length of 25 feet.

Chapter 7

Test Results of the Olfactometer

During each test, the LabVIEW VI (virtual instrument) recorded and displayed all the measurements of the fluctuating voltage when acetone passed through the quartz tube between the UV light source and detector. Different concentrations of linalyl acetate and acetone were used as a testing odorant because acetone could not be used in actual olfactory stimulation. Linalyl acetate is the olfactory stimulus, which will be used in human olfactory stimulation. This combination mixture will provide some information of the performance of the olfactometer with actual stimulus.

7.1 Results of testing the impulse response of the olfactometer

One of the most important features of any dynamic system is its time response function, which is a description of the accuracy or fidelity of the system in response to control signals. Delivery delay times and accuracy of timing is important for any brain activation study.

For testing the time response and the characteristic of the olfactometer, different durations of pulses were generated by the control VI, which triggered the valves of the olfactometer. The durations were set at 0.1, 0.5, 1, 2, 4, 8, 10 and 20 seconds. There was a 30-second 'OFF' time before and after each pulse. Eight pulses were generated for each duration. The flow rate was set at 1 LPM and the full tubing length of 25 feet was attached to the olfactometer. Pure acetone concentration was used as a testing odorant.

Each trial of duration was taken 1 second before the trigger pulse, the time of the trigger pulse and 5 seconds afterwards from the collected data. The first trial from the data set was excluded, which usually created a larger drop in the voltage compared to the others. Then the average of the seven trials was calculated (figure 7.1-1). All results are shown in figure 7.1-2 as the durations listed above respectively.

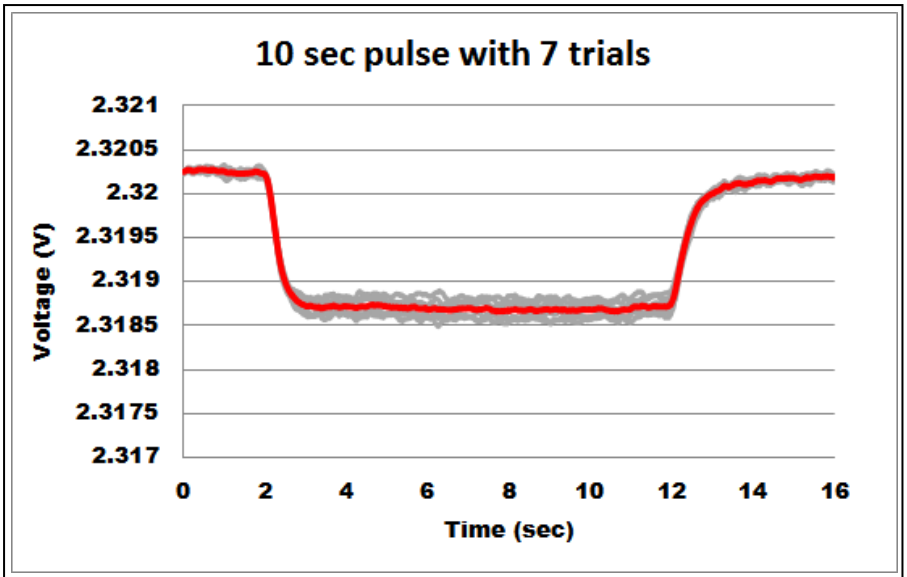

Figure 7.1-1: The average was calculated from 7 trials. Red line is the average and the grey lines are the trials.

One may notice that in figure 7.1-2 the voltage varied from each duration test. This was due to the instability of the power supply to the detecting circuit. The maximum varied voltage was 1 mV. It was a very small change in voltage. However, the power supply that was used here was not able to be adjusted or fine-tuned to control these small voltage changes.

The maximum, minimum, and pulse width were calculated and were shown in table 7.1-1. Pulse width of each curve has two time points on the curve. The first time point 'T1' is on the left hand side of the curve, and the second time point 'T2' is on the right.

The time response of the olfactometer is shown in figure 7.1-2, 0.1 second pulse response. The width of the 0.1 second pulse response curve is 0.494 of a second (as listed in table 7.1-1). From figure 7.1-3, one can see that there is a similar pattern (linearly increasing) when the pulse duration increases. Also, we can see that the duration at pulse width (in sec) matches with the pulse duration from 1 second onward. We plot the pulse duration at pulse width to show the linear relationship in figure 7.1-4. It shows that this custom-built

olfactometer's characteristic is almost the same as the duration of the input pulse. Also, the standard deviations are very small from each of the duration tests – from 7 to 16 milliseconds. It shows the accuracy of the calculated-duration values at pulse width.

Pulse duration	**Max (V) ±SD(mV)**	**Min (V) ±SD(mV)**	**Voltage drop (mV)**	**Voltage at pulse width (V) ±SD(mV)**	**T1 ±SD(ms)**	**T2 ±SD(ms)**	**Time at pulse width (sec)**
0.1 sec	2.32 ±0.06	2.32 ±0.04	0.73	2.32 ±0.05	2029.00 ±12.52	2522.57 ±8.28	0.49
0.5 sec	2.32 ±0.05	2.32 ±0.07	1.71	2.32 ±0.06	2111.57 ±8.10	2834.71 ±9.38	0.72
1 sec	2.32 ±0.08	2.32 ±0.08	1.74	2.32 ±0.08	2024.71 ±8.52	3141.43 ±12.59	1.12
2 sec	2.32 ±0.02	2.32 ±0.07	2.06	2.32 ±0.04	2210.42 ±9.22	4317.57 ±13.53	2.11
4 sec	2.32 ±0.03	2.32 ±0.05	1.90	2.32 ±0.02	2228.14 ±14.82	6288.43 ±13.67	4.07
8 sec	2.32 ±0.04	2.32 ±0.07	1.78	2.32 ±0.04	2226.14 ±14.61	10269.29 ±14.58	8.04
10 sec	2.32 ±0.03	2.32 ±0.09	1.62	2.32 ±0.06	2299.43 ±7.19	12313.00 ±18.01	10.01
20sec	2.32 ±0.05	2.32 ±0.14	1.47	2.32 ±0.09	211814 ±10.64	22109.43 ±15.89	19.99

Table 7.1-1: The measurement results from different pulse durations (mean value ± standard deviation). Voltage dropped = max – min, and the pulse width (sec) = T2 – T1.

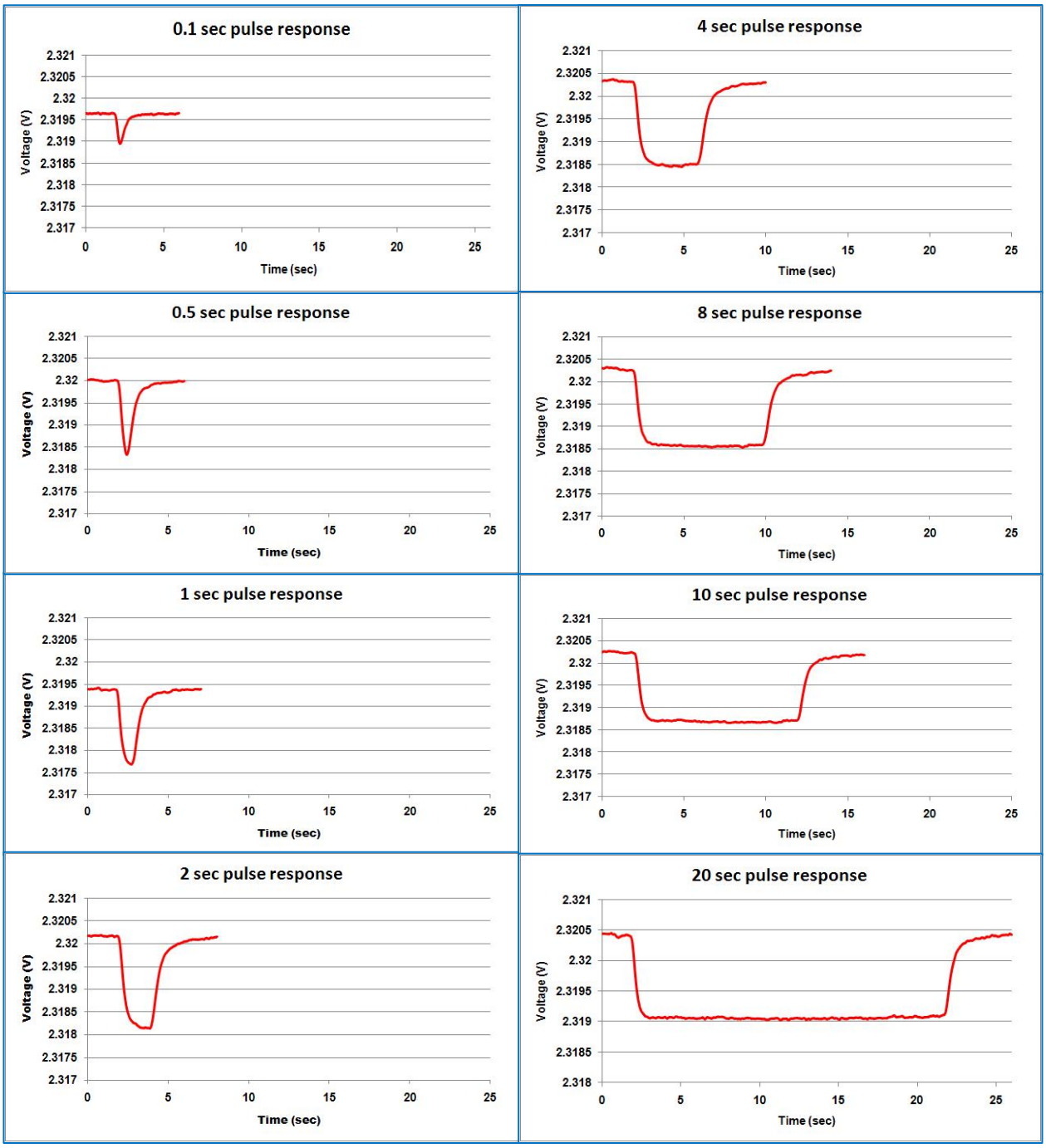

Figure 7.1-2: Characteristics of the olfactometer. From top left down and continuing on the right – 0.1, 0.5, 1, 2, 4, 8, 10 and 20 seconds respectively.

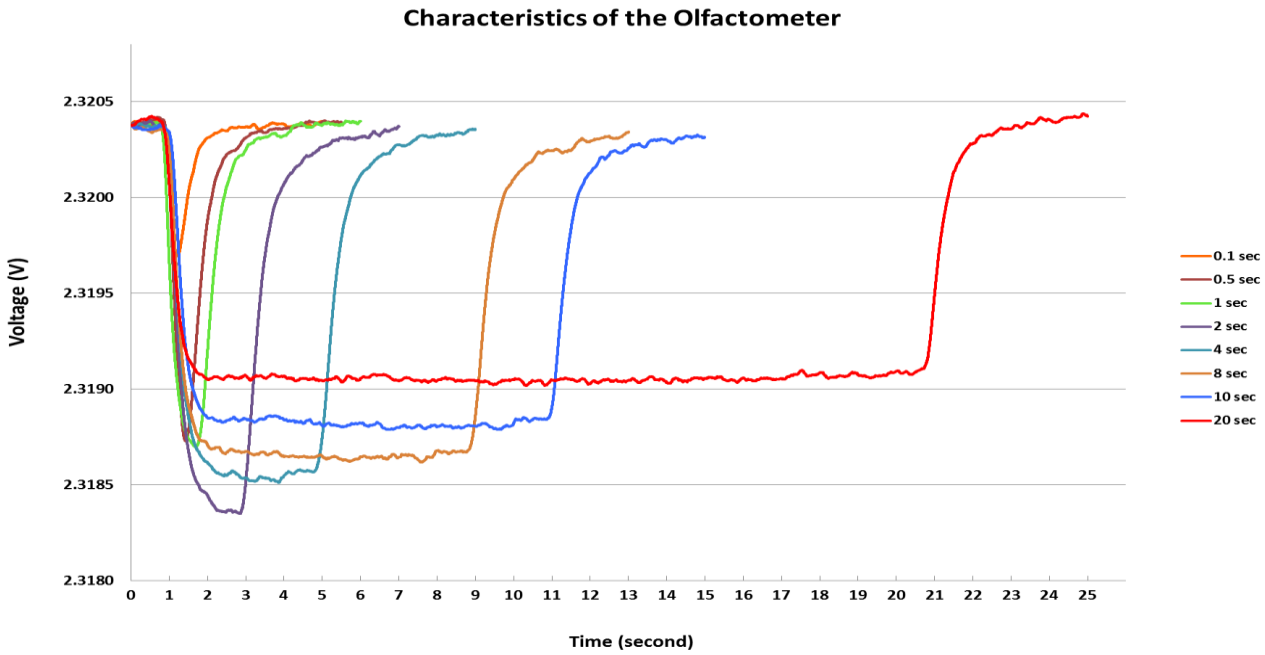

Figure 7.1-3: The characteristics of the olfactometer.

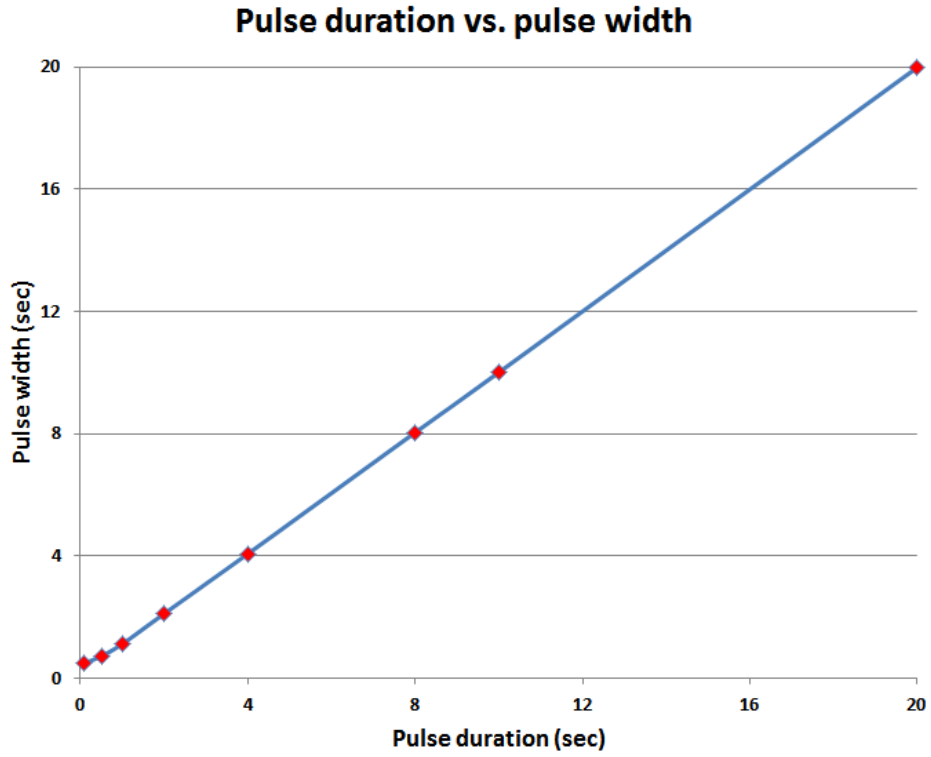

Figure 7.1-4: Pulse duration vs. the durations at pulse width to show the linear relationship between these two parameters.

To determine the point spread function (PSF) of the olfactometer, curve fitting was used to characterize this response function. In figure 7.1-5, all the curves are matched to the minimum voltage drop point. It is clear that they have a similar on and off pattern. The front and back portions of the curves were separated by removing the middle sections – not setting them to zero. The curves of 0.1, 0.5 and 1 second were eliminated since these curves never reached minimum potential (figure 7.1-6). An average curve was created individually from all the curves of the front and back portions.

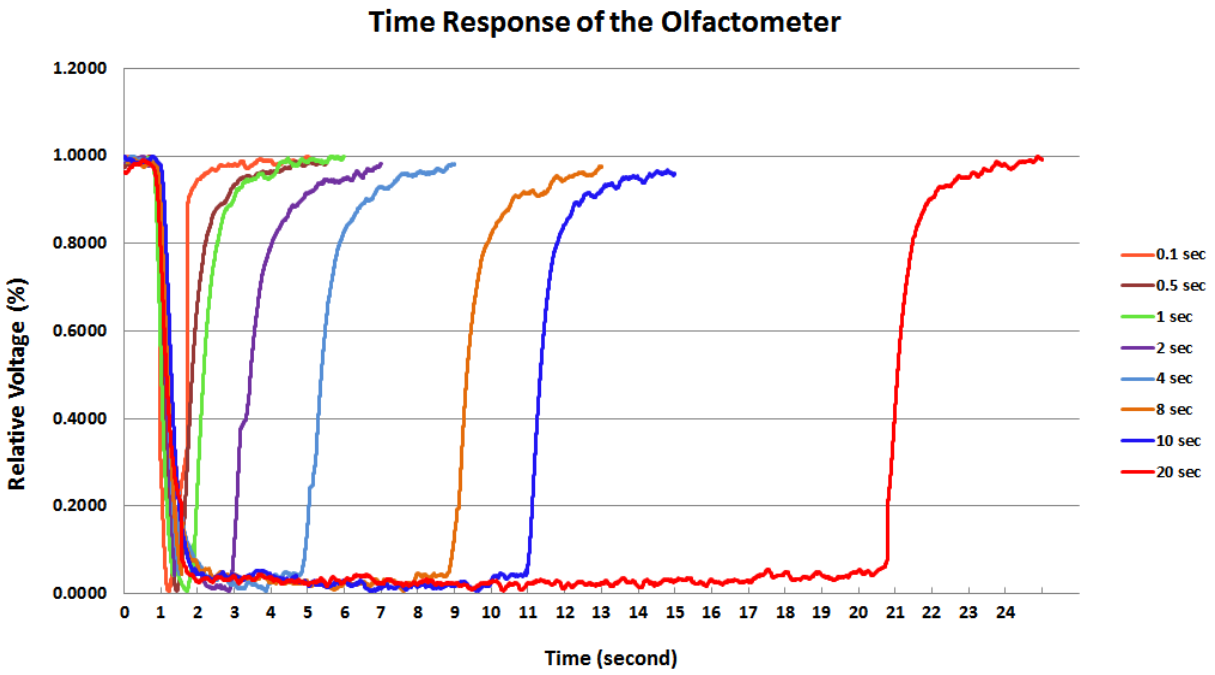

Figure 7.1-5: The time response of the olfactometer with all curves at the same level of voltage drop.

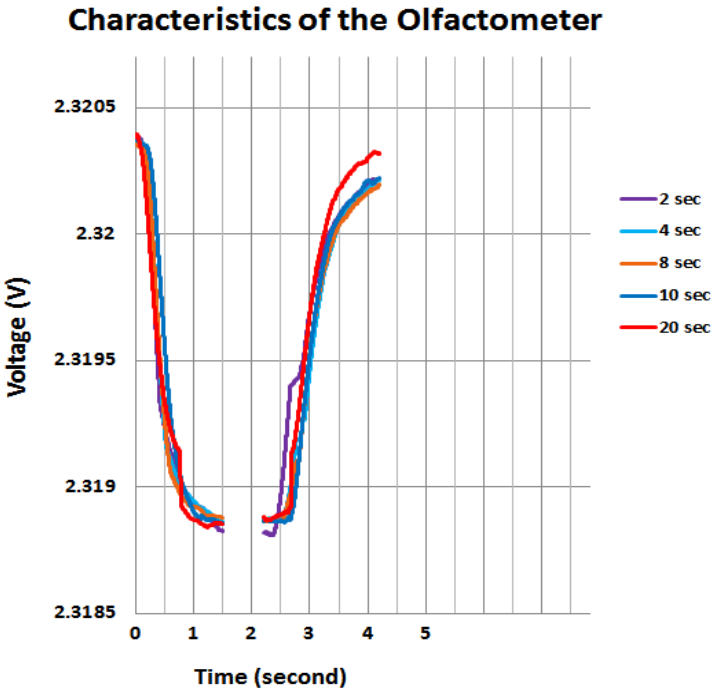

Figure 7.1-6: The separation of the front and back portions of all curves at the same level of voltage dropped, where 0.1, 0.5 and 1 sec pulses were eliminated.

The "Curve Fitting Tool" in Matlab was used for the curve fitting of each portion. Different higher degrees of Polynomial were tested. The front part of the average curve was fitted with the 7th degree of Polynomial,

$$f(x) = P_1 * x^7 + P_2 * x^6 + P_3 * x^5 + P_4 * x^4 + P_5 * x^3 + P_6 * x^2 + P_7 * x + P_8$$

and the back part was fitted with the 9th degree of Polynomial.

$$f(x) = P_1 * x^9 + P_2 * x^8 + P_3 * x^7 + P_4 * x^6 + P_5 * x^5 + P_6 * x^4 + P_7 * x^3 + P_8 * x^2 + P_9 * x + P_{10}$$

These curve fitting results are shown in table 7.1-2.

Poly7		Poly9	
P_1	5.61E-18	P_1	8.88E-18
P_2	-0.00015	P_2	5.06E-05
P_3	-7.24E-18	P_3	-4.86E-17
P_4	0.00072	P_4	-0.00043
P_5	-4.14E-17	P_5	8.11E-17
P_6	-0.00033	P_6	0.0010
P_7	2.59E-17	P_7	-4.48E-17
P_8	-0.0015	P_8	-2.89E-05
		P_9	1.12E-17
		P_{10}	-0.0013
R^2: 0.991		R^2: 0.998	

Table 7.1-2: Results data from the Polynomial Curve Fitting of the front (Poly7) and back (Poly9) portions of the average curve.

Both of these curves have very high values of R^2, which is known as the goodness of fit, and the value closer to 1 indicates a good fit.

Using the data from table 6.1-2, a response curve of each portion was reproduced. Then the front and back portions were combined (figure 7.1-7). The same "Curve Fitting Tool" in Matlab was used in this new curve to determine the response function of the olfactometer.

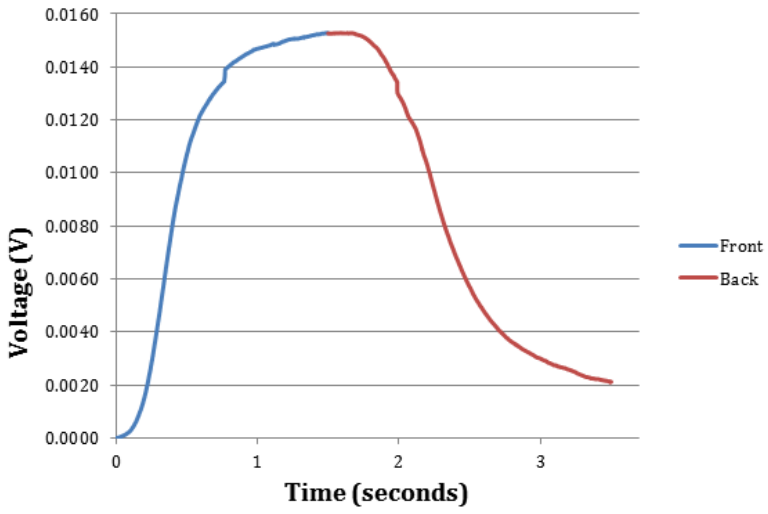

Figure 7.1-7: Both portions (front and back) of the response curve were combined as one.

The sums of Gaussians fitting method was used for this curve fitting. Different sums of

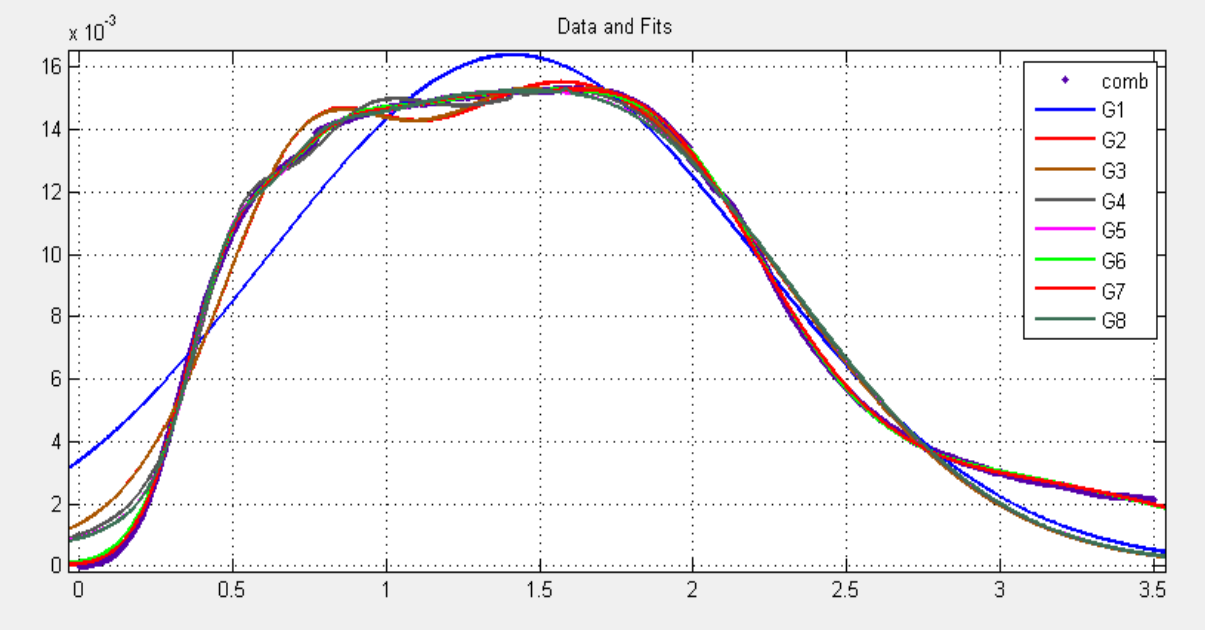

Figure 7.1-8: Different sums of Gaussians fitting trials are shown above with the data set from Matlab.

Gaussians were tested for the curve fitting, shown in figure 7.1-8. From these fittings, Gauss7 was the best fit for the response curve, in which $R^2 = 0.9998$.

$$f(x) = a_1 * e^{-\left(\frac{x-b_1}{c_1}\right)^2} + a_2 * e^{-\left(\frac{x-b_2}{c_2}\right)^2} + a_3 * e^{-\left(\frac{x-b_3}{c_3}\right)^2} + a_4 * e^{-\left(\frac{x-b_4}{c_4}\right)^2} + a_5 * e^{-\left(\frac{x-b_5}{c_5}\right)^2}$$

$$+ a_6 * e^{-\left(\frac{x-b_6}{c_6}\right)^2} + a_7 * e^{-\left(\frac{x-b_7}{c_7}\right)^2} + a_8 * e^{-\left(\frac{x-b_8}{c_8}\right)^2}$$

The result was shown in table 7.1-3 and figure 7.1-9 below.

Gauss7			
	a	b	c
1	-2.46E-05	1.67	0.092
2	0.0084	1.09	0.41
3	0.014	1.76	0.65
4	0	1.90	4.14E-05
5	0.0057	0.46	0.21
6	0.0026	3.02	0.89
7	0.0074	0.73	0.29
R^2: 0.9998			

Table 7.1-3: Results data from the sums of Gaussians Curve Fitting of the combined response curve.

However, this information does not indicate the limitation of the olfactometer. Even though the regular Gaussian curve fitting (Gauss1) did not fit very well with this combined curve, where R^2 is 0.9262, it still provided certain information as to the limitation of the olfactometer (figure 7.1.10). Matlab's curve fitting tool only provided the standard deviation; and no information with the FWHM. Therefore, OriginPro 8.5.1 (OriginLab, Northampton MA) was used to determine the standard deviation (σ) and FWHM with a Gaussian curve fitting function. The curve fitting result is shown in figure 6.1-10. The standard deviation is 0.756, the center point of the curve (x_c) is 1.406 seconds and the FWHM is 1.780 seconds. If one wants to optimize the olfactometer, protocol must be designed to be greater than 1.41 seconds for the 'ON' period until the stimulus reaches its maximum.

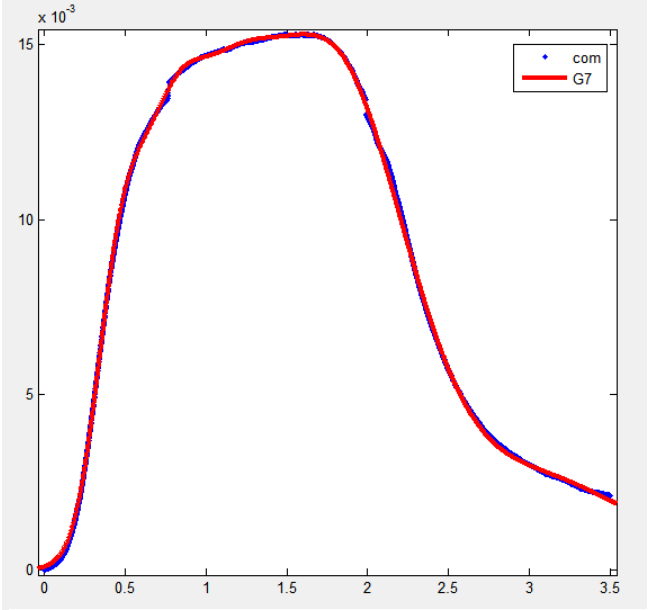

Figure 7.1-9: Curves of the data set with sums of Gaussians (Gauss7) curve fitting from Matlab.

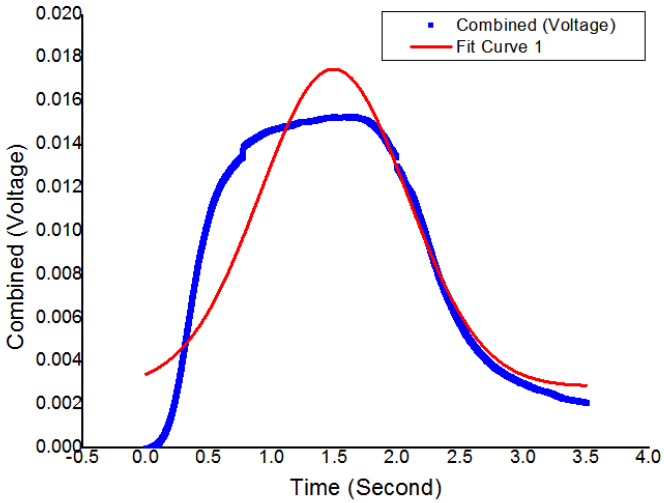

Figure 7.1-10: Curves of the data set with Gaussian curve fitting from OriginPro.

When one has a closer look at figure 7.1-2, one can notice that there is a time delay before the testing odorant is being delivered. Figure 7.1-11 is a close-up of the time period from 1 second to 3 second points in figure 7.1-3. The trigger point is rescaled at 0 second point mark. After the triggering point, all pulses are delayed approximately 0.9 of a second before the voltage starts decreasing. The artifact of 1 second pulse (slightly faster than all the other pulses) may due to triggering the stimulation and acquiring data programs together at the same time (left and right hands sync-delay). This delay time may be caused by the length of the connected tubing. However, it is not a long delay compared to the hemodynamic response function (HRF), which will be a few seconds. Therefore, it will not affect the results of the olfactometer by much. Moreover, one must take this into account when analyzing the functional data.

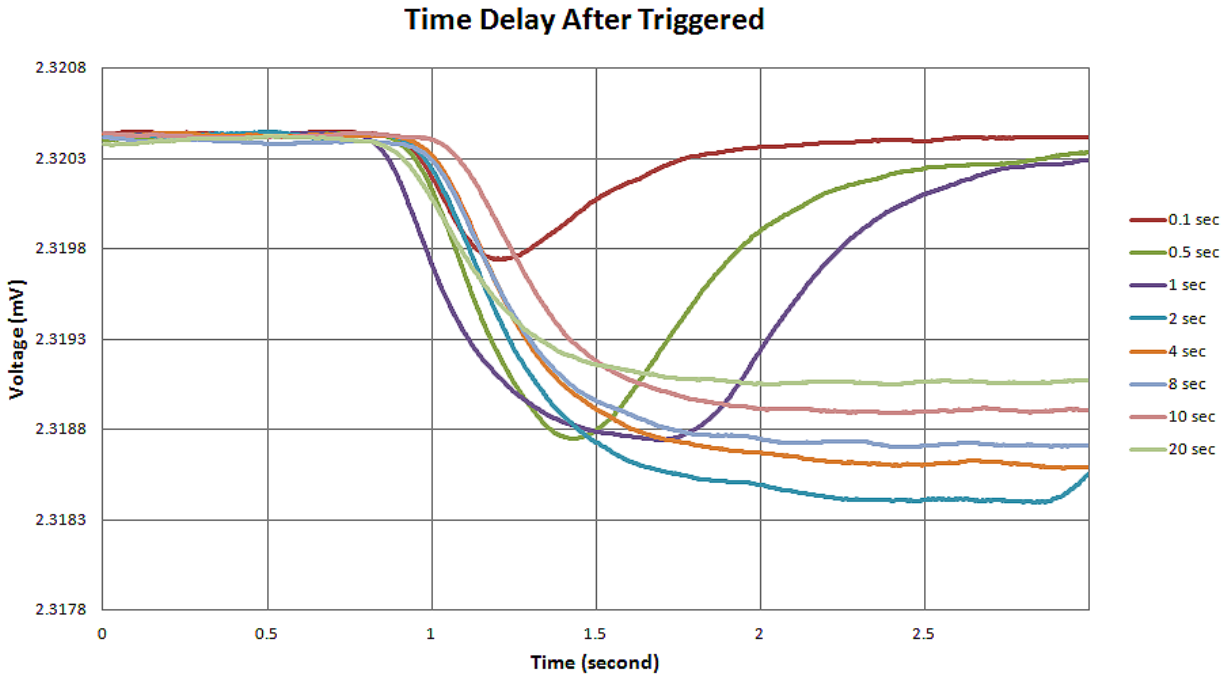

Figure 7.1-11: The time delay after each trigger pulse.

7.2 Results of testing the shortest possible duration

The olfactometer was still connected with the full length of 25 feet Teflon tubing, and the flow rate was set to 1 LPM. Testing odorant was 100% concentration of acetone. In the control VI interface, the 'ON' time was set from 0.25 to 6 seconds with different 'OFF' times from 1 to 8 seconds. This test was aimed to find what the shortest possible presentation time or 'ON' time and 'OFF' time would be that could be used in a real experiment. After a sequence of combinations of 'ON' and 'OFF' time tests, the shortest possible presentation time was 0.5 of a second for the 'ON' time and 2 seconds for the 'OFF' time, if and only if, a certain block paradigm would be used – such as Westermann's (figure 5.2-1).

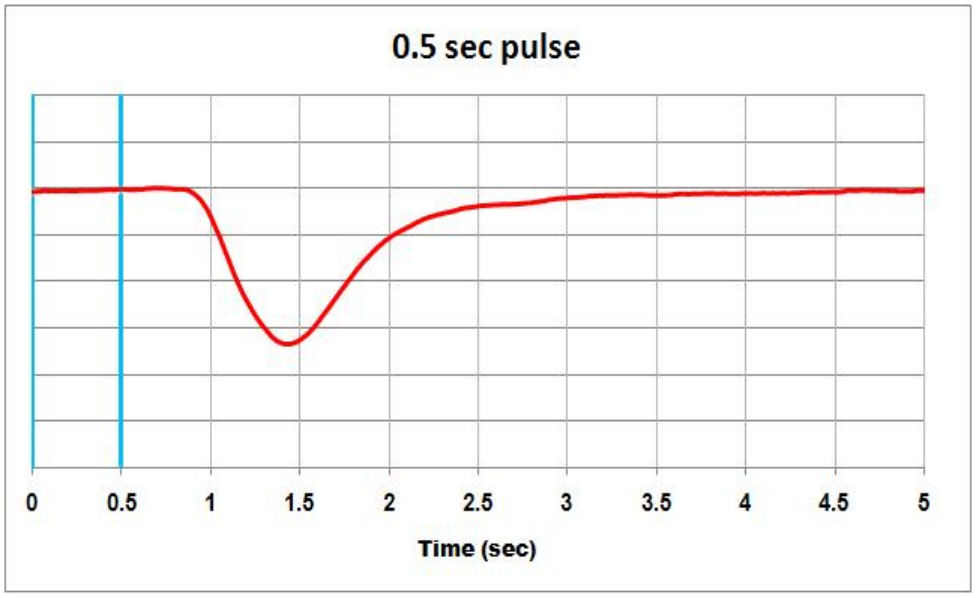

Figure 7.2-1: Recovery time after a pulse response. Blue line is the 0.5 second pulse, and the red line is the pulse response. The pulse needed approximately 2 seconds to recover to its 90% amplitude; and approximately 3 seconds to return close to its full amplitude as shown above.

From table 7.1-1, one can see that the 0.1 second pulse response has fluctuated approximately 0.7 mV between the maximum and minimum value. It may not deliver enough quantity of odorant stimulus to the subject, whom may not possibly be able to detect this small

amount of the stimulus. Therefore, 0.1 second pulse duration is out of consideration. The next shortest duration is 0.5 second. It has almost double the voltage changes as a 0.1 second pulse response. The trigger point is at the 0 time point mark. There was approximately a 0.5 second time delay after the trigger pulse (see figure 7.2-1). The testing odorant was delivered during the 'OFF' period. When it started to recover its amplitude, the next pulse may be triggered if the 'OFF' period is short, such as 0.5 of a second. It was not able to recover its maximum amplitude. However, it recovered to approximately 85% of its original amplitude. The odorant stimulus might not be detected if using a regular boxcar protocol and will not trigger any or enough olfactory stimulation response to be recorded. Even if a pulse-sequence paradigm is used, the subject may not be able to detect the odorant stimulus since the 'ON' block is a sequence of pulses with a short 'OFF' time. Usually 1 second is used in between each pulse (refer to figure 5.2-1). The amplitude will only recover approximately to 50 to 60% of its original amplitude. Therefore, one should reasonably choose at least a 2 second minimum as the 'OFF' time. This might not work in practice since the hemodynamic response is in seconds. This short duration pulse may not have the optimal result of the olfactory stimulation.

This brought up the question as to how long it would take to fully recover or attain 90% of its original amplitude. From figure 7.1-3, all pulse durations need approximately 2 seconds to rise back to 90% amplitude and approximately 3 to 4 seconds to rise close to its original amplitude. A longer 'OFF' time will guarantee recovery to the original amplitude totally before the next 'ON' trigger begins.

7.3 Results of testing the concentration being delivered with two methods

For this test, the length of the Teflon tubing to the olfactometer was not changed – still 25 feet long. The flow rate remained at 1 LPM. The parameter boxcar protocol was set at 1 second

'ON' and 2 seconds 'OFF' for 16 blocks. The testing odorants pentyl acetate, linalyl acetate and acetone, were used with a volume of 5 ml and each was placed in an individual gas-washing bottle. Each stimulus bottle was connected to the olfactometer, and ran through the above protocol test with the UV test apparatus circuit. As predicted, the stimuli pentyl acetate and linalyl acetate, did not absorb any UV energy; therefore there was no fluctuation of the voltage at the UV detector.

Using a 4-way multiport connector (Cole-Parmer), the Teflon tube was connected to two gas-washing bottles, one containing either pentyl acetate or linalyl acetate and the other one acetone. This method is similar to Lorig et al. 1999 which used air to dilute the two stimuli [31], but in our case the mixture only had 50% of each stimulus. The 'ON' time was set at 2 seconds, and the 'OFF' time was set at 6 seconds. The protocol was set to 6 blocks. The averaged voltage dropped approximately 1.5 mV when the odorant stimulus passed through the quartz tube on either air-diluted mixture.

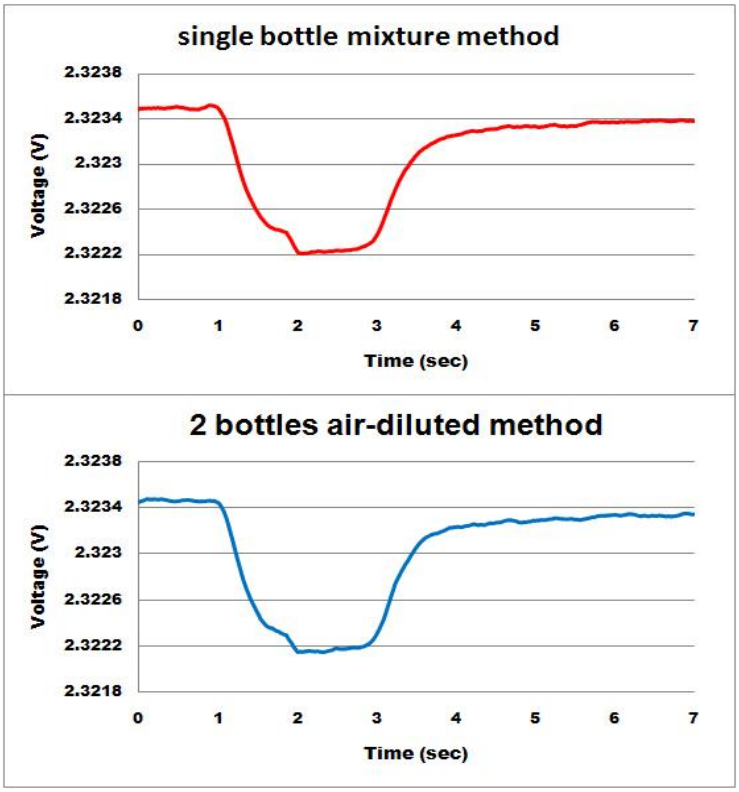

Figure 7.3-1: Results of using two different methods using 50% of the acetone.

The same length of tubing was still connected to the olfactometer, and a 50% concentration of each testing stimulus, acetone and linalyl acetate, were mixed in a single gas-

washing bottle. This would match with the concentration of the air-diluted stimulus as above. The same boxcar protocol was run and the average voltage dropped approximately 1.4 mV. The two methods had similar voltage attenuation (figure 7.3-1). This shows that either method can be used for the UV apparatus circuit testing. Using the mixture method will be best for our testing since the custom-built olfactometer was not built under the concept of air-diluting the stimulus.

6.4 Results of testing the delay time with different flow rates

Three different flow rates of 0.25, 0.5 and 1 LPM were tested with the full Teflon tubing length of 25 feet attached to the olfactometer. 100% of acetone concentration and 50% concentration of acetone mixture (mixed with 50% of linalyl acetate) were used as testing stimuli. The testing paradigm was set as the 'ON' time at 2 seconds and the 'OFF' time at 25 seconds. There were eight blocks of 'ON', and 10 seconds of baseline (OFF time) was introduced at the beginning of the protocol. The results are shown in figure 7.4-1. The 0.25 LPM curve in the figure shows a long delay time of approximately 8 seconds before the odorant stimulus was delivered. The voltage difference was approximately 0.5 mV. This means that there was not enough acetone concentration carried by this flow rate towards the quartz tube to absorb much of the UV energy. The result was compared with table 7.5-1; less than 15% of acetone concentration was delivered. Furthermore, this means that the subject may not detect the odorant stimulus from the olfactometer with this flow rate and short duration pulse protocol. The 0.5 LPM curve in the figure shows a 2-second time delay and the voltage difference was approximately 1.6 mV. Comparing this result with table 7.5-1, it seems that less than 75% and more than 50% of acetone concentration was delivered with this flow rate. The 1 LPM curve showed approximately a 1 second delay in delivering the odorant stimulus. The voltage

difference was approximately 2 mV. It was in the range of 75 to 100% of acetone concentration in table 7.5-1.

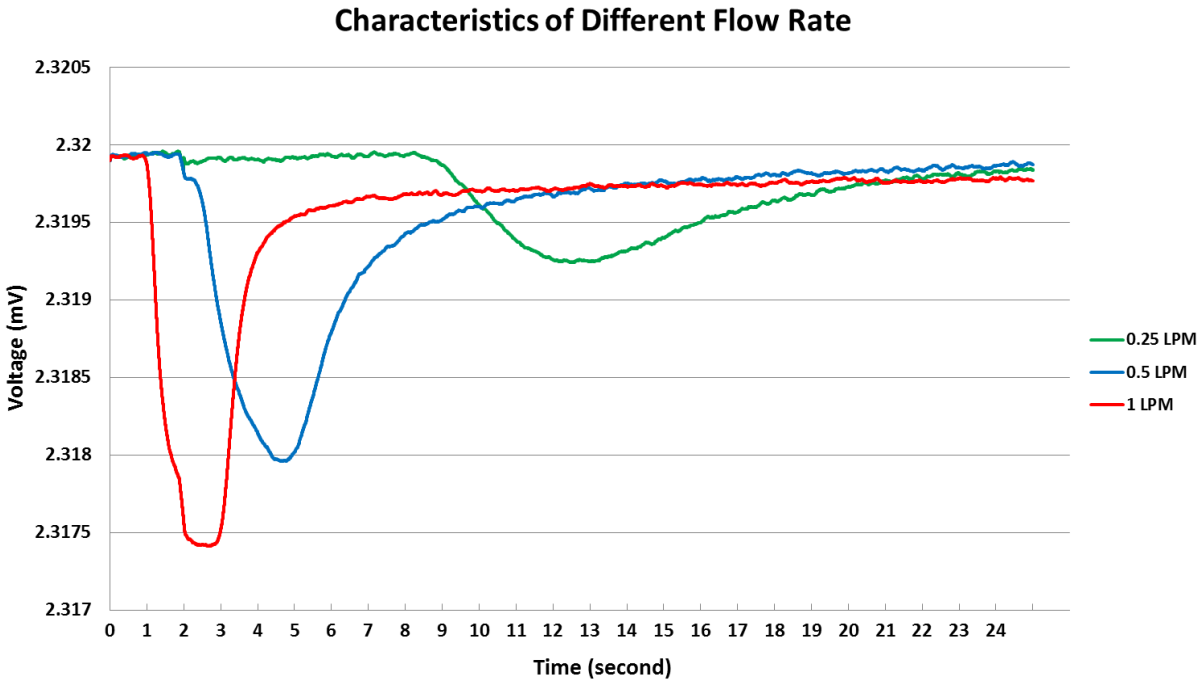

Figure 7.4-1: Characteristics of the three different flow rates.

7.5 Results of testing the different lengths of the tubing

Different concentration mixtures of linalyl acetate and acetone (five gas-washing bottles) were prepared in individual gas-washing bottles. Each concentration was tested with the same block protocol used above – 2 seconds 'ON' time and 6 seconds 'OFF' time. The flow rate was kept constant at 1 LPM for all three tests. Three different lengths of the Teflon tubing connected to the olfactometer were tested, and the testing odorant was generated by different concentrations of the acetone and linalyl acetate mixture through the UV test apparatus. The results are shown in table 7.5-1.

Length	Concent.	Max (V) ±SD(mV)	Min (V) ±SD(mV)	Voltage dropped (mV)	Voltage at pulse width (V) ±SD(mV)	T1 ±SD(ms)	T2 ±SD(ms)	Time at pulse width (ms)
1/3 of full length (8ft4in)	25%	2.32 ±0.03	2.32 ±0.05	0.77	2.32 ±0.04	1150.88 ±34.25	3251.94 ±19.51	2101.06
	50%	2.32 ±0.03	2.32 ±0.06	1.29	2.32 ±0.04	1089.19 ±27.58	3231.63 ±22.79	2142.44
	75%	2.32 ±0.04	2.32 ±0.17	1.99	2.32 ±0.10	1028.75 ±20.67	3211.94 ±26.23	2183.19
	100%	2.32 ±0.05	2.32 ±0.17	2.16	2.33 ±0.11	982.19 ±13.63	3371.44 ±19.92	2389.25
2/3 of full length (16ft7in)	25%	2.33 ±0.10	2.33 ±0.11	0.48	2.33 ±0.10	1236.63 ±17.78	3282.25 ±16.89	2054.63
	50%	2.33 ±0.08	2.33 ±0.10	1.27	2.33 ±0.09	1213.56 ±17.14	3317.69 ±15.41	2104.13
	75%	2.33 ±0.10	2.33 ±0.20	1.90	2.33 ±0.16	1149.69 ±15.20	3329.56 ±10.14	2179.88
	100%	2.33 ±0.10	2.33 ±0.19	1.90	2.33 ±0.16	1114.44 ±13.10	3329.56 ±10.14	2215.13
full length (25ft)	25%	2.32 ±0.02	2.32 ±0.07	0.43	2.32 ±0.04	1469.94 ±40.02	3210.63 ±42.60	1740.69
	50%	2.32 ±0.04	2.32 ±0.07	1.26	2.32 ±0.05	1342.00 ±20.82	3250.44 ±25.71	1908.44
	75%	2.32 ±0.10	2.32 ±0.23	1.87	2.32 ±0.18	1276.56 ±17.32	3292.00 ±16.89	2015.44
	100%	2.32 ±0.10	2.32 ±0.19	1.88	2.32 ±0.14	1273.63 ±15.67	3317.06 ±13.04	2043.44

Table 7.5-1: Results of different lengths of tubing connected to the olfactometer.

From the table 7.5-1, the length of the Teflon tube connected to the olfactometer does not have a great effect on the concentration delivery of the stimulus. It seems to have a slight effect on the lower concentration, but the fluctuation is small – approximately 0.2 to 0.5 mV. Moreover, the voltage difference of each length is proportionate with the concentrations – the higher the concentration, the higher the voltage difference.

Three different tubing lengths were tested with the olfactometer. The lengths of the tubing were 25 feet (full length), 16 feet 7 inches (2/3 of the full length), and 8 feet 4 inches (1/3

of the full length). Each length was tested with 100% of acetone and 1 LPM flow rate. Each stimulus was delivered for 2 seconds 18 times. A comparison graph of different tube lengths was constructed from the collected data sets. A time delay between each length is indicated in figure 7.5-1a. The time delay of each tube length was not longer than one second. The delay time of the full length tubing was 872 milliseconds, 2/3 length was 694 milliseconds and 1/3 length was 559 milliseconds. One would expect these results – the longer the tubing, the longer the delay time. This time delay was not significant in affecting the actual olfactory stimulation, since the hemodynamic delay function (HRF) is much greater than this delay. After stimulus delivery, HRF typically peaks at 4-6 seconds[12]. Furthermore, the pulse width (similar to full width at half maximum FWHM) of each curve was calculated (figure 7.5-1b). These rise time values were 0.967 second, 1.112 seconds and 1.257 seconds respectively to 1/3, 2/3 and full length tubing. A linear relationship was found with the increase of the tube length (figure 7.5-2a). There was a linear increase in the rise time, 0.145 second, when 1/3 of the tube length (8 feet 4 inches) was increased. Moreover, in figure 7.5-2a, one can find the delay time of the olfactometer, which was approximately 0.822 second without any tube length attached at pulse width. In figure 7.5-2b, both delay times of different tubing lengths were displayed. A trend line was drawn with the regular fall time data, and the delay time without any tubing attached was determined – 0.395 second. This delay time was possibly caused by the control VI (~ 200 ms), the valve and the testing circuit. One can take this delay into account when acquiring or analyzing the functional data. The concentration difference between each length is shown in figure 7.5-3, and it was similar as one would expect. The shorter the length of the tubing, the higher concentration of the stimulus. It was similar as the results in figure 7.4-1, the higher the flow rate, the higher the concentration.

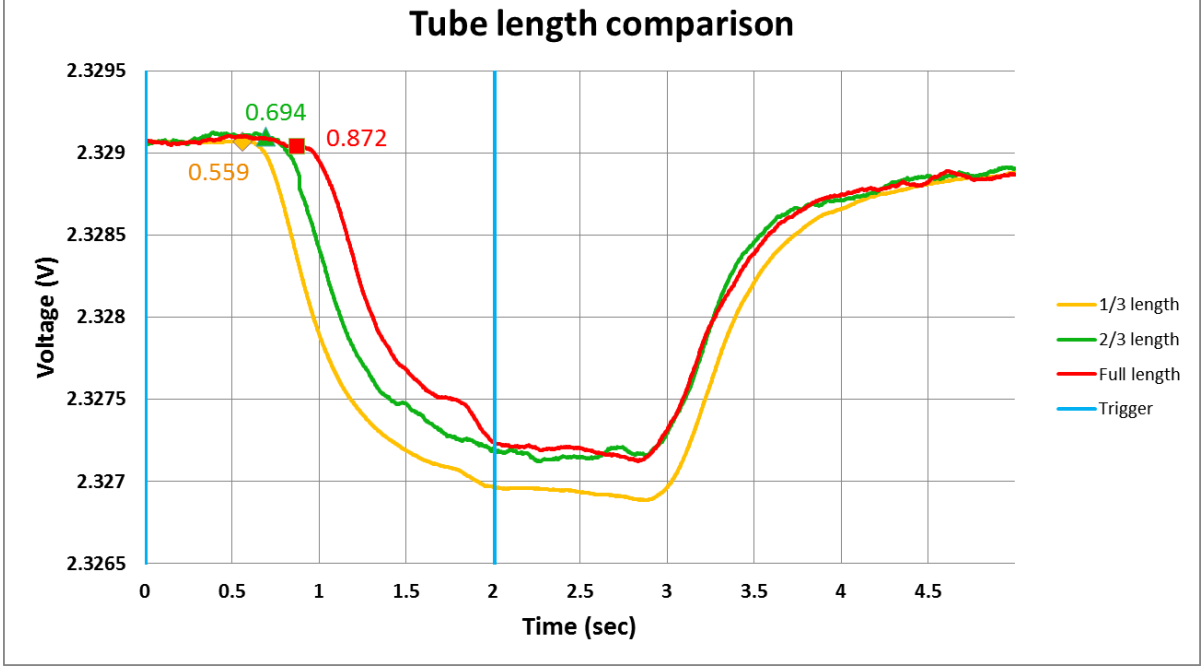

Figure 7.5-1a: Tube length comparison graph shows the delay time of each tube length with 100% acetone and 1 LPM flow rate.

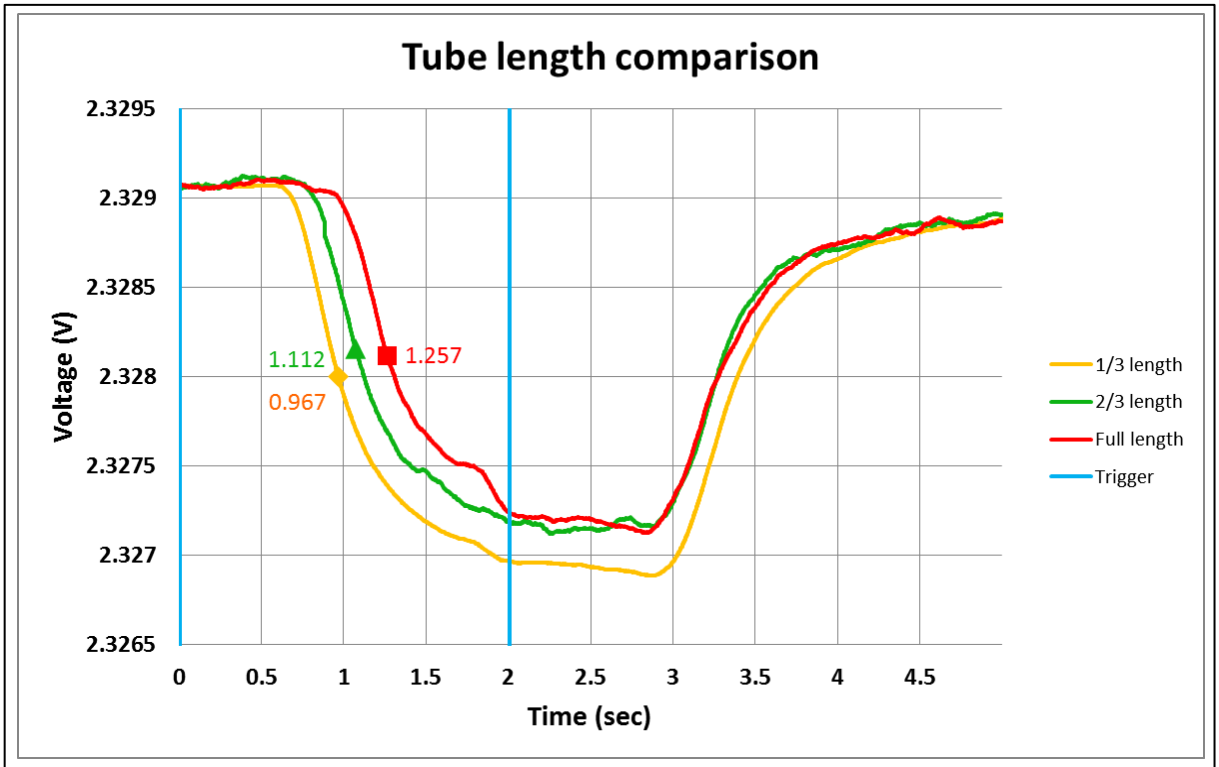

Figure 7.5-1b: Tube length comparison graph shows the pulse width delay time of each tube length with 100% acetone and 1 LPM flow rate.

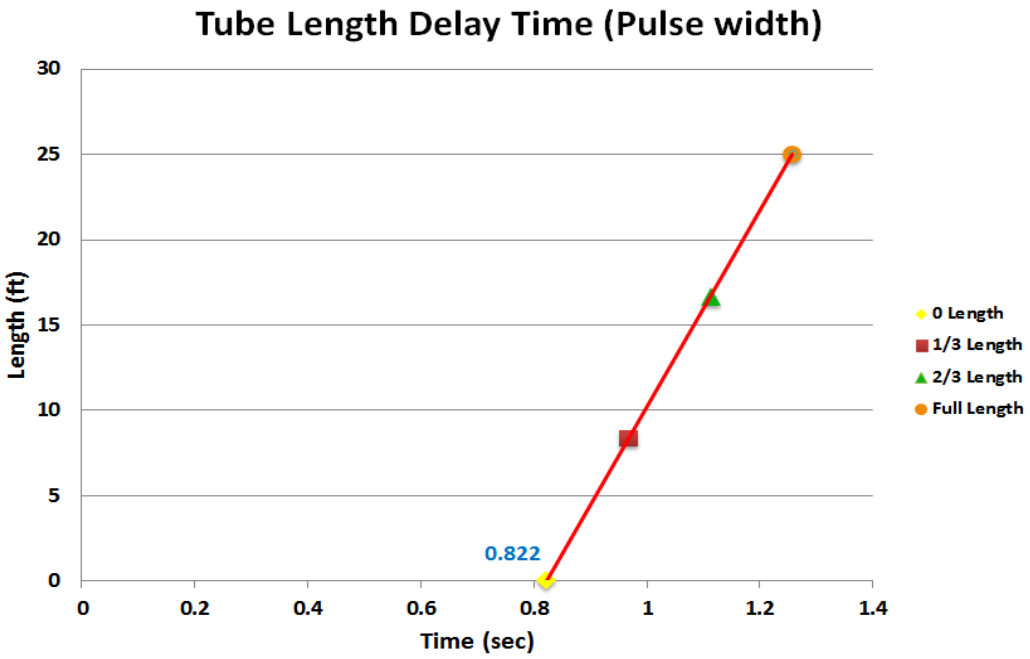

Figure 7.5-2a: Indicates the linear relationship of the time delay from different tubing lengths at pulse width. Other delay time can also be measured from this graph.

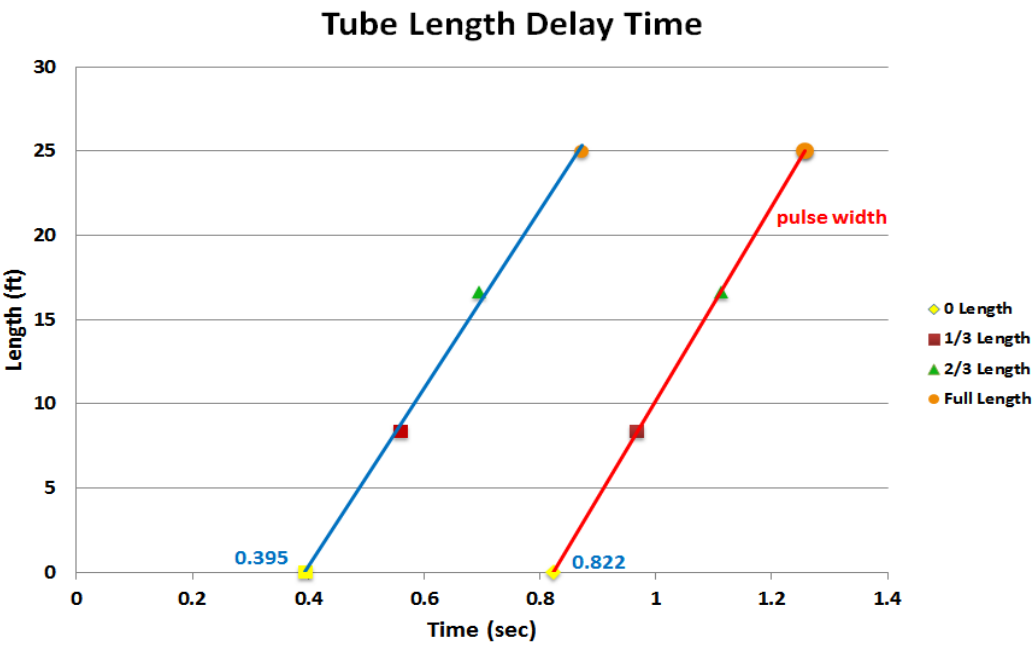

Figure 7.5-2b: Indicates both time delays from different tubing lengths. Other delay time can also be measured from this graph.

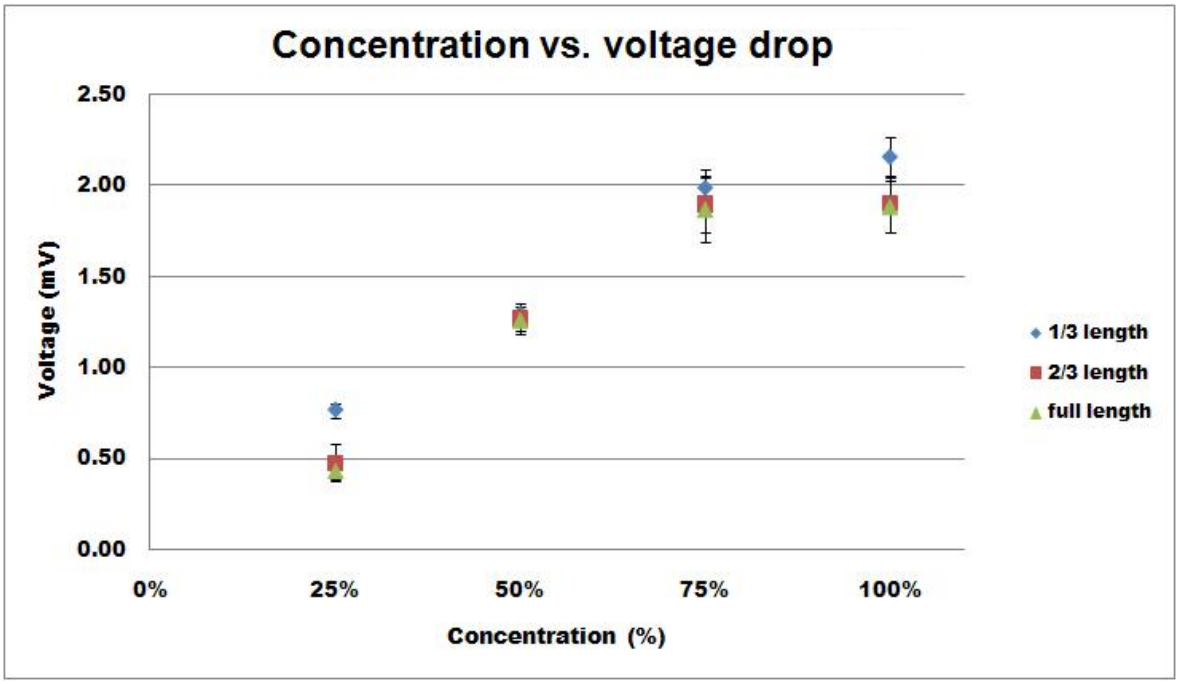

Figure 7.5-3: The relationship of different concentrations from different tubing lengths as their voltage dropped.

7.6 Results of testing the durability of the olfactometer

During this test, the olfactometer was running for a long period of time – approximately 30 minutes. The 'ON' time was set at 2 seconds, and the 'OFF' time was set at 6 seconds. 5 ml of acetone was used as the odorant stimulus. The display was set to register every 5 minutes (300 seconds). The test was run three times on three consecutive days. Unfortunately, the whole data set was too large to record and store, and therefore the first 5 minutes of data was recorded. The beginning of the test results is shown in figure 7.6-1. The olfactometer performed well with each test run. The display of the signal durations during every 5 minute period was consistent; only the waveform shifted upward approximately 0.25 mV. Moreover, the amplitude of the waveform noticeably shrank. Otherwise, the waveform shape remained the same. Further investigation was performed: the UV apparatus was powered, no stimulus (acetone) was used, and after 10 minutes the voltage was measured from the output with a voltage meter. The results were plotted in

figure 7.6-2. The voltage dropped approximate 3 mV during a 30-minute test. This showed that the power supply was not stable during the first 13 minutes, possibly due to fluctuation in mV for which the power supply was not designed in adjusting to these small changes. It could only adjust 100 mV at a time. All the above experiments were performed when the power supply was on longer than 30 minutes. This was the reason that the waveform shifted in a small amount. Therefore, for longer period of testing, the UV LED was chosen for the apparatus, because it generated less heat and a longer life span. Furthermore, another reason for the reduced amplitude of the waveform was the evaporation of the acetone which changed the gas-washing bottle's temperature. With the temperature lower, the concentration of the acetone being carried by the air flow would be lower. Therefore, the amplitude of the waveform shrank at the beginning of the experiment. Until the temperature reached the saturation point, the amplitude would remain at the same level.

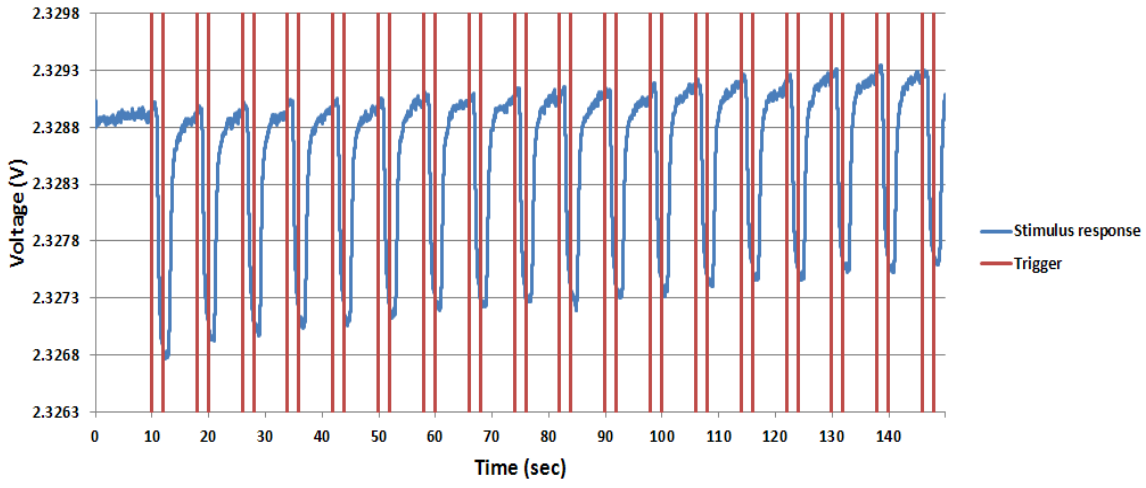

Figure 7.6-1: Test ran for 30 minutes with regular box-train protocol and used acetone only. The first 2 ½ minutes of waveform displayed.

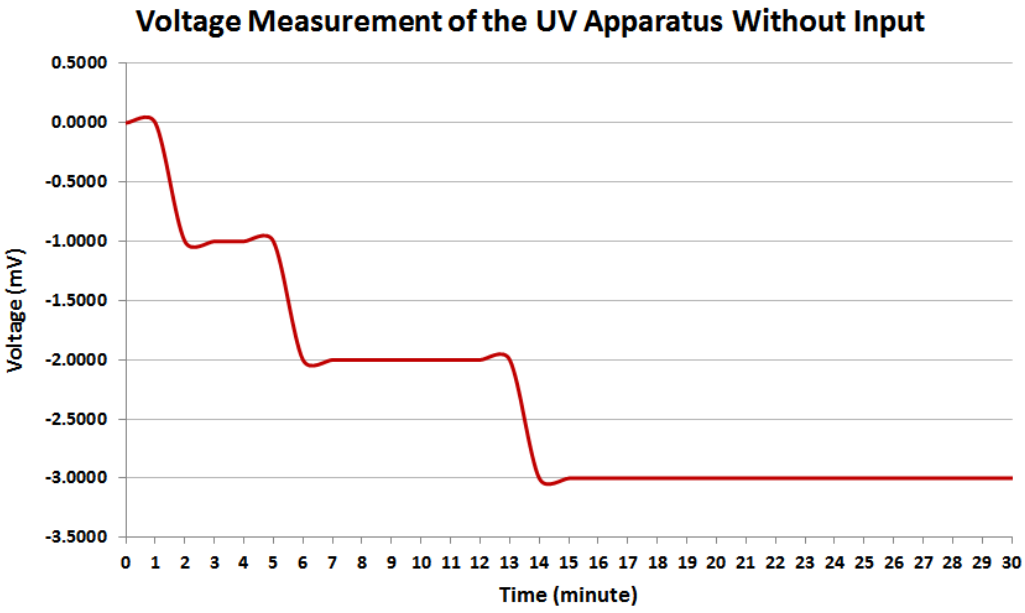

Figure 7.6-2: Test of the UV apparatus ran for 30 minutes without any acetone as stimulus.

Chapter 8

Stimuli and Human Subjects

8.1 Stimuli

All the stimuli used in this project are in liquid form. Pentyl acetate (banana and apple scent; Sigma-Aldrich), linalyl acetate (strong sweet floral scent; Fluka, Sigma-Aldrich), chocolate and lavender fragrances (Bell Flavors & Fragrances, Inc., Northbrook, IL) and white vinegar (standard 5% strength and commercially available) will be used as the stimulus/stimuli for the first part of the research. They were mainly used to test with the nasal cannula. The odorants (except vinegar) are considered as pleasant odorants, and have been shown to stimulate the olfactory system[64, 79, 80].

Chocolate fragrance (Bell Flavors & Fragrances, Inc., Northbrook, IL), luscious vanilla, banana base, urine, musty, rubbish acrid and flatulence (Carvansons LLP, Lancashire, UK) are used in the second part of the research. This part is mainly focused on testing with the phantom nasal CPAC mask (SleepNet Corporation, Hampton, NH). The first three odorants are considered as pleasant odorants. The rest are considered as unpleasant[81].

All the olfactory stimuli can be diluted with propylene glycol (tasteless, odorless and colorless; Sigma-Aldrich) to create different concentrations (10%, 20%, 40%, 60%, 80% and 100%)[82]. The white vinegar can be mixed with an equal amount of water to yield 2.5% acetic acid to control the intensity of the odorant stimulus. Small surveys (10 to 15 people) were conducted to decide what concentration should be used in the second part of the research for testing with human subjects.

8.2 Survey of the stimuli

The main purpose of this survey was to determine which stimulus belongs to either the “pleasant” (positive hedonic value) or “unpleasant” (negative hedonic value) group and its intensity. Seven odorant stimuli were chosen for this survey, and one of them would be

eliminated. The stimuli were: chocolate, luscious vanilla, banana base, urine, musty, rubbish and flatulence.

Fourteen healthy subjects participated in this pleasant/unpleasant and intensity survey: 6 males and 8 females. Each subject was placed in a well-ventilated room. A small bottle of each stimulus was placed near the subject's nose for a few seconds, one at a time in random order. After each bottle was placed, the subject graded the odorant stimulus's pleasantness, unpleasantness and its intensity. The results of the pleasantness and intensity were shown in figure 8.2-1 and 8.2-2.

8.3 Participants

Eleven healthy volunteers (5 males and 6 females, mean age = 29.82; mean age for male is 34.2 and for female is 36.17) were recruited and participated in this project. Three males and a female participated with the coronal fMRI acquisitions. The others participated with the axial acquisition. These results are shown in the later "Results" chapter. The project was approved by IRBs of Mount Sinai School of Medicine and the Graduate Center of New York.

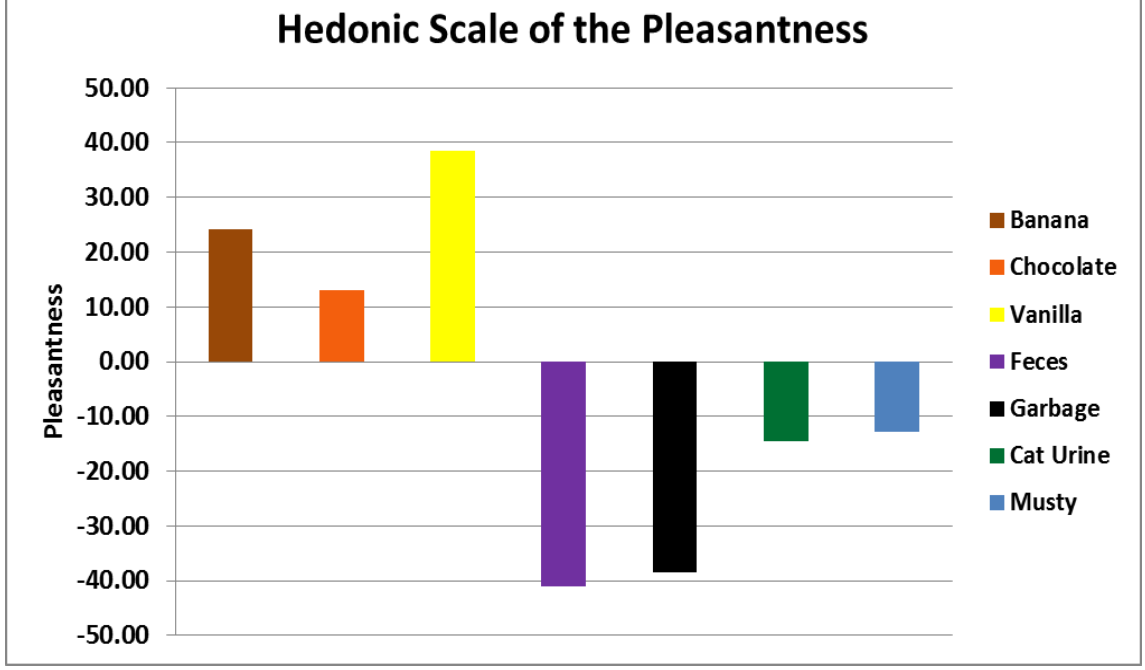

Figure 8.2-1: The Hedonic Scale of the pleasantness of the stimuli.

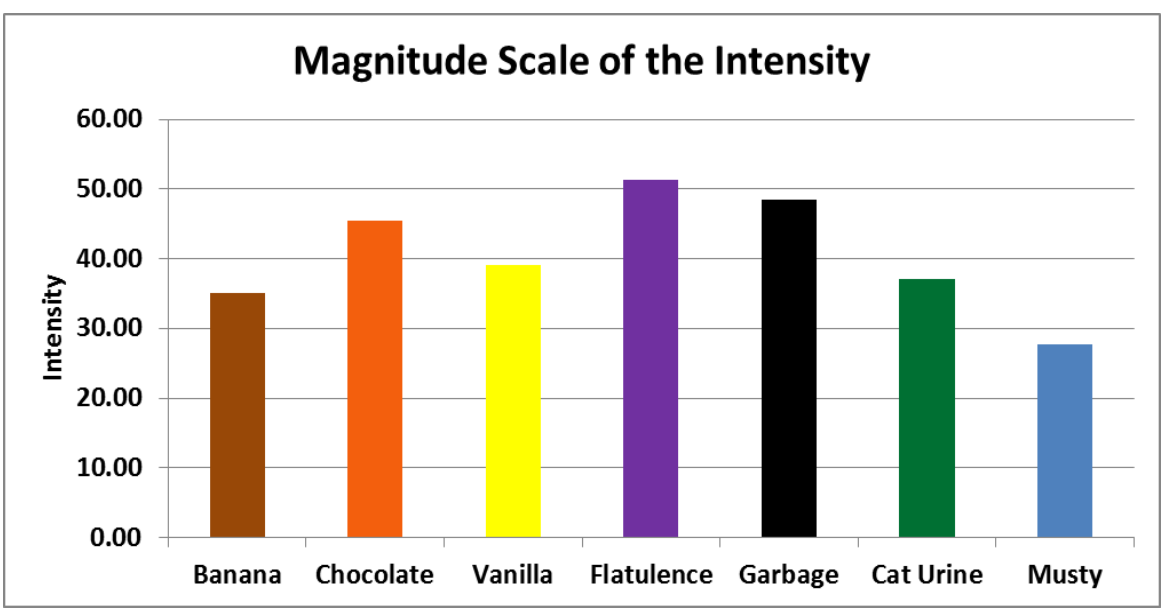

Figure 8.2-2: The Magnitude Scale of the intensity of the stimuli.

Chapter 9

Imaging Technique

9.1 Functional Magnetic Resonance Imaging (fMRI)

Neuronal activity involves many complex physiological processes. These physiological functions in the brain respond regionally to brain activity. Functional magnetic resonance imaging (fMRI), a noninvasive method, measures the changes in hemodynamic events in the brain tissue[83, 84]. A momentary increase in neuronal activity within a region of the brain begins consuming additional oxygen in the blood proximal to these cells; however it also causes local vasodilation. This means the increase in blood flow causes a slight increase in blood volume in this region. As a result, blood near the region of local neuronal activity has a higher concentration of oxygenated hemoglobin than blood in locally inactive areas. Through the blood oxygenation level dependent (BOLD), fMRI detects these hemodynamic changes in neuronal activity in the proximal brain tissue, which is the magnetic susceptibility of hemoglobin (Hb)[85-91]. Deoxygenated Hb is paramagnetic, and oxygenated Hb is diamagnetic. The presence of the paramagnetic deoxygenated Hb distorts the static magnetic field (B_0). Spins in this non-uniform magnetic field will precess at different frequencies causing more rapid phase dispersal and decay of the MR signal[85, 92]. Therefore, changes in the blood oxygenation can cause changes in the MR decay parameter, T_2*, leading to changes in the image intensity in the T_2*-weighted images[85].

9.2 fMRI Data Acquisition

All MRI studies will be performed on Philips Achieva 3T MRI systems (Philips Medicine System, Netherlands) with echo planar imaging (EPI). The trade-off in using a 3T MRI system rather than the 1.5T is an increase in the resolution of the imaging, but also an increase in the susceptibility effect. We will use 3T MR systems to acquire MR images with the custom-built olfactometer.

A standard clinical head coil will be used. The MRI system is located in the MRI center of the Department of Radiology, B1 level, Annenberg Building, Mount Sinai Hospital. In each MRI study, a proton density fast spin echo imaging (PD T2 Dual Echo image) will be acquired as the anatomic image. Functional MRI BOLD images will be acquired with a gradient echo-planar sequence using the following protocol: 34 coronal slices or 19 axial slices will be acquired, TR=4000 or 2000 ms, TE=30 or 27 ms, (coronal and axial acquisitions respectively) the field of view will be 21cm, the slice thickness will be 3mm with 4 mm spacing, the matrix size will be 112X112, and the flip angle=90°. During the fMRI imaging, the odorant stimulus/stimuli will be delivered to the subject by a custom-built olfactometer. Also, a high-resolution structural MP-RAGE (Magnetization Prepared Rapid Gradient Echo) scan will be acquired with the following parameters: 144 Slices, thickness=1.0 mm, matrix size = 256 ×256, FOV=256 mm, TR=1900ms, TE=3.5ms and a 15° flip angle.

9.3 Procedure and Method

The subject sat on the table of the scanner. A mask was placed over the subject's nose only with the hornet support to his/her head (figure 9.3-1a). Earplugs were given to the subject before placing a headphone over his/her ears. The mask was connected to a fresh air/stimulus tube on the bottom and two vacuum tubes on both sides of the mask (figure 9.3-1b). The subject then lay down on the scanner table; a head coil was placed over the subject's head (figure 9.3-1c).

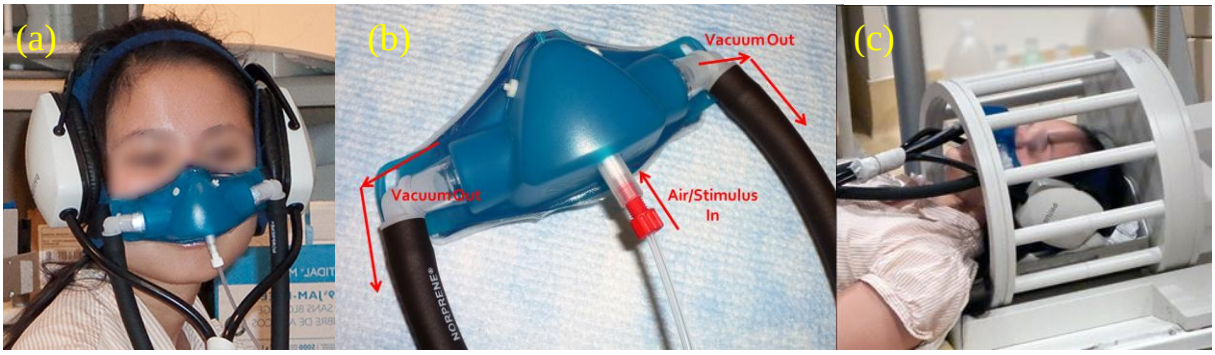

Figure 9.3-1: (a) Subject wearing a mask, which is supported by a hornet on the subject's head. (b) Connections of the air/stimulus and vacuum tubes of the mask. (c) Head coil is placed over the subject's head.

The odor stimuli were delivered to the subject by the computer-controlled olfactometer. This system is free of auditory, tactile and thermal shifts that could cue the subject to the onset of the odor delivery. Since the nasal cannula/mask is a non-metallic material, it is safe to be used inside the scanner. The gas washing bottles were placed near the subject and were outside the scanner to minimize any delay in delivering the stimuli (figure 9.3-2). All the tubing was extended through a porthole (waveguide vent) connected to the technician's booth or equipment room, which is next to the MRI room. Moreover, all the connectors of the tubing are color-coded to identify which valve is connected to which stimulus. A constant airflow was generated behind the participant's head during the entire time the participant was in the scanner. The subject must avoid sniffing or blocking his/her breathing. A regular rhythm of breathing will have better results. The olfactometer is located outside the scanning room, since the magnetic environment of the scanning room hinders the use of electronic devices.

Figure 9.3-2: Subject was positioned inside the scanner and the stimuli holder was placed as close as possible to the scanner.

9.4 Data Processing and Analysis

The time-series fMRI data is processed using SPM8 (Statistical Parametric Mapping, The Wellcome Department of Imaging Neuroscience, University College London, UK). Images are first corrected for the staggered order of slice acquisition during echo planar scanning and make the data on each slice correspond to the same point in time – *slice timing correction*. It is accomplished by a simple shift of the phase of sine that makes up the signal. Motion correction is performed to realign each volume with the first of each scanning series by using a rigid-body transformation to correct movement artifacts - *realigning*. Spatially normalized images are transferred into a standard space – the Montreal Neurological Institute brain template – *spatial normalization*. The last step is to smooth the data sets with a 6 mm FWHM (Full Width Half Maximum) isotropic Gaussian kernel to improve the signal to noise ratio by reducing the high frequency noise – *smoothing*[93].

The statistical analysis is based on the general linear model (GLM), which defines the design matrix embodied in the fMRI experiment. The statistical parametric map (SPM) is calculated by correlating voxel intensities of the time-series images with the experiment protocol (stimulation). Then it convolves with the canonical hemodynamic response function (HRF) and impulse response of the olfactometer. The statistical parametric map indicates the likeliest voxels associated with the hemodynamic response. Then the results are overlaid to the corresponding anatomical images.

Chapter 10

Imaging the Orbitofrontal Cortex

The exploration of the human frontal lobes started with the dramatic case of Phineas Gage, who was injured in an accidental explosion by an iron rod passing through his head in 1848 in Cavendish, Vermont. The iron rod must have torn through the frontal lobe and a substantial part of the orbitofrontal cortex (OFC) as described by Dr. John Harlow, who treated Gage after the incident. Gage survived and recovered. However, there was a dramatic shift of his personality towards the irresponsible and secular[94, 95]. One would think that would have led to all kinds of developments in behavioral neurology to clarify the functions of the frontal lobe, including the OFC. Nonetheless, research on the orbitofrontal cortex has lagged behind other brain regions for much of the last century. Over the decade, there has been an enormous increase of research data addressing the OFC's structure, connections and functions. Especially after Zald and Kim's published papers in 1996[96, 97], there was an explosion of research in this region. There were dramatic advances in knowledge regarding the OFC's structure, neurocircuitry, functional contributions to sensation, emotion, social processing, decision-making and memory.

The OFC is located in the inferior, or orbital, surface of the frontal lobe. It gets its name from its position immediately above the orbits (the cavity or socket of the skull) in which the eyes are situated. In humans it consists of Brodmann area 10, 11 and 47 (figure 10-1). It is also the area of the prefrontal cortex commonly defined as the region that receives the projections from the thalamus. Moreover, clinical neuroscience increasingly implicates the OFC and adjacent ventral frontal regions with different psychiatric and neurological conditions, including

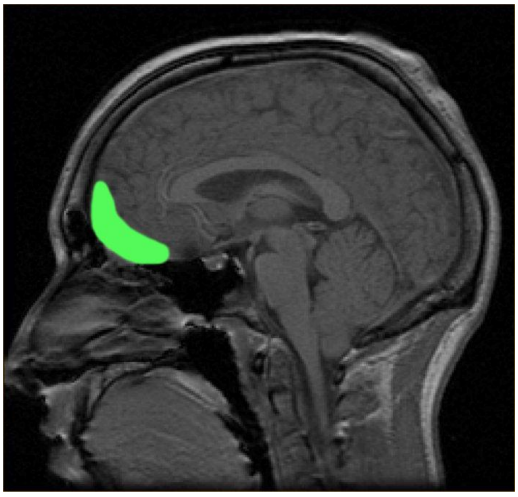

Figure 10-1: The area of the orbitofrontal cortex. *Phychology Wikia*

anxiety, mood and addictive disorders, and frontotemporal dementia. However, its location makes it vulnerable to lesions, such as head injury, tumor, vascular and neurodegenerative processes. It has bi-directional connections with the olfactory tubercle, piriform cortex, amygdala, and entorhinal cortex; and it is one of the higher order olfactory regions or secondary connections. There is probably hierarchical arrangement within OFC. The posteromedial OFC receives olfactory signals from the piriform cortex and amygdala, and transfers this information to more rostral areas of the OFC. In many human neuroimaging experiments, there is an OFC area activated by olfactory stimuli. Moreover, the pleasantness or reward value of odor is also represented in the OFC. Furthermore, the frontal lobe in the brain is involved in the cognitive processing of decision-making and the functions of the OFC are involved in emotion and reward; some consider the OFC as part of the limbic system.

Research has recently reported an increased number of neurological and psychiatric diseases associated with olfactory dysfunction. These diseases are: Alzheimer's disease (AD), schizophrenia, multiple sclerosis (MS), epilepsy, Parkinson's disease (PD) and obsessive-compulsive disorder (OCD). The most common theme associated with OCD is contamination concern, which is an intense feeling of having been polluted or infected. There is a well-established relationship between olfactory identification and the orbitofrontal cortex (OFC), which is the key structure affected in OCD[98]. Previous studies using functional magnetic resonance imaging (fMRI) show activations in OFC during olfactory stimulation with pleasant and unpleasant odorant stimuli[32, 98, 99]. However, it is always problematic imaging the OFC due to its location. It is near an air/tissue interface (air-filled sinuses) which has great different susceptibilities, may cause image distortions and signal losses[100]. As an earlier chapter stated that the signal intensity changes in fMRI are based on the difference of the susceptibility

between the oxygenated and deoxygenated blood (the BOLD effect). Moreover, the gradient-echo imaging sequences which are used mostly with functional MR imaging are rely on the T2* contrast arising from the dephasing spins due to local variations of the magnetic field caused by susceptibility differences. Nonetheless, it is a challenge to perform imaging of the OFC with fMRI due to its location. The other reason for limited studies of the OFC with fMRI may have been non-availability of the olfactometers.

Recently there was a research study, which showed great interest in the OFC area with pleasant and unpleasant stimuli with OCD patients. The olfactometer built for this thesis is being used to deliver the stimuli to the subjects in this study. Since OFC is the focus area with the OCD subjects, higher activations are suspected with the odorant stimuli. Two different approaches are attempted – axial and coronal imaging acquisitions. Moreover, both of these acquisitions do not acquire the entire brain – shown in figure 10-2. The axial acquisition is acquired with 19 slices, 150 volumes with TR=2000ms. The images are acquired from inferior to superior in ascending order. The angle of acquisition is approximately a 10 degrees angle to the AC-PC (anterior and posterior commissure) line. The coronal acquisition is acquired with 34 slices, 80 volumes, with TR=4000ms. The images are acquired from anterior to posterior in ascending order. The angle of acquisition is perpendicular to the AC-PC line.

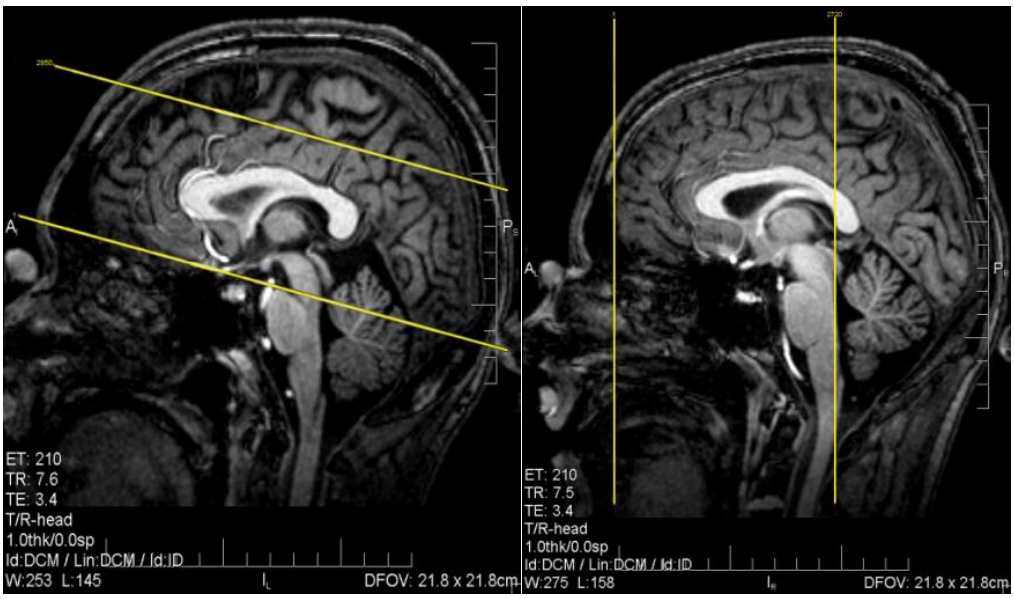

Figure 10-2: The coverage of the axial (left) and coronal (right) acquisitions are shown with first and last reference lines.

There is a large portion of the inferior OFC area not covered with the axial direction image acquisition due to the susceptibility artifacts (figure 10-3 – top figures). Since the OFC is the most interesting region of the OCD study, the coronal direction acquisition was used to acquire the images to minimize the artifacts. It reduced the susceptibility artifacts caused by the OFC and the phase-encoding component of the susceptibility-induced gradient, which might cause a severe drop in EPI. The result was much better compared to axial acquisition, even though it was still not totally covering the entire OFC region (figure 10-3 – bottom figures). However, it is only a smaller area of the posterior OFC that was not covered compared to the axial direction. Detail of the imaging results is discussed in Chapter10.

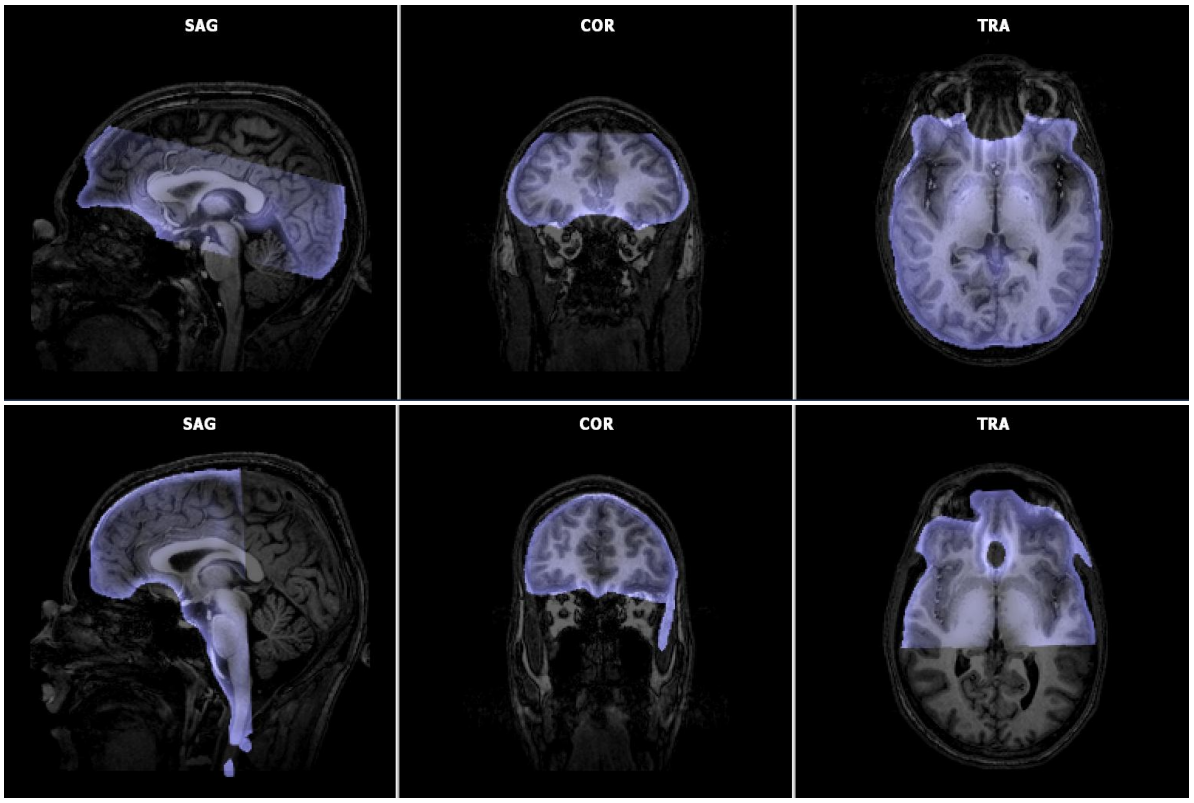

Figure 10-3: The overlays of functional images infused with the anatomical images. The axial acquisition is on the top, and the coronal acquisition is on the bottom.

Chapter 11

Test Results with Human Subjects

A birhinal nasal cannula, which was placed in front of the subject's nose, had been tested at the beginning of the project – olfactometer only. Ten volunteers (six male and four female) participated in this testing. However, the results were not conclusive and did not have consistent olfactory activations. Volunteers also responded, after the functional scans, that they could not distinguish the 'ON' and 'OFF' periods. The stimulus also lingered inside the scanner. A mask was chosen as the final choice for this olfactometer, with a vacuum system added. Therefore, the results presented here were based on the fMRI scanning with the mask to deliver the odorant stimulus. All fMRI images were acquired with Philips 3T Gemini (the Netherlands).

11.1 Set up procedures with a subject

As described in chapter 9.3, the subject was sitting on the table of the scanner. A mask was put over his/her nose only, with the hornet supported on his/her head. Ear plugs were given to the subject before placing a headphone over his/her ears. The mask was connected to a fresh air/stimulus and vacuum tubes (figure 9.3-1a & b). The subject lay down on the table and was given the instruction to breathe normally through his/her nose only. The subject also was instructed to try to determine what kind of stimulus was delivered and its intensity during the 'ON' period. Then the birdcage head coil was placed over the subject's head, and the subject entered the scanner (figure 9.3-1c and 9.3-2). The stimuli were placed in the holder of the magnetic safe stand, and the stand was rolled as close as possible to the scanner. The subject was ready to be scanned.

11.2 Functional MR scanning results

Four females and two males participated in the testing of the protocol, olfactometer and odorant stimuli for the OCD project. Data was acquired in the axial direction (as mentioned in chapter 9). From these pilot data, activations were observed with some of the subjects in the amygdala, insular cortex and dorsolateral prefrontal cortex (DLPFC) (figure 11-2.1). No activation was detected in the OFC area. When data acquisition was in the axial direction, there was a large portion of the OFC not covered (shown in figure 10-3 – top figure). This might be the reason why activations in the OFC area were not observed with all the subjects. However, the OFC region was the main area of concern with the OCD project. Optimum scanning protocol was needed to observe the activations in the OFC region.

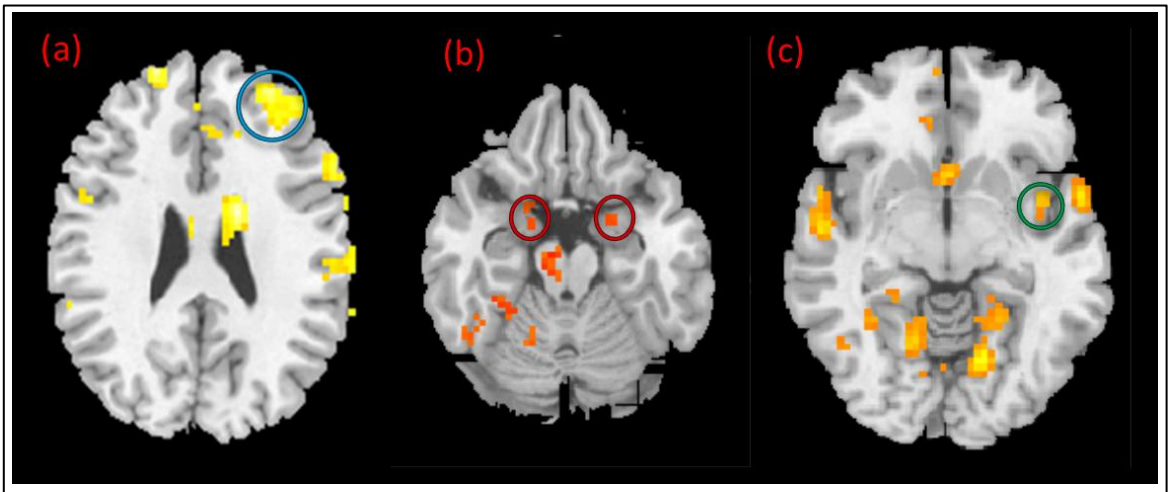

Figure 11.2-1: (a) Activation in the left DLPFC. (b) Activations in the both sides of the Amygdala. (c) Activation in the left insula cortex.

Coronal direction acquisition was then used to acquire the functional images. Changing the slice orientation reduced the phase-encoding component of the susceptibility-induced gradient, which might cause severe dropout in EPI. Four subjects, three male and one female, participated in this part of the testing. Activations in the OFC were observed in most of the subjects' scans. However, the number of the subjects was too small for one to conclude that this

method is the optimum. Nevertheless, it is encouraging from the results thus far. Figure 11.2-2 shows the activations of the correlation maps from one subject.

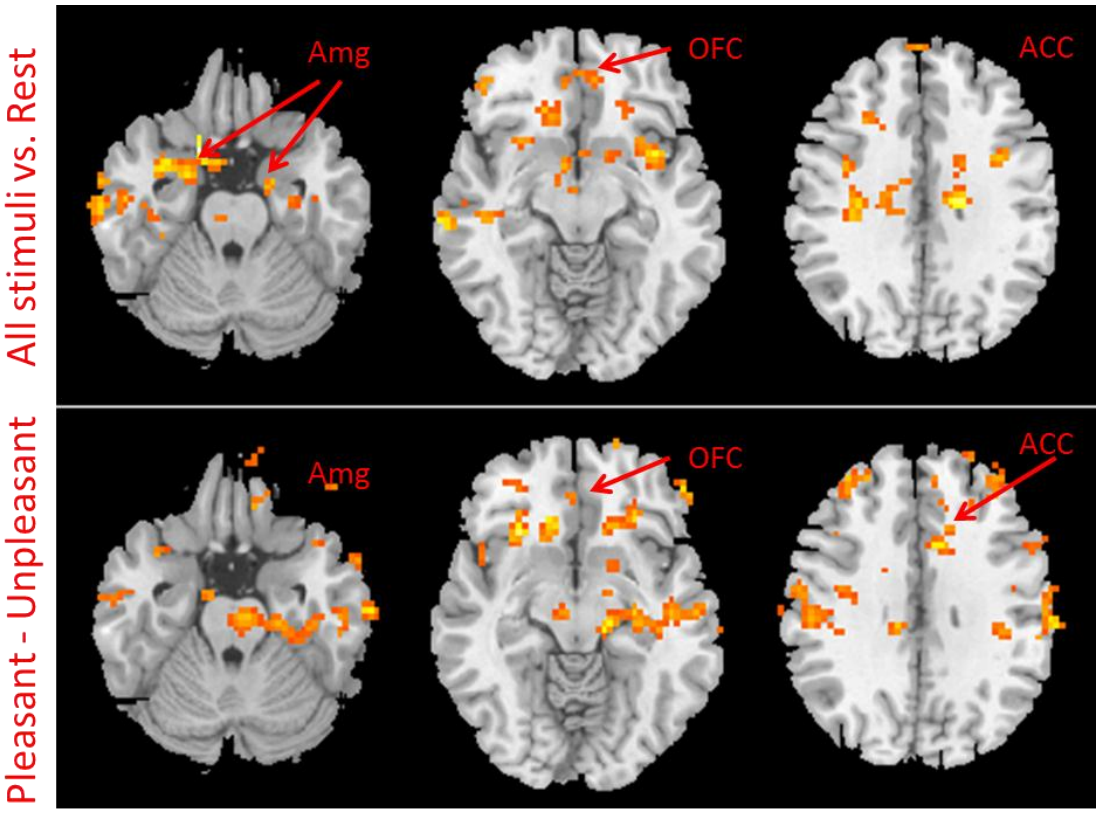

Figure 11.2-2: Correlation maps of one subject's scan with the OCD project protocol.

Two correlation maps were generated with the data: all stimuli versus the rest period and pleasant versus unpleasant. Analysis of stimuli versus rest showed activations in the amygdala, OFC and insular cortex. In pleasant-unpleasant comparisons, activations were found in OFC and anterior cingulate cortex (ACC), but not in the amygdala. These areas had very similar activations with olfactory stimulation from previous studies[32, 73]. The medial orbitofrontal cortex correlated with pleasantness; activations were shown in both correlation maps. In a previous investigation, activations in ACC were negatively correlated with pleasantness[73]. That may be the reason why there were activations in this area with pleasant versus unpleasant, and

not in all stimuli versus rest. In Grabenhorst et al. 2007, the activations in the primary olfactory areas were correlated with the intensity rather than pleasantness. This may be the reason why there were activations in the amygdala in stimuli versus rest, but not in pleasant versus unpleasant.

Chapter 12

Discussion

Compared to other sensory systems, especially visual and auditory, the olfactory system is the one of least interest in research – especially with fMRI (table 12-1). The main issue of limiting olfactory research with fMRI is probably the lack of accessibility of an olfactometer. The other issue is probably the susceptibility artifacts in some parts of the olfactory system. With the OCD project, the issue is the susceptibility artifacts of the OFC area. Also, there is no gold standard of the particular stimulus to stimulate certain parts of the olfactory system. Determining what stimuli to be used makes research in the olfactory system more difficult. There are advantages and disadvantages with the custom-build olfactometer versus a commercial olfactometer, and mask versus nasal cannula.

	Google	PubMed
Visual	709,000	16,425
Auditory	313,000	5,003
Somatosensory	119,000	3,127
Olfactory	73,100	837
Gustatory	20,800	112

Table 12-1: Search results from Google and PubMed websites for each sensory system with fMRI. *June 2011*

12.1 Advantages and disadvantages between nasal cannula and mask

In this research, a birhinal nasal cannula and a mask were used and tested. Due to different configurations of different magnets and their bird-cage head coils, when using a mask there is some difficulty to maneuver inside the head coils with its limited space. It also depends on the subject's head size. To resolve this problem, the padding inside the head coil, which is placed under the head for support, has to be adjusted in thickness to accommodate the fitting of the mask. Some people are borderline claustrophobic, and using a mask may increase their tension and fear. It is better to let the subject wear the mask for a short period, getting used to it before putting him/her inside the scanner. Depending on the design of the mask, there may be turbulence inside the mask. This also is related to the flow rate which one is using; the higher the

flow rate such turbulence can be created inside the mask. If a mask is desired with this design, one should be aware of this turbulence effect.

The mask can be expensive (depending on the kind and type, or special configuration) to maintain, and it takes time to be thoroughly cleaned after each use. If more subjects are to be tested, cleaning time may delay the next test. The test also depends on the material of the mask, which will or will not absorb the stimulus. A second mask is suggested if a large volume of scans is scheduled. On the other hand, the nasal cannula is inexpensive and can be replaced for each subject. It can easily be found in a hospital environment. It will reduce maintenance costs.

The odorant/smell lingers in the MR coil when using the nasal cannula. Even though the fan in the MR coil was set to high speed, the odorant was still not totally clear. Sometimes subjects will not inhale enough olfactory stimuli due to the evacuation from the fan, which is blowing in the opposite direction of the stimuli being delivered, especially when the intensity of the stimuli is low. On the other hand, some subjects also reported that they could still detect the stimulus during the 'OFF' period. Even though a vacuum tube was attached on the head coil, it was still difficult to evacuate the entire stimulus after it was delivered. Some also reported that they could not really distinguish the 'ON' or 'Off" period in the middle of the scanning. On the other hand, when a mask is used, the stimulus was contained inside the mask. When the vacuum pump started to operate, it took a second or two to evacuate the entire delivered stimulus. At the same time, fresh air was delivered to the mask. Subjects reported that they could distinguish the 'ON' and 'OFF' period very clearly; and they could no longer detect any stimulus during the 'OFF' period. The advantage of using a mask is the shortening of the stimulus delivery time, since the stimulus is in a more confined environment. Moreover, the flow rate has to be increased (from 1.5 LPM to 2 LPM) when using a mask.

12.2 Advantages and disadvantages compared to a commercial olfactometer

As far as we know, there is only one commercial olfactometer manufacturer in the market (Burghart Medizintechnik, Hamburg-Blankenese, Germany) that is compatible with magnetic resonance imaging. Most other researchers do not use this brand of olfactometers; they build their own or have individually custom built olfactometers. Most laboratories have limited space; the commercial olfactometer (especially when using more than one channel) is usually quite large in size. For example, the measurement of the 8 channel and birhinal olfactometer is 4 x 2.6 x 7 ft^3 (width x depth x height) and weighs about 882 pounds. Laboratories have to designate a specific area to install the olfactometer, and it needs to be near the MR scanner. The supplied tubing is just 2 meters long – extended tubing would need to be purchased from the company. This device's size will be an issue in a clinical setting, where space is at a premium or specific allocated space to accommodate this large machine is not available. This is one reason why transportability is important in a clinical environment. A custom-built olfactometer will be much smaller and lighter than a commercial one. It is easy to transport and disassemble. It is ideal for a clinical environment with limited space. It also has the possibility of more channels than the current commercial olfactometer offers at a fraction of the price. The commercial olfactometers may also build in some functions that research projects will never use. It will not be economically efficient for limited budget projects.

Commercial olfactometers from Burghart need time to warm up before the experiment, and will take approximately half an hour to prepare the device and patients. After each experiment, the device must run dry for at least 10 minutes before shut down. The custom-built olfactometer does not have this problem. It will take approximately 15 minutes to prepare the device and the patient. Also, it does not require time to warm up before or run dry after each the experiment.

Commercial olfactometers are very expensive with the basic system, and maintaining the olfactometer is costly in the long term. The most commonly used olfactometer manufacturer is Burghart Medizintechnik, Hamburg-Blankenese, Germany. They have a few models of olfactometer (depending on how many channels and monorhinal or birhinal are offered) and the price ranges from 32,000 to 170,000 EUR (approximately US$ 45,000 to 240,000). These prices do not include transportation, training and installation costs, which mainly depend on the location of the country of delivery and installation. This could be a large amount for a laboratory's budget if it is not mainly doing olfaction research. A custom-built olfactometer can satisfy research needs and does not require a large portion of the budget. Our custom-built olfactometer costs approximately $4600 with most of the main components and the testing equipment.

Chapter 13

Conclusion

We built an MR compatible olfactometer that can reliably present olfactory stimuli to a subject during fMRI. The stimulus was delivered in the absence of thermal, auditory and tactile indication. The vacuum pump does well in evacuation. The whole system is compact and can easily be transferred to different locations, especially in a clinical environment, as space is essential. Moreover, the total cost to build this system is just a fraction of the cost of a commercial MR compatible olfactometer.

The current Obsessive-Compulsive Disorders project is using this custom-built olfactometer to deliver the stimuli to the subjects. It gives great confidence to the stability and efficiency of the final product. While acquiring the pilot data, subjects could identify the pleasantness and unpleasantness of the odorant stimuli, but could not completely identify what the stimuli were. They also reported that the intensity detection was moderate, and not overwhelmingly strong, especially with the unpleasant stimuli. Axial orientation was tried with EPI-acquisition. However, regions in the OFC were either not visualized or had severe distortion and no activation was detected in the OFC. When acquisition was changed to the coronal plane with segmented EPI-acquisition, there were significant increased activations not only in the OFC area, but were also found in the ACC. These are the pilot data to determine the optimum protocols, improving acquired OFC images and choice of stimuli to be used. We conclude that we have a workable protocol to study the OFC using an olfactometer in an fMRI paradigm.

There are some areas, which can be improved with this olfactometer when performing functional experiments. A respiration amplifier (RSP 100C, Biopac Systems Inc., Goleta CA) can be added to monitor the subject's respiration. This can also confirm the subject is breathing normally during the 'ON' period, rather than holding his/her breath if the unpleasant stimulus is being delivered. Furthermore, this respiration signal can be implemented into the LabVIEW

program, which can trigger the delivery of the stimulus when the subject is inhaling. An auditory cue program (written with E-Prime 2.0, Psychology Software Tools Inc., Sharpsburg, PA), for the breathe-in and breathe-out instructions, can also be implemented if investigators want to include auditory cuing as part of their protocols when respiration monitoring is not used. Also, investigating on the molecular level of the stimuli may help to determine and find better stimuli, which can increase activations in the olfactory system. With these stimuli, more activation may then be obtained from the functional imaging in the focus areas, such as OFC in this study. Moreover, the most important task is to recruit more subjects and collect enough fMRI data to confirm our findings.

Publications and Abstracts

Publications:

Cheuk Y. Tang, Joseph I. Friedman, David M. Carpenter, Vladan Novakovic, Emily Eaves, Johnny Ng, Ying-Wei Wu, Stephanie Gottlieb, Sylvan Wallenstein, Erin Moshier, Michael Parrella, Leonard White, Stephanie Bowler, Thomas G. McGinn, Lauren Flanagan, Kenneth L. Davis, The Effects of Hypertension and Body Mass Index on Diffusion Tensor Imaging In Schizophrenia, Schizophrenia Research, 2011, 130 (1-3): 94-100.

Cheuk Y. Tang, David M. Carpenter, Emily L. Eaves, Johnny Ng, Nimalya Ganeshalingam, Clifford Weisel, Gudrun Lange, and Nancy L. Fiedler, Effects of occupational solvent exposure on brain function: an fMRI study. Environmental Health Perspectives, 2010, 119 (7):908-13

Cheuk Y Tang, Eaves EL, Ng JC, Carpenter DM, Mai X; Schroeder DH, Condon DH; Colom R, Haier RJ, Brain networks for working memory and factors of intelligence assessed in males and females with fMRI and DTI. Intelligence, 2010, 38: 293-303

Friedman J, Tang C, Carpenter D, Buchsbaum M, Schmeidler J, Flanagan L, Golembo S, Kanellopoulou I, Ng J, Hof PR, Harvey PD, Tsopelas ND, Stewart D, Davis KL, Diffusion Tensor Imaging Findings in First-Episode and Chronic Schizophrenia Patients. Am J Psychiatry 2008 165: 1024-1032

Tang C Y, Friedman J, Shungu D, Chang L, Ernst T, Steward D, Carpenter D, Ng J, Hajianpour A, Mao X, Hof P, Buchsbaum M S, Davis K and Gorman J M, Correlations between Diffusion Tensor Imaging (DTI) and Magnetic Resonance Spectroscopy (1H MRS) in schizophrenic patients and normal controls, BMC Psychiatry 2007, 7:25 (19 Jun 2007)

Abstracts and Posters:

Ng J, Berlin H, Goodman W, Eaves E, Carpenter D and Tang C Y, Optimized fMRI imaging protocol and custom-built olfactometer for studying the orbitofrontal cortex, The 2nd Annual TMII Symposium - 2011, New York

Ng J, Eaves E, Carpenter D and Tang C Y, An MR Compatible Olfactometer for Clinical Research Use, ISMRM 2011, Montreal Quebec Canada

Ng J, Berlin H, Goodman W, Eaves E, Carpenter D and Tang C Y, Optimized fMRI Imaging Protocol and Hardware for Studying the Orbitofrontal Cortex in the Presence of Olfactory Stimulation, ISMRM 2011, Montreal Quebec Canada

Ng J, Tang C Y, Eaves E, Kanellopoulou I, Mai X, Carpenter D, Schroeder, Condon C and Haier R J, Gender differences in correlations of regional white matter integrity with intelligence factor scores, ISMRM 2009, Honolulu Hawaii

Eaves E, Tang C Y, Ng J, Carpenter D, Schroeder D, Condon C, Colom R and Haier R J, Gender differences in correlations of functional brain activation with intelligence factor scores, ISMRM 2009, Honolulu Hawaii

Ng J, Tang C Y, Eaves E, Kanellopoulou I, Mai X, Carpenter D, Schroeder, Condon C and Haier R J, Gender differences in correlations of regional white matter integrity with intelligence factor scores, Neuroscience 2008, Washing DC

Eaves E, Tang C Y, Ng J, Carpenter D, Schroeder D, Condon C, Colom R and Haier R J, Gender differences in correlations of functional brain activation with intelligence factor scores, Neuroscience 2008, Washing DC

Carpenter D, Tang C Y, Ng J and Leung E, Modulation of the Inverse Functional Relation of Resting and Working Memory Networks, ISMRM 2007, Berlin Germany

References

1. Doty, R.L., *Clinical studies of olfaction.* Chemical Senses, 2005. **30**(suppl 1): p. i207-i209.
2. Özdener, M.H. and N.E. Rawson, *Olfactory dysfunction in neurodegenerative dieases.* European Journal of General Meddicine, 2004. **1**(3): p. 1-11.
3. Murphy, C., et al., *ERP, fMRI and Functional Connectivity Studies of Brain Response to Odor in Normal Aging and Alzheimer's Disease.* Chemical Senses, 2005. **30**(suppl 1): p. i170-i171.
4. Murphy, C., et al., *Prevalence of olfactory impairment in older adults.* JAMA, 2002. **288**(18): p. 2307-2312.
5. Rawson, N.E., *Olfactory loss in aging.* Science Aging Knowledge Environment, 2006. **2006**(5): p. pe6.
6. Kern, R.C., et al., *Pathology of the olfactory mucosa: implications for the treatment of olfactory dysfuction.* The Laryngoscope, 2004. **114**: p. 279-285.
7. Doty, R.L., et al., *Olfactory dysfunction in patients with head trauma.* Archives of Neurology, 1997a. **54**(9): p. 1131-1140.
8. Landis, B.N., et al., *Differences Between Orthonasal and Retronasal Olfactory Functions in Patients With Loss of the Sense of Smell.* Archives of Otolaryngol - Head & Neck Surgery, 2005. **131**: p. 977-981.
9. Connelly, T., et al., *Olfactory dysfunction in degenerative ataxias.* J. Neurol. Neurosurg Psychiatry, 2003. **74**(1435-1437).
10. Thomann, P.A., et al., *Reduced olfactory bulb and tract volume in early Alzheimer's disease - A MRI study.* Neurobiology of Aging, 2007.
11. Swaab, D.F., *The Human Hupothalamus: Basic and Clinical Aspects (Volumes I and II).* 1st ed, ed. M.J. Aminoff, F. Boller, and D.F. Swaab. Vol. 2. 2003, Amsterdam, The Netherlands: Elsevier. Volume 1: 476 pp; Volume 2: 597 pp.
12. Bonakdarpour, B., T.B. Parrish, and C.K. Thompson, *Hemodynamic response function in patients with stroke-induced aphasia: Implications for fMRI data analysis.* Neuroimage, 2007. **36**(2): p. 322-331.
13. Doty, R.L., et al., *Olfactory dysfunction in three neurodegenerative disease.* Geriatrics, 1991. **46**(Suppl 1): p. 47-51.
14. Kivity, S., O.D. Ortega-Hernandez, and Y. Shoenfeld, *Olfaction - A Window to the Mind.* The Isreal Medical Association Journal, 2009. **11**(4): p. 238-243.
15. Moberg, P.J. and R.L. Doty, *Olfactory Function in Huntington's Disease Patients and At-risk Offspring.* International Jounral of Neuroscience, 1997. **89**: p. 133-139.
16. Doty, R., *Olfactory Deficit in Alzheimer's Disease?* American Journal of Psychiatry, 2001. **158**(9): p. 1533-1534.
17. Olofsson, J.K., et al., *Odor Identification Deficit as a Predictor of Five-Year Global Cognitive Change: Interactive Effects with Age and ApoE-e4.* Behavior Genetics, 2009. **39**: p. 496-503.
18. Segalas, C., et al., *Olfactory Identification and Discrimination in Obsessive-Compulsive Disorder.* Depression and Anxiety, 2011. **0**: p. 1-9.
19. Doty, R.L., *The Olfactory System and Its Disorders.* Seminars in Neurology, 2009. **29**(1): p. 74-81.
20. Graeber, M.B., *Biomarkers for Parkinson's disease.* Experimental Neurology, 2009. **216**(2): p. 249-253.

21. Craig-Schapiro, R., A.M. Fagan, and D.M. Holtzman, *Biomarkers of Alzheimer's disease.* Neurobiology of Disease, 2009. **35**(2): p. 128-140.
22. Berne, R.M., et al., *Physiology, 5th Edition*. Vol. Chapter 8. 2004: Mosby. 148-153.
23. Doty, R.L., in *Handbook of Olfaction and Gustatin, 2nd Edition*, R.L. Doty, Editor 2003, Marcel Dekker: New York.
24. Ganong, W.F., *Review of Medical Physiology, 21st Edition*2003: Lange Medical Books/McGraw-Hill.
25. Kandel, E.R., J.H. Schwartz, and T.M. Jessell, *Principles of Neural Science, 4th Edition*. Smell and Taste: The chemical senses2000: McGraw-Hill Companies, Inc.
26. Kandel, E.R., J.H. Schwartz, and T. Jessell, *Principles of Neural Science, 4th Edition*. 4th ed2000: McGraw-Hill Companies, Inc.
27. Jafek, B.W., et al., *Biopsies of human olfactory epithelium.* Chemical Senses, 2002. **27**: p. 623-628.
28. Murphy, C., et al., *ERP, fMRI and functional connectivity studies of brain response to odor in normal aging and Alzheimer's disease.* Chemical Senses, 2005. **30**(1): p. i170-i171.
29. Wang, J., et al., *Functional Magnetic Resonance Imaging Study of Human Olfaction and Normal Aging.* Journal of Gernotology: Medical Science, 2005. **60A**(4): p. 510-514.
30. Kareken, D.A., et al., *Olfactory system activation from sniffing: effects in piriform and orbitofrontal cortex.* NeuroImage, 2004. **22**(1): p. 456-465.
31. Lorig, T.S., et al., *A computer-controlled olfactometerr for fMRI and electrophysiological studies of olfaction.* Behavior Research Methods, Instruments & Computers, 1999. **31**(2): p. 370-375.
32. Rolls, E.T., M.L. Kringelbach, and I.E.T. de Araujo, *Different representations of pleasant and unpleasant odours in the human brain.* European Journal of Neuroscience, 2003. **18**: p. 695-703.
33. Tabert, M.H., et al., *Validation and optimization of statistical approaches for modeling odorant-induced fMRI signal changes in olfactory-related brain areas.* NeuroImage, 2007. **34**(4): p. 1375-1390.
34. Poellinger, A., et al., *Activation and Habituation in Olfaction - An fMRI Study.* NeuroImage, 2001. **13**(4): p. 547-560.
35. Gottfried, J.A., et al., *Functional Heterogeneity in Human Olfactory Cortex: An Event-Related Functional Magnetic Resonance Imaging Study.* The Journal of Neuroscience, 2002. **22**(24): p. 10819-10828.
36. Negoias, S., et al., *New ways to understand aroma perception.* Food Chemistry, 2008. **108**(4): p. 1247-1254.
37. Albrecht, J., et al., *Activation of olfactory and trigeminal cortical areas following stimulation of the nasal mucosa with low concentrations of S(-)-nicotine vapor--an fMRI study on chemosensory perception.* Human Brain Mapping, 2009. **30**(3): p. 699-710.
38. Boyle, J.A., et al., *Cross-modal integration of intranasal stimuli: A functional magnetic resonance imaging study* Neuroscience, 2007. **149**(1): p. 223-231.
39. Wikipedia. *Ernst von Fleischl-Marxow*. 2009-a [cited 2009 2 July]; Available from: http://en.wikipedia.org/wiki/Ernst_von_Fleischl-Marxow.
40. Prah, J.D., S.B. Sears, and J.C. Walker, *Modern approaches to air dilution olfactometry*, in *Handbook of Olfaction and Gustation*, R.L. Doty, Editor 2003, Marcel Dekker: New York. p. 227-256.

41. Nuno Teixeira's Portfolio. *Smellit - Taste your movies like you never have*. 2008 [cited 2009 2 March]; Available from: http:.//www.behance.net/Gallery/SMELLIT--TASTE-YOUR-MOVIES-LIKE-YOU-NEVER-HAVE/141582.
42. designeRoof. *Smell it by Nuno Teixeira*. 2008 [cited 2009 2 March]; Available from: http://www.designeroof.com/smell-it-by-nuno-teixeira.
43. Fox, K. *The Smell Report: An overview of facts and findings*. 1999 [cited 2008 January]; Available from: http://www.sirc.org/publik/smell.pdf.
44. Gardner, J.W. and P.N. Bartlett, *Electronic Noses. Principles and Applications.* Measurement Science and Technology, 1999. **11**(7).
45. Gardner, J.W., H.W. Shin, and E.L. Hines, *An electronic nose system to diagnose illness.* Sensors and Actuators B: Chemical, 2000. **70**(1-3): p. 19-24.
46. Deborah. *Science of the Smell Factor*. 2007 [cited 2009 27 June]; Available from: http://www.lifeinthefastlane.ca/science-of-the-smell-factor/weird-science.
47. ETH Zurich. *Odor Matching: The Scent Of Internet Dating*. [electronic news] 2009 [cited 2009 April 14]; Available from: http://www.sciencedaily.com/releases/2009/04/090412080748.htm.
48. Wikipedia. *Smell-O-Vision*. 2009-b [cited 2009 5 March]; Available from: http://en.wikipedia.org/wiki/Smell-O-Vision.
49. Kimmelman, C.P., *Clinical review of olfaction.* American Journal of Otolaryngology, 1993. **14**(4): p. 227-239.
50. Jones, N. and D. Rog, *Olfaction: a review.* The Journal of Laryngology & Otology, 1998. **112**: p. 11-24.
51. Hawkes, C.H. and R.L. Doty, *The Neurology of Olfaction*. 1st ed2009: Cambridge University Press.
52. Herz, R., *The Scent of Desire: Discovering our enigmatic sense of smell*. 1 edition ed2007: William Morrow.
53. Hansel, D.E., B.A. Eipper, and G.V. Ronnett, *Regulation of olfactory neurogenesis by amidated neuropeptides.* Journal of Neuroscience Research, 2001. **66**: p. 1-7.
54. Mombaerts, P., *How smell develops.* Nature Neuroscience Supplement, 2001. **4**: p. 1192-1198.
55. Özdener, M.H. and N.E. Rawson, *Olfactory dysfunction in neurodegenerative diseases.* Eur J Gen Med, 2004. **1**(3): p. 1-11.
56. Robinson, A.M., et al., *Apoptosis in the aging olfactory epithelium.* The Laryngoscope, 2002. **112**: p. 1431-1435.
57. Firestein, S., H. Breer, and C.A. Greer, *Olfaction: what's new in the nose?* Journal of Neurobiology, 1996. **30**(1): p. 1-2.
58. Lewcock, J.W. and R.R. Reed, *ORs rule the roost in the olfactory system.* Science, 2003. **302**: p. 2078-2079.
59. Friedman, D. and B.W. Strowbridge, *Functional role of NMDA autoreceptors in olfactory mitral cells.* Journal of Neurophysiology, 2000. **84**: p. 39-50.
60. Cleland, T.A. and C. Linster, *Computation in the olfactory system.* Chemical Senses, 2005. **30**: p. 801-813.
61. Breer, H., *Sense of smell: Recognition and transduction of olfaction signal.* Biochemical Society Transactions, 2003. **Vol. 31**(part 1).
62. Doty, R.L., *Olfaction.* Annual Review of Psychology, 2001. **52**: p. 423-452.

63. Finger, S., *Origins of Neuroscience: A History of Explorations Into Brain Funciton*. 1st Edition ed1994: Oxford University Press, USA. 480.
64. Lowen, S.B. and S.E. Lukas, *A low-cost, MR-compatible olfactometer.* Behav Res Methods, 2006. **38**(2): p. 307-313.
65. Philpott, C.M., A. Bennett, and G.E. Murty, *A brief history of olfaction and olfactometry.* The Journal of Laryngology & Otology, 2008. **122**(7): p. 657-662.
66. Doty, R.L., *Studies of Human Olfaction from the University of Pennsylvania Smell and Taste Center.* Chemical Senses, 1997b. **22**: p. 565-586.
67. Berglund, B., U. Berglund, and T. Lindvall, *Theory and methods for odor evaluation.* Cellular and Molecular Life Sciences, 1986. **42**(3): p. 280-287.
68. Altawell, N. *What is Electronic Nose?* 2008; Available from: http://ezinearticle.com/?What-is-Electronic-Nose?&id=1037705.
69. Wenzel, B.M., *Techniques in Olfactometry: A Critical Review of The Last One Hundred Years.* Psychological Bulletin, 1948. **45**(3): p. 231-247.
70. Hall, G.S., E.C. Sanford, and E.B. Titchener, *The American Journal of Psychology*. Vol. Vol. X. 1898-99, Clark University, Worcester, MA: Louis N. Wilson.
71. Eibenstein, A., et al., *Mordern psychophysical tests to assess olfactory function.* Neurological Sciences, 2005. **26**(3): p. 147-155.
72. Popp, R., et al., *Olfactometry in fMRI studies: odor presentation using nasal continuous positive airway pressure.* Acta Neurobiologiae Experimentalis, 2004. **64**: p. 171-176.
73. Grabenhorst, F., et al., *How Pleasant and Unpleasant Stimuli Combine in Different Brain Regions: Odor Mixtures.* The Journal of Neuroscience, 2007. **27**(49): p. 13532-13540.
74. De Wijk, R.A., et al., *An injection olfactometer for humans and a new method for the measurement of the shape of the olfctory pulse.* Behavior Research Methods, Instruments & Computers, 1996. **28**(3): p. 383-391.
75. Hummel, T., *Olfactometry*, in *Encyclopedia of perception*, E.B. Goldstein, Editor 2009, Sage Publications, Inc. p. 674-676.
76. Westermann, B., et al., *Functional imaging of the cerebral olfactory system in patients with Parkinson's disease.* Journal of Neurology, Neurosurgery, and Psychiatry, 2008. **79**: p. 19-24.
77. Roon, T.v. *555 timer tutorial*. 1995; Available from: http://www.sentex.ca/~mec1995/gadgets/555/555.html.
78. Johnson, B.N., J.D. Mainland, and N. Sobel, *Rapid Olfactory Processing Implicates Subcortical Control of an Olfactometer System.* Journal of Neurophysiology, 2003. **90**: p. 1084-1094.
79. Onoda, N., T. Sugai, and H. Yoshimura, *Odor-intensity Coding in the Anterior Piriform Cortex.* Chemical Senses, 2005. **30**(suppl 1): p. i162-i163.
80. Murphy, C., et al., *Olfactory event-related potentials and aging: normative data.* Internaltional Journal of Psychophysiology, 2000. **36**: p. 133-145.
81. Heining, M., et al., *Disgusting smells activate human anterior insula and ventral striatum.* Annals of The New York Academy of Sciencies, 2003. **1000**: p. 380-384.
82. Rolls, E.T., F. Grabenhorst, and B.A. Parris, *Neural Systems Underlying Decisions about Affective Odors.* Journal of Cognitive Neuroscience, 2010. **22**(5): p. 1069-1082.
83. Savic, I., *Brain imaging studies of the functional organization of human olfaction.* The Neuroscientist, 2002. **8**(3): p. 204-211.

84. Heeger, D.J. and D. Ress, *What does fMRI tell us about neuronal activity* Nature Reviews: Neuroscience, 2002. **3**: p. 142-151.
85. Bammer, R., et al., *Foundations of advanced magnetic resonance imaging.* The Journal of the American Society for Experimental NeuroTherapeutics, 2005. **2**: p. 167-196.
86. Buckner, R.L., *Event-related fMRI and the hemodynamic response.* Human Brain Mapping, 1998. **6**: p. 373-377.
87. Heeger, D.J. and D. Ress, *What does fMRI tell us about neuronal activity?* Nature Reviews: Neuroscience, 2002. **3**: p. 142-151.
88. Kobal, G. and B. Kettenmann, *Olfactory functional imaging and physiology.* International Journal of Psychophysiology, 2000. **36**: p. 157-163.
89. Cacioppo, J.T., et al., *Just because you're imaging the brain doesn't mean you can stop using you head: A primer and set of first principles.* Journal of Personality and Social Psychology, 2003. **85**(4): p. 650-661.
90. Budinger, T.F., *Functional biomedical imaging.* National Academy of Engineering of The National Academies, 2000. **30**(1): p. Spring 2000.
91. Raichle, M.E., *Functional brain imaging and human brain function.* The Journal of Neuroscience, 2003. **23**(10): p. 3959-3962.
92. Pekar, J.J., *A brief introduction to functional MRI: History and today's developments,* in *IEEE Engineering in Medicine and Biology Magazine*2006. p. 24-26.
93. Friston, K.J., et al., *Spatial Registration and Normalization of Images.* Human Brain Mapping, 1995. **2**: p. 165-189.
94. Harlow, J.M., *Passage of an Iron Rod Through the Head* The Journal of Neuropsychiatry & Clinical Neurosciences, 1999. **11**: p. 281-283.
95. Barker II, F.G., *Phineas among the phrenologists: the American crowbar case and nineteenth-century theories of cerebral localization.* Journal of Neurosurgery, 1995. **82**: p. 672-682.
96. Zald, D.H. and S.W. Kim, *Anatomy and function of the orbital frontal cortex, I: anatomy, neurocircuitry; and obsessive-compulsive disorder.* Journal of Neuropsychiatry & Clinical Neurosciences, 1996. **8**: p. 125-138.
97. Zald, D.H. and S.W. Kim, *Anatomy and function of the orbital frontal cortex, II: Function and relevance to obsessive-compulsive disorder.* Journal of Neuropsychiatry & Clinical Neurosciences, 1996. **8**: p. 249-261.
98. Saxena, S. and S.L. Rauch, *Functional neuroimaging and the neuroanatomy of obsessive-compulsive disorder.* Psychiatric Clinics of North America, 2003. **23**(3): p. 563-586.
99. Katata, K., et al., *Functional MRI of regional brain responses to 'pleasant' and 'unpleasant' odors.* Acta Oto-laryngologica, 2009. **129**(s562): p. 85-90.
100. Deichmann, R., et al., *Optimized EPI for fMRI studies of the orbitofrontal cortex.* NeuroImage, 2003. **19**(2): p. 430-441.